ministerie van verkeer en waterstaat

koninklijk nederlands meteorologisch instituut

A comparison of numerical methods for air-quality models

Th.L. van Stijn, J.C.H. van Eijkeren, N. Praagman

scientific reports WR-nr. 87-6

wetenschappelijke rapporten WR-87-6

RIVM report nr. 95 87 02 007

in samenwerking met

rivm

Rijksinstituut voor Volksgezondheid en Milieuhygiëne, Bilthoven

de bilt, 1987

KNMI

A Comparison of Numerical Methods for Air-Quality Models

Th. L. van Stijn,

Royal Netherlands Meteorological Institute,
P.O. Box 201,
3730 AE De Bilt, The Netherlands

J.C.H. van Eijkeren,
N. Praagman,

National Institute for Public Health
and Environmental Hygiene,
P.O. Box 1,
3720 BA Bilthoven, The Netherlands

TABLE OF CONTENTS

SUMMARY

In realistic air-pollution models a variety of physical and chemical processes have to be taken into consideration. The most important processes for constituents are advection and (turbulent) diffusion in the atmosphere, emission from diffuse and concentrated sources, wet and dry deposition and (photo-)chemical interactions. A mass balance, that reflects these processes is difficult to solve directly with numerical mathematical methods. However, the method of fractional steps (Yanenko, 1971) makes it possible to treat the different processes separately. Thus an algorithm that is most suitable for the approximation of a particular sub-process, such as advection, can be chosen.
Photo-chemical interactions play a substantial role in air-pollution situations. They are described by non-linear mathematical equations, which in many cases demand for their numerical solution that the chemical constituent concentrations remain non-negative. It turns out to be especially hard to construct numerical advection schemes that are non-negative as well as mass conserving and accurate enough. Therefore the larger part of this study is devoted to a comparative study of a number of special numerical methods that approximate the solution of the advection equations with two spatial dimensions. The best methods that came out of previous comparison studies have been chosen, together with some methods which appeared in recent literature.

To get a clear and coherent impression of the performance of these advection schemes a consistent set of tests has been made on a VAX 11/750 under the UNIX 4.1 system. A number of objective criteria discriminate between the various outcomes. Also practical results such as computer time consumption and storage requirements are given.
The results indicate that the Second Moment Method is a robust and relatively cheap method for the resolution of the advection equation, although its storage requirements can be prohibitive. For a more detailed discussion see section 2.11.

Numerical methods for the treatment of the vertical structure and the non-linear chemical interactions are not included in this report. These will be the subject of a subsequent investigation.

This study is a part of the RIVM (National Institute for Public Health and Environmental Hygiene)-KNMI (Royal Netherlands Meteorological Institute) cooperation for the development of operational air-pollution models.

1. INTRODUCTION

In the last decade simulation models have become important instruments for the understanding and the abatement of air quality problems. Much effort is given by physicists and chemists to design urban scale, regional or global models which describe the transport of air pollutants. There are many other related problems in environmental science where the main concern is the way in which transport of a contaminant is taking place by a moving fluid. Next to the air pollution problem there is e.g. the question of transport of trace constituents in the ocean, in estuaries or by rivers. However, all these problems have the following in common. When practical situations are to be simulated using a numerical model, the governing model equations have to be discretized. To this end the equations are approximated utilizing numerical mathematical methods. Such a process unavoidably will introduce errors, which even can defile the entire solution (e.g. if negative concentrations are produced) when an incorrect method is chosen. Therefore, if the careful model-research is not to be nullified, it is of paramount importance to use advanced numerical methods. Here the rule can be employed that numerical errors should be of smaller order than the uncertainty that is present in the results of measurements and model approach to obtain results that are interpretable.

Usually several mechanisms can be distinguished in the model equations for the transport of contaminants. The important mechanisms are advection (transport by wind), turbulent diffusion and chemical and photochemical reactions. Each of these has its own numerical characteristic difficulties and therefore the method of fractional steps (Yanenko (1971)) is attractive to use. This method makes it possible to employ for each sub-mechanism separately an efficient numerical solution technique.

In this report a number of special numerical methods for solving the advection equation with two spatial dimensions are compared. Although even before the advent of the computer algorithms for the transport of chemical constituents were designed, many specialized methods have appeared in the literature recently. Many of them have a heuristic basis which makes it difficult to trace their formal accuracy. Therefore it is desirable to test these methods on one computer with one set of test problems, so that the properties of the methods will be demonstrated in a clear manner. In this study the best methods of previous comparison studies have been

chosen together with some methods which appeared in recent literature. For testing purposes the methods have been programmed directly from the original papers. Here the important features of the numerical algorithms are compiled; more detailed descriptions and results can be found in [1]-[6].

The available computer configuration on which a simulation must be performed puts a strong bias on the choice of the numerical algorithm. It must be stated, however, that in the near future powerful computers become within reach of many users. Hence memory limitations will be not as severe anymore and it will be easy to couple an attached array processor to any computer. This implies that the mathematical properties of an approximating scheme are the most important items to take into consideration in any comparison study. In this report no account has been taken of methods which are designed for vector or parallel computers. This promising subject is left for future study.

In the remaining part of this chapter the basic conservation laws for the transport of air pollution will be explained. Moreover, the method of fractional steps, the initial conditions and the forcing will be elucidated. The subsequent chapters deal with numerical methods for the advection equation. Special numerical methods, which treat the vertical structure in the atmosphere and the stiff differential equations that emerge from the chemistry will be left for future investigation.

1.1 The conservation laws

The equations that govern the air pollution process are the result of conservation laws. If s chemical species $c_i(\underline{x},t)$ $(i = 1,\ldots,s)$ are considered suspended in a turbulent flow, then the following nonlinear partial differential equations express conservation of mass (Businger (1984), Pasquill and Smith (1983)),

$$\frac{\partial c_i}{\partial t} + \nabla.\ (\underline{U}\ c_i) = \nabla.\ (IK\ .\ \nabla\ c_i) + f_i\ (c_1,\ldots,c_s,t) + S_i\ . \qquad (1.1.1)$$

In this set of equations $\underline{U}\ (\underline{x},t) = [U,V,W]^t$ is the advective velocity field, imposed by meteorological conditions, $\underline{x}$ is a spatial point and t represents time. IK is a second-order eddy diffusivity tensor. The functions f_i render the complicated non-linear interactions among the chemical components. The term S is a source or sink term that describes the influence of surface sources, point sources and deposition processes.

In general it is not necessary nor desirable to solve (1.1.1) in its full form. In many cases it suffices to solve a simplified equation which reads in cartesian coordinates

$$\frac{\partial c_i}{\partial t} + \frac{\partial U c_i}{\partial x} + \frac{\partial V c_i}{\partial y} = - \frac{\partial F_i}{\partial z} + f_i + S_i, \quad i = 1,\ldots,s \; . \tag{1.1.2}$$

The most essential transport phenomena described by (1.1.2) are horizontal advection and vertical eddy diffusion. The mechanism for effective horizontal diffusion is provided by the horizontal shear in the wind velocity profile. The flux F_i expresses both vertical eddy diffusion and vertical transport.

The equations (1.1.2) must be solved on a limited spatial domain Ω which is bounded by $\partial\Omega$. It is assumed that Ω is fixed in time. The mathematical formulation of (1.1.2) is completed if initial and boundary conditions are added. The initial conditions for $\underline{x}$ in Ω can be written as

$$c_i\ (\underline{x},o) = c_{io}\ (\underline{x}), \quad i = 1,\ldots,s \; . \tag{1.1.3}$$

With respect to the horizontal boundary conditions distinction has to be made between in- and outflow boundaries. For that part $\partial\Omega_1$ of the boundary where an inflow of contaminant is taking place the local value must be prescribed by

$$c_i\ (\underline{x},t) = c_{i1}\ (\underline{x},t), \quad i = 1,\ldots s\ , \quad \underline{x} \in \partial\Omega_1 \; . \tag{1.1.4}$$

At the remaining part $\partial\Omega_2$ of the boundary the concentration is largely determined by advection outwards Ω.
At the top and at the bottom of the model expressions for the flux F_i have to be prescribed.

In the analysis of the numerical methods it will be assumed that the meteorological windfield $\underline{U}$ and the initial concentrations c_{io} are given on a prescribed grid. Moreover, it is supposed that relations are available for the vertical flux F_i and the chemical interactions f_i.

1.2 An approach to the forcing

The forcing term S in eq. (1.1.2) consists of a number of complex source and sink terms, namely

$$S = S_p + S_s - S_d \ . \qquad (1.2.1)$$

The depletion term S_d describes the deposition process at the earth's surface or the removal of material by wet processes. These processes usually are parameterized, see Pasquill and Smith (1983).

The other terms are the surface source term S_s and the point-emission term S_p. The surface source term is constructed from an emission inventory. It is usually a sufficient smooth function of $\underline{x}$ and therefore will not cause any difficulties in the numerical integration procedure.

Point sources, however, bring about strong sub-grid chemical interactions. It is virtually impossible to incorporate them in a numerical grid point approximation without introducing large errors, which makes it necessary to treat point sources separately. This is done by tracking the plume of each point source with a Gaussian model (Pasquill and Smith (1983)) for several time steps, until this concentration distribution is smooth enough to be incorporated in the large-scale grid point model. The air pollution model must thus provide for a bookkeeping section, which traces the trajectories of the point sources. An analysis can be found in Karamchandani et al. (1983). The Gaussian model has as an additional advantage that the chemical reactions between the relatively high concentrations of pollutant that are present in the initial stages of the plume can be described much better by this subgrid procedure. Numerical methods that are most suited for a direct treatment of point sources are Lagrangian methods of the particle-in-cell class (see section 2.9).

1.3 The method of fractional steps

As was pointed out in the introduction, several mechanisms for the transport of contaminants can be distinguished in eq. (1.1.2), all having a totally different numerical behaviour. These mechanisms are advection in a horizontal plane, vertical diffusion and chemical reactions. To get a feel for the numerical difficulties two out of many problems are illustrated below.

In the atmosphere the large scale dispersion of pollutants is chiefly a result of advection processes, whereas turbulent diffusion has a local mixing effect. Approximating the advection part of (1.1.2) with several numerical schemes on a grid, Sheih and Ludwig (1985) found that for realistic gridsizes of 50 km, which are used in regional scale models, about half of the schemes produced an artificial diffusion larger than the

natural eddy diffusion.

Another example which is of numerical concern can be found in the terms f_i that reflect the chemical reactions between the concentrations c_i. Apart from the fact that the terms are non-linear, they also complicate the numerical solution process because the spectrum of reaction time-scales is very large. In photochemical situations it is realistic to encounter reaction times that differ by an order of 10^8 seconds (McRae et al. (1982)). This phenomenon will dominate the entire solution process if this type of process is not resolved by a special method.

There are several ways in which the above mentioned difficulties can be removed. The most appropriate option seems to be the method of fractional steps, that was introduced by Yanenko (1971) and elaborated by Marchuk (1975). In this method the original differential operator (1.1.2) is factorized, thus obtaining a sequence of manageable equations. Here we may obtain

$$\text{Advection} \qquad \frac{\partial c_i}{\partial t} + \frac{\partial U c_i}{\partial x} + \frac{\partial V c_i}{\partial y} = S_{1i} \,, \tag{1.3.1}$$

$$\text{Diffusion} \qquad \frac{\partial c_i}{\partial t} = -\frac{\partial F_i}{\partial z} + S_{2i} \,, \tag{1.3.2}$$

$$\text{Chemistry} \qquad \frac{\partial c_i}{\partial t} = f_i\,(c_1,\ldots,c_s,t) \,. \tag{1.3.3}$$

The source term S must be incorporated in both (1.3.1) and (1.3.2). The advection step (1.3.1) will be used in this form in the upper air (above the mixed layer) where vertical diffusion is considered negligible. The homogeneous advection step will be used in combination with the diffusion step (1.3.2) in the mixed layer (Van Dop et al. (1982)).

In each timestep Δt of the numerical calculation these equations are solved. Observe, however, that equations (1.3.1-2) are uncoupled from (1.3.3) and therefore each of them constitutes a set of s uncoupled equations themselves. The investigation can now be restricted to numerical methods which are specific for the physical character of the three composing parts indicated above, thus leading to an efficient and stable overall scheme.

Further denote the part that approximates the advection equation numerically by the operator N_a, the diffusion equation by N_d and the chemistry equation by N_c, then it is possible to write the numerical process symbolically as

$$\underline{c}^{n} = N_c \, N_d \, N_a \, \underline{c}^{n-1} \quad . \tag{1.3.4}$$

Here the index n indicates time level t_n. It can be proved that the operator splitting in this method of fractional steps formally is of first order accuracy in time. To accomplish second order accuracy in time it is necessary that the numerical operators commute, which in general is not the case. If the order in which the operators are applied is reversed in each alternate timestep, i.e.

$$\underline{c}^{n+1} = N_a \, N_d \, N_c \, N_c \, N_d \, N_a \, \underline{c}^{n-1} \quad , \tag{1.3.5}$$

then the method is of second order accuracy.

2. NUMERICAL METHODS FOR THE ADVECTION EQUATION

In this chapter several numerical schemes are compared, that seem most appropriate to discretize the advection equation in two spatial dimensions (1.3.1) for a single concentration field c, viz.

$$\frac{\partial c}{\partial t} + \frac{\partial Uc}{\partial x} + \frac{\partial Vc}{\partial y} = 0 \ . \qquad (2.1)$$

This is possible, since it was shown in section 1.3 that the set of s equations becomes uncoupled when the method of fractional steps is involved. Moreover, first the homogeneous equation (without source term S) will be considered in the analysis.

The most important physical properties for the understanding of the transport equation are given in the next section. Thereupon a few numerical properties will be displayed. In section 2.3 it is mentioned which methods are investigated, together with the testproblems and objective criteria that will point out the most suitable method. In the sections 2.4-2.9 the methods are described in a short fashion, if necessary supplemented with indications concerning the technical implementation.

2.1 Physical properties

The solution of the advection equation (2.1) possesses a large number of properties that fruitfully can be employed in the search for the most suitable numerical approximation.

In the first place it is noted that in many occasions it is allowed to consider the windfield to be divergence-free at each horizontal level z, which is expressed by

$$\frac{\partial U}{\partial x} + \frac{\partial V}{\partial y} = 0 \ . \qquad (2.1.1)$$

Therefore, it is equally possible to start the numerical analysis from the conservation equation (2.1) or from its advection form

$$\frac{\partial c}{\partial t} + U \frac{\partial c}{\partial x} + V \frac{\partial c}{\partial y} = 0 \ . \qquad (2.1.2)$$

A very important requirement for the simulation is the positivity of the solution. This means that a positive initial concentration field will remain positive during the evolution process. Especially when non-linear

photochemical reactions (1.3.3) are used in the simulation it is imperative to design a positive scheme. In the following this is made plausible. Chemical reactions usually are modelled by the equation

$$\frac{dc_i}{dt} = P_i - L_i\, c_i, \quad i = 1,\ldots,s\ , \tag{2.1.3}$$

where the time constant $\tau_i = 1/L_i$ gives an indication of the time scale on which the reaction takes place. The production term P_i and the loss term L_i are in general functions of c_j, $j = 1,\ldots,s$, and are polynomial in form. Therefore a negative concentration c_j, which is due to the numerical procedure, can strongly influence the terms P_i and L_i. If as a consequence L_i becomes negative a violent non-linear instability may occur. This, together with the usual broad spectrum of time constants in the photochemical simulation can have a disastrous effect.

Next, it is observed that the exact solution of equation (2.1) has the property of mass conservation. This is shown by integrating (2.1) over Ω, which yields

$$\frac{d}{dt}\int_{\Omega} c\,d\underline{x} = -\int_{\partial\Omega} c\ \underline{U}.\underline{n}\ ds\ . \tag{2.1.4}$$

The right hand side designates the flux of material over the boundary $\partial\Omega$ with normal $\underline{n}$.

It is recommendable to incorporate both the positiveness and the conservative properties in a numerical scheme. This objective turns out to be a very restrictive one, since only a very small class of methods satisfies these demands.

If boundary fluxes are not present, not only mass conservation results from (2.1). In fact, then there is an infinity of conservation laws. Next to conservation of moments of the concentration distribution in a uniformly moving fluid, there follow

$$\frac{d}{dt}\int_{\Omega} c^m d\underline{x} = 0, \quad m\varepsilon IN\ . \tag{2.1.5}$$

This is a consequence of the very strong property of conservation of form in a uniform velocity field. For, in this case the solution of equation (2.1) with initial condition $c(x,y,o) = c_o(x,y)$ simply is

$$c(x,y,t) = c_o(x - {}_o\int^t U dt,\ y - {}_o\int^t V dt) \ . \qquad (2.1.6)$$

This in turn demonstrates a special Lagrangian solution of (2.1), which states that the material derivative Dc/Dt is zero, or c is constant along a characteristic defined by dx/dt=U and dy/dt=V. A more fundamental treatment can be found in Whitham (1974).

In numerical schemes it is impossible to satisfy (2.1.6), except for special, often trivial cases. However, the relations that are described in this section are very useful to measure the performance of a particular method.

2.2 Numerical properties

Within the scope of this report it is not possible to deal with all the elementary implications of numerical schemes. Comprehensive accounts on this subject are found in Richtmyer and Morton (1967), Roache (1976) and Peyret and Taylor (1983). Here only some topics which are of interest to the approximation of the advection equation will be discussed.

It is found from theory that mass conservation can easily be incorporated into higher-order schemes. In general, however, these schemes produce solutions that are very dispersive (wave-like) in character, thus resulting in undesirable negative concentrations. On the other hand, it is easy to construct lower-order positive schemes. They, however, suffer in the most cases from an extensive artificial diffusion, which brings on an unacceptable (Gauss-like) smoothing of sharp gradients, such as peak concentrations. Yet, these peaks are of great interest in air quality simulation models.

This contradistinction is the basis of the theses that an "optimal" scheme in general is not the simplest one. Another point is that it is desired that the numerical scheme yields high accuracy, whilst the grid-resolution is as low as possible. Also the advection calculation effort must be in balance with the remaining parts of the simulation. Again this will introduce a certain complexity in the algorithms.

The performance of the numerical schemes can be measured by observing in test situations the time evolution of moments, the conservation of peak values, gradients and other criteria that were described in the foregoing section. For the tests criteria will be defined in an exact manner in the

following section.

Intimately related to the performance is the numerical stability of a scheme, which is expressed in the Courant number $\gamma = U\Delta t/\Delta x$ by

$$| \gamma | \leq \alpha \ . \qquad (2.2.1)$$

Here Δx is the spatial mesh size. Formula (2.2.1) actually indicates the possibility to transfer information among neighbouring gridpoints. Implicit schemes often yield $\alpha=\infty$. Not only (2.2.1) determines the effectiveness of a scheme. Also the accuracy imposes restrictions on the timestep Δt (Praagman (1979)), which can render implicit schemes less effective than (2.2.1) suggests.

A complicating, but important issue is the fact that the simulation is organized on a limited area. This makes it necessary to specify boundary conditions.
For inflow boundaries c is prescribed. Outflow boundaries are treated differently by each method. If they are not designed carefully, high wavenumber oscillations may reflect at the numerical outflow boundaries and spoil the solution or even jeopardize the stability of the method (Trefethen (1985)).

Furthermore it can be remarked that the method of fractional steps from section 1.3 allows for a sub-factorization of the advection step (1.3.1) by

$$\frac{\partial c}{\partial t} + \frac{\partial Uc}{\partial x} = 0 \ , \qquad (2.2.2a)$$

$$\frac{\partial c}{\partial t} + \frac{\partial Vc}{\partial y} = 0 \ . \qquad (2.2.2b)$$

Or, in terms of the numerical operators N,

$$N_a = (N_a)_y \, (N_a)_x \ . \qquad (2.2.3)$$

Some methods actually employ (2.2.2) and therefore only the analysis of a one-dimensional numerical scheme is necessary. The greater number of methods that are tested here are true multi-dimensional methods, thus diminishing the error that is involved in the operator splitting.

Finally, in some situations one may consider the use of a non-equidistant grid. One situation is encountered when the input data is irregularly distributed over the domain Ω. A second occasion arises when a local refinement of the mesh is desired.
The last case can be treated by means of introducing a nested grid, but both cases can be handled in a flexible way by the finite element method of which an account is given in Strang and Fix (1973).
Here methods on an equidistant grid, or on grids that are topologically equivalent to it are dealt with only.

2.3 Advection schemes, testproblems and criteria

The many advection schemes, that have been developed until today can be subdivided into two fundamental classes, namely the class of Eulerian methods, where the solution is found relative to a fixed grid and the class of Lagrangian methods, where the solution is traced along local characteristics. When the underlaying mathematical methodology is taken as a reference, it is possible to make the following classification: finite difference, spectral, variational, particle-in-cell and non-classified methods. A specimen of each will here be encountered.

In the framework of this comparison study a starting point is the outcome of previous comparison studies. The best methods have been selected from these studies to be investigated on one computer and with identical sets of testproblems and criteria. Moreover, some new methods that were published in recent literature have been adopted for the comparison study.

In the following a table of methods is displayed. The first number in it denotes the section in which a résumé is found, which is, whenever necessary, supplemented with indications concerning the technical implementation. Next the name of the method, an acronym and a reference are given. In this report the features of most concern are presented. A separate report on each method is issued which contains a more detailed exposition of the outcome of the testproblems. The number in square brackets refers to these reports and can be found in the list of references.
The methods are

2.4 The pseudo-spectral method, PS/DH, De Haan (1981), [1],
PS/CP, Christensen and Prahm (1976), [1].

2.5 The second moment method, SM, Long and Pepper (1981), [2].

2.6 A chapeau function method, CF, Chock (1985), [3].

2.7 A multi-dimensional positive advection transport algorithm, MPAT, Smolarkiewicz (1984), [4],

2.8 A multi-dimensional flux-corrected transport algorithm, MFCT, Schere (1983), [5].

2.9 A particle method, PM, Praagman (1986), [6].

Four problems have been selected to test the quality of the afore mentioned methods. All methods are capable of handling smooth concentration fields, without sharp gradients, quite well. Therefore the testproblems have been directed toward a number of important phenomena that proved to be difficult in practice. For all the testproblems an exact solution is present.

T1 Sharp gradients and boundary crossing.

a. To obtain an impression of the performance of the inflow boundaries a local block-concentration

$$c_o(x,y) = 1 \quad \text{for } (x,y) \in B,$$
$$= 0 \quad \text{for } (x,y) \in \Omega \backslash B$$

is defined, with $\Omega = [0,L] \times [0,L]$ and B by

$$B = \{ (x,y) \;/\; i_1 \Delta x \leq x \leq i_2 \Delta x,\ j_1 \Delta y \leq y \leq j_2 \Delta y \} .$$

In this test $L = N_x \Delta x = N_y \Delta y = 320000$, where N_x and N_y are the number of intervals in x- and y-direction, resp. and the velocities are $U = V = 20000/3600$ m/sec. The initial condition is $c(x,y,0)$ 0. The block-concentration is enforced by the boundary conditions. The exact result is shown in figure 2.3.1a.

b. An impression of the action on sharp gradients by the numerical method under consideration is obtained by starting with the block-

concentration c_o in the middle of Ω and by applying the velocity field of T1-a. Subsequently the effect of the outflow-boundary implementation is tested when the block goes outside of the domain Ω, see figure 2.3.1b.

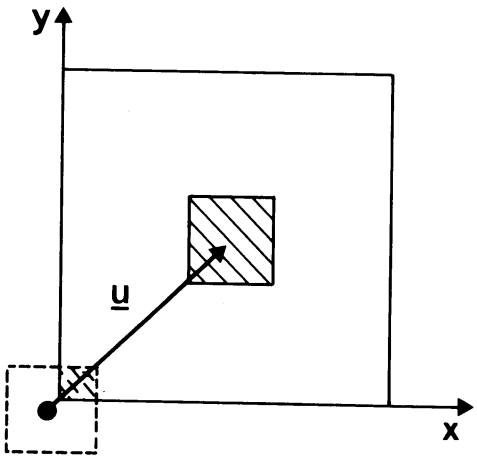

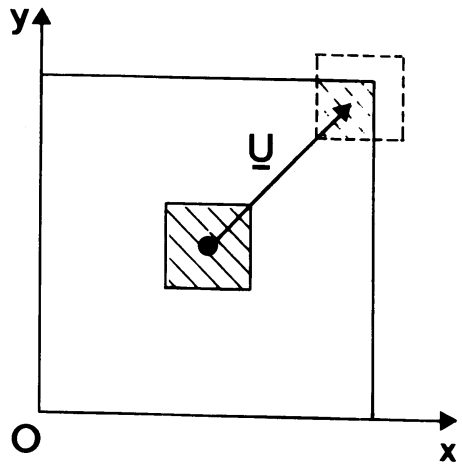

Figure 2.3.1a.

b.

T2 A local concentration in a rotating windfield (the "Molenkamp" test).

This standard test, first mentioned by Molenkamp (1968), is very instructive, since it combines a simple solution with a non-cartesian windfield.

In a windfield that is uniformly rotating with angular velocity $\underline{\omega} = \omega \underline{e}_z$, the advection equation (2.1) yields in polar coordinates (r,ϕ)

$$\frac{\partial c}{\partial t} + \omega \frac{\partial c}{\partial \phi} = 0 \ , \qquad (2.3.1)$$

which has as a solution

$$c(r,\phi,t) = c_o(r,\phi-\omega t) \ . \qquad (2.3.2)$$

The initial concentration here is chosen to be

$$c_o(r,\phi) = \begin{cases} A \cos^2 \left(\frac{\pi}{2L} \| \underline{x}-\underline{x}_o \| \right) & \text{if} \quad \| \underline{x}-\underline{x}_o \| \leq L \\ 0 & \text{in the rest of } \Omega. \end{cases}$$

The parameters have the values

$L = 3\ N_x\ \Delta x/16$, $\underline{x}_o = [\ N_x\ \Delta x/4,\ 0\ ]^t$,

$\omega = 2\pi\ /\ (6*3600)$, $N_x\ \Delta x = N_x\ \Delta y = 320000$,

N_x = number of intervals in the x and y direction. The origin is at the centre of Ω.

In figure 2.3.2 the Molenkamp test is depicted.

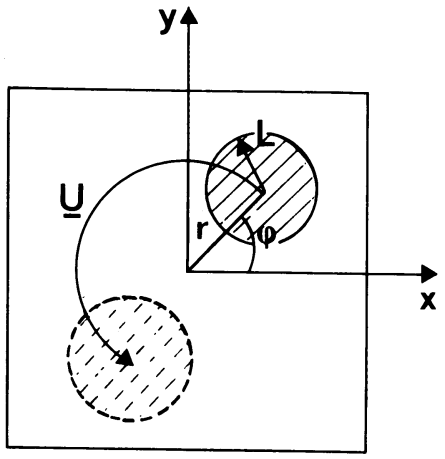

Figure 2.3.2

T3 A source term test.

Until here the source term in (1.3.1) remained undiscussed. This test, however, gives a possibility to measure the performance of the implementation of the source term.

In this test the windfield is assumed to be constant and in the positive x-direction. Define a time-independent source term to be

$$S(x,y,t) = \begin{cases} g(x) & \text{if } x_0 < x < x_1, \\ 0 & \text{elsewhere.} \end{cases} \qquad (2.3.3)$$

For a zero initial condition the advection equation yields as a solution with forcing (2.3.3)

$$c(x,y,t) = \frac{1}{U} \int_{x-Ut}^{x} g(\xi)\, d\xi\ . \qquad (2.3.4)$$

If $g(x) = c_o/\tau$, with c_o and τ constant, $x_{min} = \min\ (x_o+Ut, x_1)$ and $x_{max} = \max\ (x_0+Ut, x_1)$ then (2.3.4) yields for $t \geq 0$ the trapezoidal solution

$$\frac{c(x,y,t)}{c_o} U_\tau = \begin{cases} 0 & \text{for } x \leq x_0 \text{ or } x \geq x_1 + Ut \,, \\ x - x_o & \text{for } x_o < x < x_{min} \,, \\ x_{min} - x_o & \text{for } x_{min} < x < x_{max} \,, \\ x_1 + Ut - x & \text{for } x_{max} < x < x_1 + Ut \,. \end{cases} \qquad (2.3.5)$$

After some time the source is switched off, so that the trapezoid will travel towards the outflow boundary.

This situation is displayed in figure 2.3.3. Of course this test can be used in a Molenkamp version by interchanging x with ϕ.

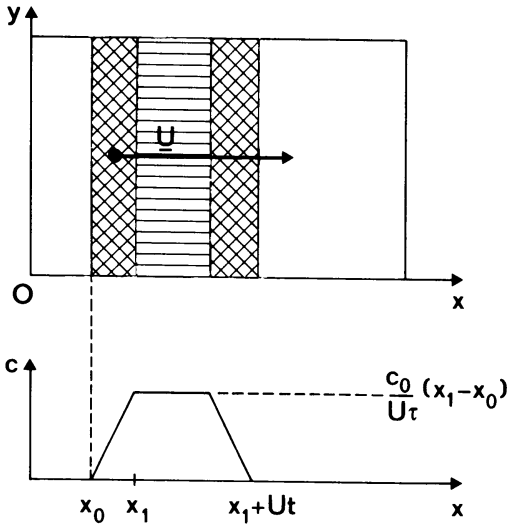

Figure 2.3.3 The source term test.

To determine the magnitude of the deviations of the numerical solution to the advection equation (2.1) for a testproblem with respect to the exact solution, objective criteria must be introduced. To this end property (2.1.6) is utilized, i.e. the form of a concentration distribution in a uniform flow field is conserved. This includes that parameters which are related to the shape of the distribution, such as e.g. the mean, the variance or the kurtosis, but also the moments from (2.1.5) are potential criteria.
Here a number of illustrative criteria are used. These are

C1 The detailed impression of the shape during its evolution, by inspection of contour plots and three dimensional plots.

C2 Peak conservation: $\max_{x_i,y_j} c_{ij}^n$,

C3 Negative concentrations: $\min_{x_i,y_j} c_{ij}^n$,

C4 Mass conservation: $\sum_{i,j} c_{ij}^n$,

C5 Norms. If N is the number of gridpoints, then

- mean absolute error (ℓ_1 norm): $\frac{1}{N} \sum_{i,j} | c_{ij}^n - c(x_i,y_j,t_n) |$,

- mean quadratic error (ℓ_2 norm): $(\frac{1}{N} \sum_{i,j} [c_{ij}^n - c(x_i,y_j,t_n)]^2)^{\frac{1}{2}}$,

- maximum absolute error (ℓ_∞ norm): $\max_{i,j} | c_{ij}^n - c(x_i,y_j,t_n) |$.

C6 Two special criteria for the Molenkamp test T2. These are in polar-coordinates the conservation of the radius r_o and the angle deviation $\Delta\phi_o$ of the centre of mass of the cosine distribution.

To get a normalized impression the criteria have been taken relative to the exact solution.

2.4 The pseudospectral method

The first pseudospectral model with emphasis on practical application for atmospheric computations was introduced by Christensen and Prahm (1976). They showed that, compared to finite difference methods, this method has a high resolution and yields a numerical solution within an a priori prescribed tolerance in less computing time and with less storage requirements. In this report the pseudospectral method is considered in connection with the method of fractional steps (2.2.2), hence only the one-dimensional algorithm will be outlined.

Consider the segment [0,L], and define collocation points

$$x_j = (j-1).\Delta x;\ j = 1,\ldots,N;\ \Delta x = \frac{L}{N-1} \qquad (2.4.1)$$

Expand $c(x_j,t)$ in the following Fourier series

$$c(x_j,t) = \sum_{k=-(N-3)/2}^{(N-1)/2} A(k,t) \cdot \exp\left(\frac{2\pi i}{L} kx_j\right) , \qquad (2.4.2)$$

$$j = 1,\ldots,N-1 \ (N-1 \text{ even}) ,$$

where the Fourier transform of $c(x_j,t)$ is defined by

$$A(k,t) = (N-1)^{-1} \cdot \sum_{j=1}^{N-1} c(x_j,t) \cdot \exp\left(-\frac{2\pi i}{L} kx_j\right) , \qquad (2.4.3)$$

$$k = -\frac{N-3}{2},\ldots,\frac{N-1}{2} .$$

From this definition it follows that $c(x_j,t)$ is periodic in the sense that

$$c(x_j,t) = c(x_{j+N-1},t) .$$

Let the function $\bar{c}(x,t)$ be defined by

$$\bar{c}(x,t) = \sum_{k=-(N-3)/2}^{(N-1)/2} A(k,t) \cdot \exp\left(\frac{2\pi i}{L} kx\right) ,$$

where the coefficients $A(k,t)$ are defined by (2.4.3), and interpret this function as an approximation to $c(x,t)$. Note that in the collocation points $\bar{c}(x_j,t) = c(x_j,t)$. Then, in the collocation points, the space derivative $\frac{\partial c}{\partial x}(x_j,t)$ can be calculated, and formally,

$$\frac{\partial c}{\partial x}(x_j,t) = \frac{\partial \bar{c}}{\partial x}(x_j,t) = \sum_k \frac{2\pi i}{L} k \cdot A(k,t) \cdot \exp\left(\frac{2\pi i}{L} kx_j\right) . \qquad (2.4.4)$$

The procedure of expanding a function at collocation points in a finite series and taking formal derivatives as outlined is known as collocation. The rationale for such a procedure is that in between the collocation points the approximating function and its derivatives are supposed to be close to the exact solution.

One could proceed now by calculating

$$\frac{dc}{dt}(x_j,t) = \sum_k \frac{dA(k,t)}{dt} \cdot \exp\left(\frac{2\pi i}{L} kx_j\right)$$

in order to derive for constant U the (full) spectral method

$$\frac{dA(k,t)}{dt} = -\frac{2\pi i}{L} k\, U\, A(k,t)$$

which constitutes a set of N-1 ordinary differential equations; $k = -(N-3)/2,\ldots,(N-1)/2$. In the pseudospectral method such a procedure is not followed, but instead the time derivative is taken in "physical" space by an RK4 method, while the space derivative is calculated in the "spectral" space to which the collocation functions belong. This procedure makes it possible to handle a varying velocity field U(x,y) without for the full spectral method resolving the convolution, which is due to the product of U and c. Moreover, the boundary conditions are easily incorporated in the pseudospectral method. In fact one may choose an arbitrary set of collocation functions, e.g. Chebychev polynomials, at suitable collocation points x_j, instead of the Fourier series expansion. The reasons for using Fourier series expansion are that the set of collocation points form an equidistant grid and that fast Fourier-transform algorithms are available (Cooley and Tukey, 1965), which make it possible to compute the space derivatives in a modest amount of time. However, the Fourier series expansion presupposes periodicity of the solution $c(x_j,t)$ which will almost never be the case in realistic problems.

Christensen and Prahm resolve the periodicity problem by sacrificing some outer grid points. They let the concentration decay exponentially there whenever these constitute an outflow boundary, in order that the concentration flowing out will not flow in at the opposite boundary. The decay rate is chosen such that $\frac{\partial c}{\partial t} = -U\frac{\partial c}{\partial x} - \frac{c}{\tau} \approx 0$, and $\frac{\partial c}{\partial x} \approx -\frac{c}{\Delta x}$, i.e. each passage of a grid cell the concentration drops by a factor of about e^{-1}. So, $\tau = \frac{\Delta x}{U}$ is chosen.

De Haan (1981) resolves the periodicity problem by the following procedure. Let the concentration c(x,t) at any time t_n be given and consider the decomposition

$$c(x,t_n) = p(x) + q(x) ,$$

where p(x) is a $(m+1)^{th}$-order polynomial such that

$$q(0) = q(L) = 0$$

and

$$q^{(i)}(0) = q^{(i)}(L), \quad i = 1,\ldots m$$

i: i^{th} derivative, i.e. q is periodic up to and including its m^{th} derivative. The derivative of p can be found exactly. This procedure seems

mathematically rigorous: the only parameter involved is the "degree of periodicity" m which cannot exceed N-2 (Gottlieb and Orszag (1977)).

Both methods have been implemented. The time integration is performed by using a 4^{th} order Runge-Kutta procedure, which allows for a maximum Courant number $\gamma = \sqrt{8}/\pi$ (Procedure De Haan) or $\gamma \approx 0.89$ (procedure Christensen and Prahm; see [1]).

The following is concluded:

- storage requirements are minimal, i.e. one array per concentration field and 6 local help arrays;
- reasonable errors at lower grid resolutions (compared with the other methods) are to be expected;
- measures have to be taken because of the periodicity of the collocation functions.

2.5 The second moment method

The basic problem in finding a solution of the advection equation (2.1) is to design a numerical scheme that retains as much information as possible on a relative coarse grid, while some predefined restrictions are satisfied. If the positiveness and mass-conservation of the solution are considered as essential restrictions, then it is natural to look for a Lagrangian approach. One way of retaining as much information as possible is to adopt a procedure that describes information of sub-grid scale details.

Egan and Mahoney (1971) combined these elements in an algorithm which is called the Second Moment Method (SMM). This method makes it possible to realize the description of sub-grid information by the introduction of structure functions. In each grid-cell the concentration distribution is approximated by a rectangular profile, which has the property that it can completely be fixed in one space dimension by three local moments. These are a mass C, a mean F and a width R. This has as a consequence that rectangular concentration distributions, which are usually difficult to approximate with analytical methods, can be described exactly. However, in return, the cost that has to be faced is that for each quantity that is to be advected three fields must be retained in memory.

Evolution formulas for the higher moments are obtained from their definitions together with the properties of the advection equation (2.1). After each timestep Egan and Mahoney recalculate the advected distribution

onto a fixed Eulerian grid. This makes their method a quasi-Lagrangian method (Roache (1976)).

In the following the procedure will be given for a more accessible advection equation with one space dimension. The treatment for two spatial dimensions will be indicated. The technical procedure for this case can be found in [2].

For the numerical discretization of the advection equation (2.2.2a), a mesh is introduced on which cells of width Δx are situated around the nodes x_m, $m = 0,\ldots,M$, see fig. 2.5.1.
A local cell-oriented coordinate $\xi = (x-x_m) / \Delta x$ is used in the definitions for the structure functions. The mass in cell m is:

$$C_m = \frac{1}{\Delta x} \int_{x_m-\frac{1}{2}\Delta x}^{x_m+\frac{1}{2}\Delta x} c(x)\, dx = \int_{-\frac{1}{2}}^{\frac{1}{2}} \bar{C}(\xi)\, d\xi \ . \qquad (2.5.1)$$

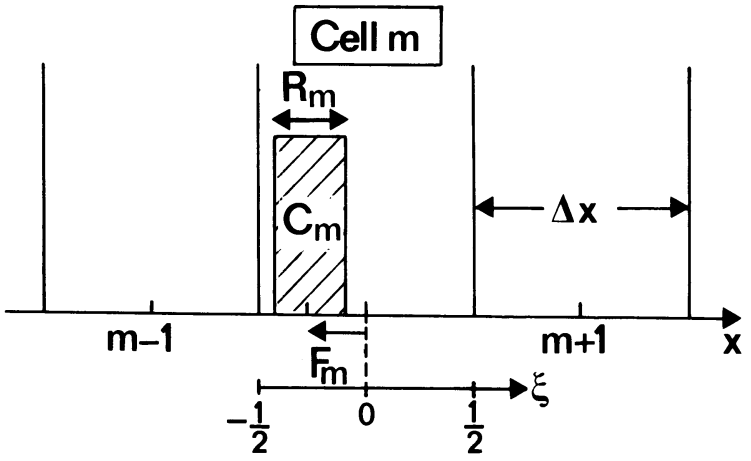

Figure 2.5.1 Grid definition

The dimensionless mean F and width R have as definition

$$F_m = \frac{1}{C_m} \int_{-\frac{1}{2}}^{\frac{1}{2}} \xi\, \bar{C}(\xi)\, d\xi \ , \qquad (2.5.2)$$

$$R_m^2 = \frac{12}{C_m} \int_{-\frac{1}{2}}^{\frac{1}{2}} (\xi-F_m)^2\, \bar{C}(\xi)\, d\xi \ . \qquad (2.5.3)$$

The factor 12 in the last definition is chosen, since then the interpretation of R_m is just the width of the rectangular distribution as indicated in fig. 2.5.1.

The evolution parameter in the advection process is the Courant number $\gamma_m = U(x_m)\Delta t/\Delta x$. In one timestep Δt the rectangular profile C_m will

be displaced with γ_m. If the transport is taking place over cell boundaries (fig. 2.5.2), new local structure functions are found from the part a that is advected into cell m and the part r that remains there (see fig. 2.5.3) with the formulas (2.5.1) - (2.5.3).

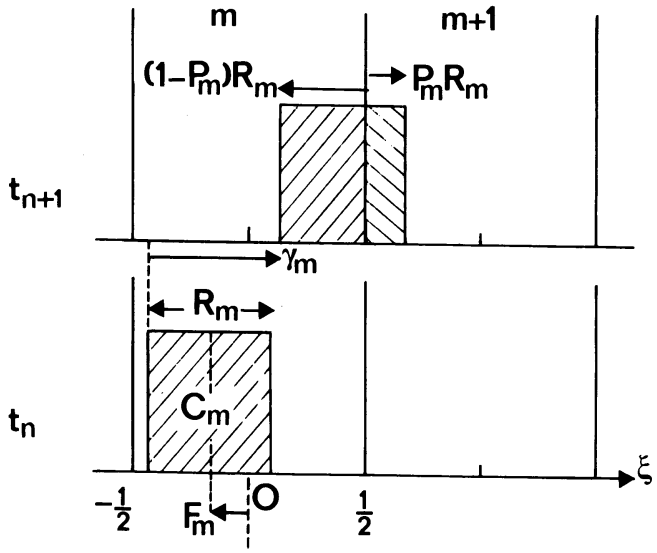

Figure 2.5.2 Transport over cell boundaries

These yield

$$C_m^{n+1} = \sum_{i=a,r} C_i \,, \tag{2.5.4}$$

$$C_m^{n+1} F_m^{n+1} = \sum_{i=a,r} C_i F_i \,, \tag{2.5.5}$$

$$C_m^{n+1} (R_m^{n+1})^2 = \sum_{i=a,r} C_i [R_i^2 + 12F_i^2] - 12C_m^{n+1} (F_m^{n+1})^2 \,. \tag{2.5.6}$$

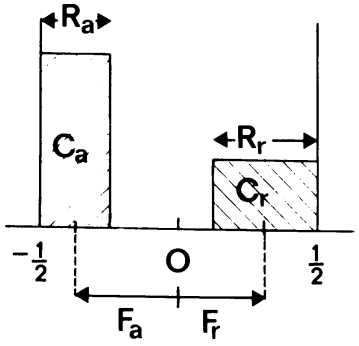

Figure 2.5.3 The definition of the advected (a) and remaining (r) parts

This formulation (Pedersen and Prahm (1974)) allows for the local advection of concentration and therefore it admits a method of calculating

the sums in a way that is customary in finite element techniques. This is particularly useful in two dimensional problems.

To complete the definition of the advection over a timestep, expressions must be found for C_i, F_i and R_i i=r,a in relation to C^n, F^n and R^n. Here a proportionality parameter P_m is used as a measure of crossing a boundary. Its definition is displayed in figure 2.5.2, which shows (dropping the index m) that

$$R\,P = \text{sign}\,(\gamma)\,(F+\gamma) + \tfrac{1}{2}R - \tfrac{1}{2}\ . \qquad (2.5.7)$$

If $P_m \leq 0$ then all mass will remain in cell m, if $P_m \geq 1$ then all mass is transported to a neighbouring cell, depending on the sign of γ_m, otherwise only a part is advected into a neighbouring cell. The rules that determine the structure functions depend on P, and can be found in Egan and Mahoney and in [2].

From the formulation it is seen that (2.5.4) in fact is an upwind method and that the formulas (2.5.5) and (2.5.6) each add a correction in the shape. This is also shown in figure 2.5.4. Fig. 2.5.4(a) displays three consecutive steps with the method (2.5.4) and a uniform Courant number of = 0.4. Fig. 2.5.4(b) shows the influence of the first moment (2.5.5), whereas fig. 2.5.4(c) shows the advection making use of the full SMM.

The present method is unconditionally stable. However, since in the actual implementation there is no provision for advection beyond one grid cell, a practical limiting condition is

$$|\,\gamma\,| \leq 1\ . \qquad (2.5.8)$$

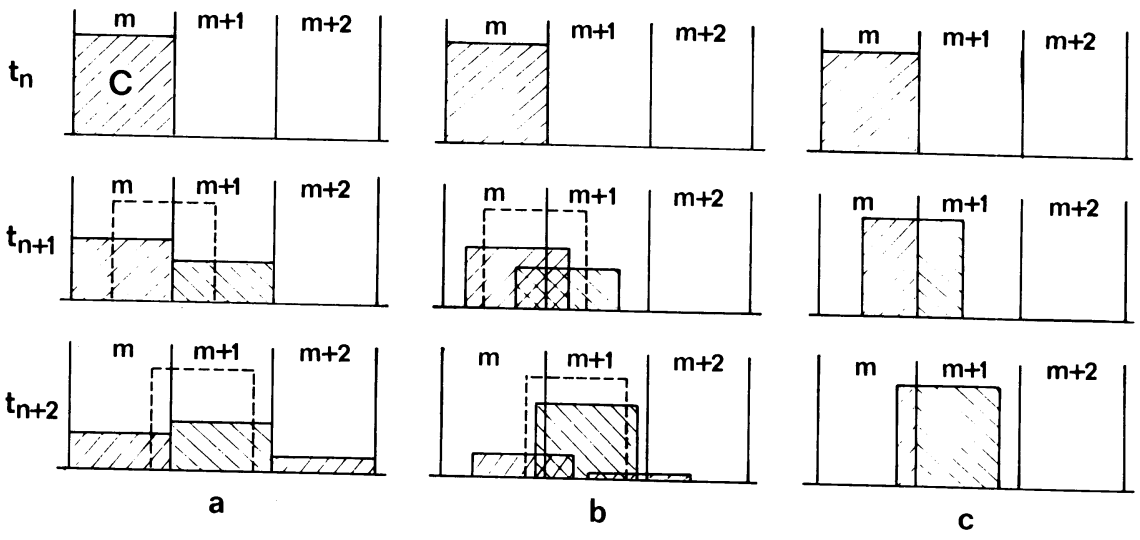

Figure 2.5.4 An initially rectangular concentration distribution advected to the right in three sequential time steps with $\gamma = 0.4$. Dashed distribution corresponds to transport by continuum advection. (a) A simple Upwind method (Eq. (2.5.4)). (b) A difference scheme using reconstruction with the first moment of the concentration distribution. (c) A difference scheme using the reconstruction with first and second moments. (Egan and Mahoney (1971)).

Although the Second Moment Method for an advection equation with two spatial dimensions is formulated in a similar way, the complexity of the method increases. This is due to the fact that there are more outflow possibilities from a two-dimensional cell to its neighbours. One such situation is shown in fig. 2.5.5.

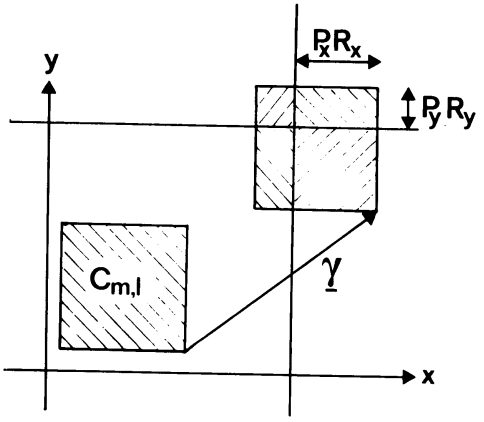

Figure 2.5.5 Transport in two dimensions

Moreover, now five fields need to be retained in memory to describe the entire structure. The limiting condition becomes

$$\max_{m,l} \left(|\gamma_x|, |\gamma_y| \right) \leq 1 \qquad (2.5.9)$$

where γ_x and γ_y are the local cartesian Courant number in x- and y-directions, resp. In [2] the technical details of the method in two dimensions are described.

The following can be concluded from the theory.
The method

- is quasi-Lagrangian,
- is positive and mass-conserving,
- describes rectangular distributions in a constant linear flow field in an exact way,
- allows for sub-grid details, which enables a local treatment of chemical reactions.

There are, however, also a number of disadvantages.

- For the full SMM approximation of each concentration field five arrays are necessary. For the implementation five help arrays are needed.
- In a non-linear velocity field the quasi-Lagrangian basis of the method causes numerical diffusion.

2.6 A chapeau function method

In their comparison studies, Chock and Dunker (1983) and Chock (1985) find that a particular chapeau function method, namely the foreward-Euler time integration method coupled with a balancing diffusion term is superior to the other methods they tested. For the two-dimensional advection equation the method of fractional steps of Yanenko (1971) is used and therefore only a one-dimensional method description will be sufficient in the following.

The method starts from the observation that the unconditional unstable foreward-Euler, centered space method can be stabilized by introducing a balancing diffusion term. This is also the basis of the highly dispersive, second order Lax-Wendroff method. If a Taylor expansion at (x_i, t_n) for one time step Δt is combined with the advection equation

$$\frac{\partial c}{\partial t} = L\, c\ , \qquad L\ .\ = -\frac{\partial}{\partial x}(U\ .)\ , \tag{2.6.1}$$

one obtains

$$c^{n+1} = c^n + \Delta t\, L\, c^n + \tfrac{1}{2}\Delta t^2\, L^2\, c^n + O(\Delta t^3)\ . \tag{2.6.2}$$

Here the quadratic term at the r.h.s. is the balancing diffusion term, and the time dependence of L is neglected.
Next, the concentration is approximated by a linear combination of basis functions $\phi_j(x)$, which are piecewise linear on elements e_j, continuous and triangular shaped and satisfy $\phi_j(x_i) = \delta_{ij}$, see fig. 2.6.1.

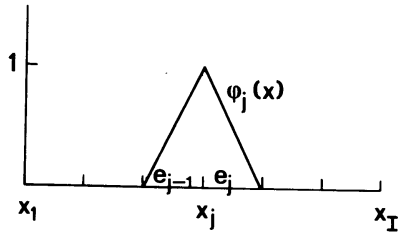

Figure 2.6.1 Chapeau function definition

This yields

$$c^n(x) = \sum_j c_j^n\, \phi_j(x)\ . \tag{2.6.3}$$

Next the method of Galerkin, as described in Strang and Fix (1973) is used. This yields the matrix equation

$$M\,(\underline{c}^{n+1} - \underline{c}^n) = S\,\underline{c}^n\ , \tag{2.6.4}$$

where $\underline{c}^n$ is the vector with elements c_j^n. At interior gridpoints the mass-matrix M and the stiffness-matrix S have as a definition:

$$M_{ij} = \int \phi_i\, \phi_j\, dx\ , \tag{2.6.5}$$

$$S_{ij} = \Delta t \int \left[\, U\, \phi_j \frac{\partial \phi_i}{\partial x} - \tfrac{1}{2}\,\Delta t\, U \frac{\partial \phi_i}{\partial x}\frac{\partial U \phi_j}{\partial x}\,\right] dx\ . \tag{2.6.6}$$

For the hyperbolic (linear) part an inflow boundary is necessary. For the elliptic term the boundary conditions are chosen to be

$$\frac{\partial Uc}{\partial x}(x_1) = \frac{\partial Uc}{\partial x}(x_I) = 0\ , \tag{2.6.7}$$

so that there will be no artificial diffusive flux across the boundaries.

Elaboration of (2.6.4) - (2.6.6) for an internal point x_i on an equidistant grid results in

$$\frac{\Delta x}{6}\left[(c_{i-1}^{n+1} - c_{i-1}^{n}) + 4\,(c_i^{n+1} - c_i^{n}) + (c_{i+1}^{n+1} - c_{i+1}^{n}) \right] =$$

$$= \tfrac{1}{2}\Delta t \left[U_{i-\frac{1}{2}}\, c_{i-1}^{n} + (U_{i-\frac{1}{2}} - U_{i+\frac{1}{2}})\, c_i^{n} - U_{i+\frac{1}{2}}\, c_{i+1}^{n} \right] +$$

$$+ \tfrac{1}{2}\frac{\Delta t^2}{\Delta x}\left[U_{i-\frac{1}{2}}^2\, c_{i-1}^{n} - (U_{i-\frac{1}{2}}^2 + U_{i+\frac{1}{2}}^2)\, c_i^{n} + U_{i+\frac{1}{2}}^2\, c_{i+1}^{n} \right] . \qquad (2.6.8)$$

The velocities at the r.h.s. are to be taken at t_n. In the evaluation the velocity was considered constant over an element e_j and represented by its mid-element value.

It should be noted that in every time-step a set of equations with coefficient matrix M from (2.6.4) must be solved. However, since M is a constant, diagonally dominant matrix, only once an LU decomposition is to be performed. It is also possible to avoid the matrix inversion by lumping the off-diagonal elements with the diagonal elements. Gresho et al. (1978), however, showed that this could highly compromise the accuracy of the numerical solution. In this context this problem is directly shown by (2.6.8) which after lumping becomes a very dispersive Lax-Wendroff scheme.

A more precise impression of the scheme (2.6.8) can be obtained by inspecting the phase and amplification properties in time. This can be done by means of the normal mode solution $c(x,t) = \exp i(\alpha x - \omega t)$. The dispersion relation of the original equation (2.6.1) reads

$$\omega = \alpha U \qquad (2.6.10)$$

A measure for amplification over a time-step Δt is the factor

$$\xi = \exp(-i\,\omega\Delta t) ,$$

which in the exact case (2.6.10) can be written as

$$\xi = \exp(-i\,\gamma\theta) . \qquad (2.6.11)$$

Here $\gamma = U\,\Delta t/\Delta x$ is the Courant number and $\theta = \alpha\Delta x$ the wavenumber. The numerical scheme (2.6.8), however, is only an approximation to (2.6.11), which yields

$$\xi = 1 + 3\gamma \{ \gamma (\cos\theta - 1) - i \sin\theta \} / (2 + \cos\theta) . \qquad (2.6.12)$$

A comparison of (2.6.12) with (2.6.11) is shown in figure 2.6.2a, where ξ is shown in the complex plane as function of θ, $0 \leq \theta \leq \pi$ and γ as a parameter. The amplification $|\xi|$ is given in fig. 2.6.2b, whereas in fig. 2.6.2c $(\arg \xi)/\gamma$ is depicted. In the exact case these quantities plot for all values of γ on the heavy lines.
Similar plots are displayed in figure 2.6.3 for the lumped scheme, which has as amplification factor

$$\xi = 1 - 2\gamma^2 \sin^2 (\tfrac{1}{2}\theta) - i \gamma \sin\theta . \qquad (2.6.13)$$

Although both methods are formally of second order it is concluded that both the amplification and the phase properties of the full scheme (2.6.8) are superior. This must be paid since the stability interval is considerably less. For stability it is needed that $|\xi| \leq 1$, which yields $|\gamma| \leq 1$ for the lumped scheme (2.6.13). However, in the case of method (2.6.4) the matrix $M^{-1}S+I$ is governing the stability. Using (2.6.12) it turns out that only

$$|\gamma| \leq \sqrt{3}/3 \doteq 0.577 \qquad (2.6.14)$$

is allowed.

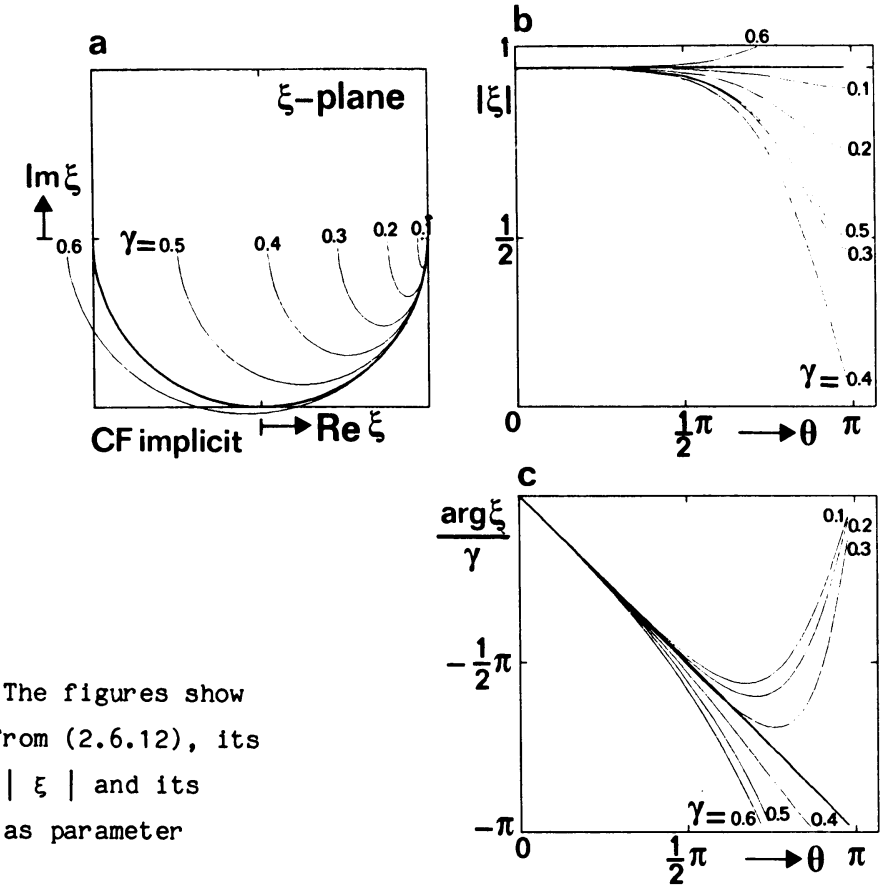

Figure 2.6.2 The figures show the factor ξ from (2.6.12), its amplification | ξ | and its phase, with γ as parameter

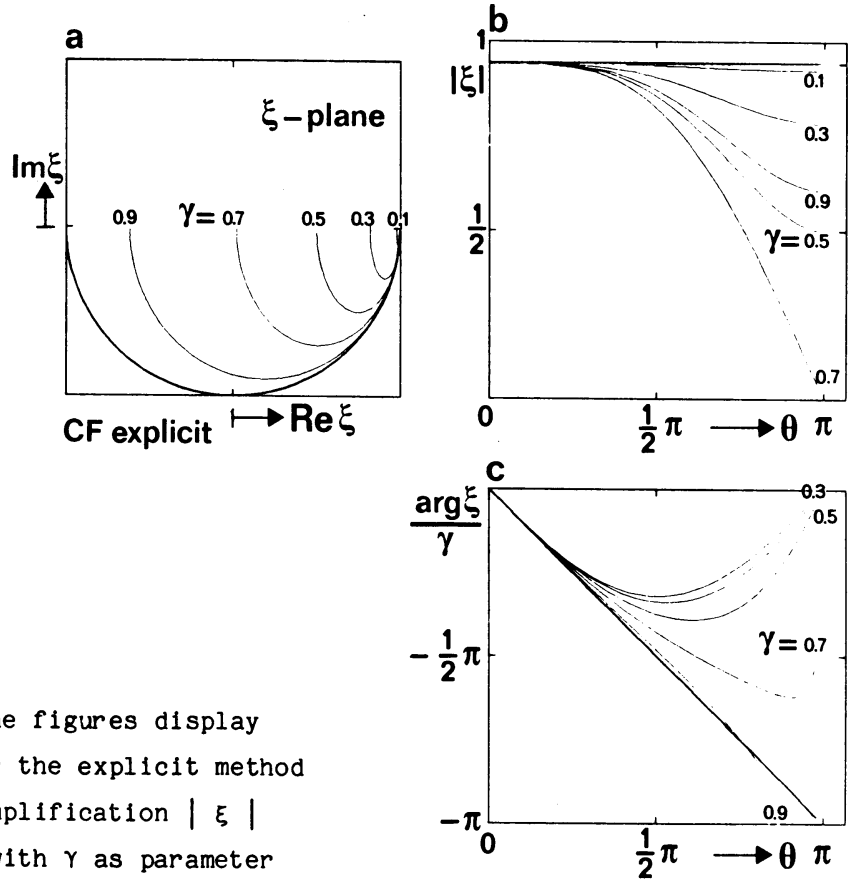

Figure 2.6.3 The figures display the factor ξ for the explicit method (2.6.13), its amplification | ξ | and its phase, with γ as parameter

Since a fractional step method is employed, (2.6.14) holds for both cartesian courant numbers γ_x and γ_y.

Although the method (2.6.8) is not as dispersive as the lumped version: a Lax-Wendroff type method, still a small amount of $2\Delta x$-ripples occurs as a consequence of phase errors. Sometimes this leads to unacceptable negative concentrations. One way of diminishing the influence of the high wavenumbers is by filtering them out. Many (non-linear) filters have been designed in the past years mainly for effectively removing computational noise from steep gradient solutions (e.g. Boris and Book (1976), Van Leer (1979), Spekreyse (1986)). Chock (1985) chooses the simple, ad-hoc filter of Forester (1977) to handle this problem. This non-linear filter selectively smoothens out $2m\Delta x$-ripples by applying a local smoothing operator, without suppressing a possible peak value significantly, if this peak region is sufficiently smooth.
The Forester filter is defined as follows

$$c_i^{n+1,k+1} = c_i^{n+1,k} + \tfrac{1}{2}\kappa \left[\Delta c_{i+\frac{1}{2}}^{n+1,k} \left(\mu_i^k + \mu_{i+1}^k\right) - \Delta c_{i-\frac{1}{2}}^{n+1,k} \left(\mu_i^k + \mu_{i-1}^k\right)\right] ,$$

$$k = 0,1,2,\ldots,K . \qquad (2.6.15)$$

where the index k is an iteration index, $\kappa < \frac{1}{2}$ is a diffusion coefficient and μ_i is a mesh parameter, which is set to zero for all values of i before each iteration. Further variables in this filter are

$$\Delta c_{i+\frac{1}{2}} = c_{i+1} - c_i , \quad S_{i+1} = \text{sign}\left(\Delta c_{i+\frac{1}{2}}\right) . \qquad (2.6.16)$$

By means of the sign function it is possible to detect $2m\Delta x$-ripples in the following way. If $S_j \neq S_{j+1}$ for a particular j, a local extremum is present. To see whether it is a true extremum, $S_{j-m},\ldots,S_j$ must have the same sign whereas $S_{j+1},\ldots,S_{j+m+1}$ are all required to have the opposite sign. If this condition is not fulfilled, then all μ_i are reset to 1 in the interval with the nodes j-m to j+m. If the sign condition holds, there is a true local extremum and the filtering process can be continued at x_{j+m}. In principle the selective smoothing can be repeated several times. Here the values that were found to be optimal by Chock (1985) are adopted: $\kappa = 0.1$ and $m = 1$ for filtering $2\Delta x$-waves and the number of iterations $k = 1$. A property of the Forester filter is that mass-conservation is not affected if the basis functions in the finite element approximation are linear.

For this method it can be concluded that

- the storage requirements are minimal, i.e. one array per concentration field, and for the implementation one help array,
- the explicit method (with mass-matrix lumping) is highly dispersive in character. The implicit method reduces this phenomenon substantially. The non-linear noise filter of Forester makes it a viable method for air-pollution simulation purposes,
- the finite-element approach makes the method flexible. However, since the fractional step method is applied, only areas that are topologically equivalent to a square can be treated.

2.7 A multi-dimensional positive advection transport algorithm

A few years ago Smolarkiewicz (1983, 1984) proposed a positive advection scheme with small implicit diffusion. His scheme is based on the upwind scheme, but this seems not to be essential: it may be based on any positive scheme for which an analytic expression, containing second order space derivatives, of the local discretization error is available. This second order term is considered to be the space derivative of a, so called, diffusive flux which is expressed as product of a diffusive velocity and the concentration.

In one dimension and for the upwind scheme the second order local discretization error is

$$\tfrac{1}{2} \frac{\partial}{\partial x} \left(|U| \, \Delta x - U^2 \, \Delta t \right) \frac{\partial c}{\partial x} \, . \tag{2.7.1}$$

The diffusive velocity then is defined to be

$$U_D = \begin{cases} -\tfrac{1}{2} \left(|U| \, \Delta x - U^2 \, \Delta t \right) \frac{1}{c} \frac{\partial c}{\partial x} & 0<c \\ 0 & 0=c \end{cases} \tag{2.7.2}$$

(In fact, whenever c=0, the only requirement for U_D is that it be finite.) The solution $\tilde{c}$ that is found after an upwind scheme step may be considered to obey the differential equation

$$\frac{\partial \tilde{c}}{\partial t} = - \left(U + U_D \right) \frac{\partial \tilde{c}}{\partial x} \, . \tag{2.7.3}$$

In order to restore the solution it is proposed to succeed the upwind scheme time step by a restauration step using the velocity field $-U_D$. Of course, this step suffers the same local error, and a second diffusive

velocity field (based on $\tilde{c}$ and $-U_D$) may be found to take another restauration step, and so on. In practice, after 3 or 4 restauration steps no essential improvement will be found anymore. Positiveness of the upwind scheme ensures positiveness of the correction scheme provided a sufficient small Courant number is taken.

For two dimensions one may apply this procedure for each direction separately, based on the concept of factorisation. Results show that it is more favourable to apply a real two-dimensional scheme, because then the cross-derivative terms $\partial^2 c/\partial x \partial y$ can be taken into account. The two-dimensional diffusive velocity field (U_D, V_D) then is defined by

$$U_D = -\tfrac{1}{2} \left(|U|\,\Delta x - U^2\,\Delta t\right) \frac{1}{c}\frac{\partial c}{\partial x} + \tfrac{1}{2}\,UV\Delta t\,\frac{1}{c}\frac{\partial c}{\partial y}$$

$$V_D = -\tfrac{1}{2} \left(|V|\,\Delta y - V^2\,\Delta t\right) \frac{1}{c}\frac{\partial c}{\partial y} + \tfrac{1}{2}\,UV\Delta t\,\frac{1}{c}\frac{\partial c}{\partial x}\,. \qquad (2.7.4)$$

For one dimension it is proved that, whenever the velocity field is defined on a staggered grid, the Courant number $\gamma = U\,\Delta t/\Delta x$ should satisfy $|\gamma| \leq 1$, and for 2 dimensions $|\gamma| = \max\left(|\gamma_x|, |\gamma_y|\right) \leq 2-\sqrt{2}$ (Smolarkiewicz (1984)). The calculation of the diffusive wind field on a staggered grid is done by an appropriate averaging procedure. For ease of computation, extra boundary points $(x_0, x_{N+1}, y_0, y_{N+1})$ are assumed in order to compute U_D and V_D. At an outflow boundary $\partial c/\partial n = 0$ is taken (Smolarkiewicz reports that a more obvious choice $\partial^2 c/\partial n^2 = 0$ results in non-positivity of the scheme!).

It is concluded that this method

- is positive and mass conserving;
- has minimal storage requirements: one array per concentration field (however, one concentration help array and two velocity help arrays are needed in a restauration step);
- in every restauration step costs the calculation of the diffusive wind velocity field and an upwind time step.

2.8 A multi-dimensional flux-corrected transport algorithm

A decade ago a new numerical method for solving the advection equation originated. This method starts from the flux equation

$$\frac{\partial c}{\partial t} + \frac{\partial f}{\partial x} = 0 \qquad (2.8.1)$$

and writes the discrete approximation in the form

$$c_i^{n+1} = c_i^n - \frac{\Delta t}{\Delta x_i} \left[F_{i+\frac{1}{2}} - F_{i-\frac{1}{2}} \right] . \qquad (2.8.2)$$

Here c and f are the concentration and the advective flux, resp., which are defined at the spatial grid points x_i and at the time t_n. The approximation F to the flux f is defined on a staggered grid. The way in which this approximation is realized determines the spatial behaviour of the scheme (2.8.2). It is well known that lower order schemes, like upstream or donor-cell, produce an extensive numerical diffusion. On the other hand, higher order schemes introduce high-wavenumber ripples, also called spurious oscillations, that cause unwanted negative concentrations.

The flux-corrected transport (FCT) method SHASTA of Boris and Book (1973) was the first to combine a low-order and a high-order scheme in such a way that the spurious oscillations are eliminated but still profits from the high-order accuracy. This is done by performing a non-linear weighing of the transportive fluxes of both schemes, and is called "flux-limiting" or "flux-correction".

Nowadays there are many investigations where this idea is used, see Van Leer (1979), Spekreyse (1986), Roe (1986). Zalesak (1979) devised a formal procedure for the FCT algorithm. This will be given below for an advection equation with two spatial dimensions, i.e.

$$\frac{\partial c}{\partial t} + \frac{\partial f}{\partial x} + \frac{\partial g}{\partial y} = 0 . \qquad (2.8.3)$$

The finite difference approximation becomes in this case

$$c_{ij}^{n+1} = c_{ij}^n - \frac{\Delta t}{\Delta V} \left[\left(F_{i+\frac{1}{2},j} - F_{i-\frac{1}{2},j} \right) \Delta y + \left(G_{i,j+\frac{1}{2}} - G_{i,j-\frac{1}{2}} \right) \Delta x \right] . \qquad (2.8.4)$$

Here $\Delta V = \Delta x \, \Delta y$ is an area element, centered at the grid point (i,j). The transportive fluxes F and G are defined as in figure 2.8.1.

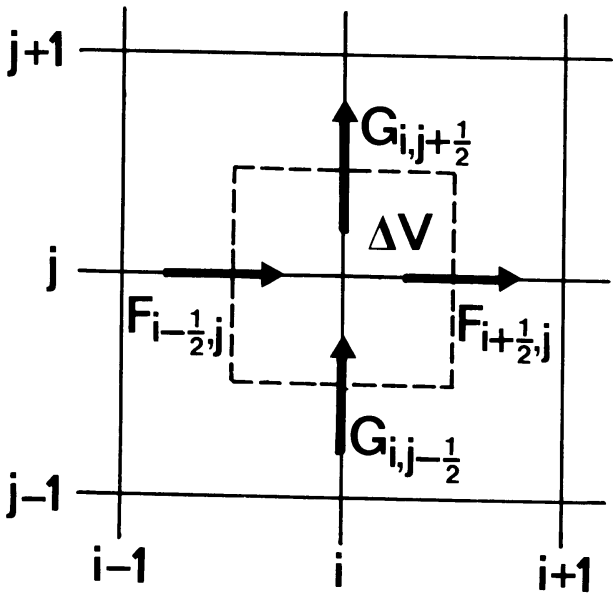

Figure 2.8.1
Definition of the fluxes

Between the square brackets in (2.8.4) the change of mass per unit time in ΔV is denoted, as is usual in finite volume methods (Peyret and Taylor (1983)).

The formal procedure is arranged into six points.

(1) Compute transportive fluxes F^L and G^L by some low-order scheme that guarantees to give monotonic and positive results for the problem.

(2) Compute the transportive fluxes F^H and G^H by some high-order scheme.

(3) Define the "antidiffusive fluxes"

$$A_{i+\frac{1}{2},j} = F^H_{i+\frac{1}{2},j} - F^L_{i+\frac{1}{2},j}$$

$$A_{i,j+\frac{1}{2}} = G^H_{i,j+\frac{1}{2}} - G^L_{i,j+\frac{1}{2}}$$

(4) Compute the low-order time advanced, "transported and diffused" solution c^{td} with (2.8.4), making use of F^L and G^L from step (1).

(5) Limit the antidiffusive fluxes, such that c^{n+1} as computed in step (6) is free of spurious oscillations:

$$\tilde{A}_{i+\frac{1}{2},j} = \mu_{i+\frac{1}{2},j} A_{i+\frac{1}{2},j}, \quad 0 \leq \mu_{i+\frac{1}{2},j} \leq 1,$$

$$\tilde{A}_{i,j+\frac{1}{2}} = \mu_{i,j+\frac{1}{2}} A_{i,j+\frac{1}{2}}, \quad 0 \leq \mu_{i,j+\frac{1}{2}} \leq 1.$$

(6) Apply the limited antidiffusive fluxes:

$$c_{ij}^{n+1} = c_{ij}^{td} - \frac{\Delta t}{\Delta V} \left[(\tilde{A}_{i+\frac{1}{2},j} - \tilde{A}_{i-\frac{1}{2},j}) \Delta y + (\tilde{A}_{i,j+\frac{1}{2}} - \tilde{A}_{i,j-\frac{1}{2}}) \Delta x \right] .$$

The most crucial step in the above procedure is the proper design of the flux-limiter μ. This is also the step where hybridization techniques differ. The choice $\mu = 1$ would result in time-advancement with the high-order scheme.

Here the method of Zalesak (1979) will be followed. The low-order fluxes are defined by the donor-cell method (Roache (1976)), given by

$$\begin{aligned} F^{L}_{i+\frac{1}{2},j} &= U_{i+\frac{1}{2},j}\, c^{dc}_{i+\frac{1}{2},j} , \\ U_{i+\frac{1}{2},j} &= \tfrac{1}{2} (U^{n}_{ij} + U^{n}_{i+1,j}) , \\ c^{dc}_{i+\frac{1}{2},j} &= \begin{cases} c^{n}_{ij} & \text{if } U_{i+\frac{1}{2},j} \geq 0 , \\ c^{n}_{i+1,j} & \text{if } U_{i+\frac{1}{2},j} < 0 . \end{cases} \end{aligned} \qquad (2.8.5)$$

Similar expressions are obtained for G^{L}.

The high-order fluxes are generated by means of the "ZIP" flux concept of Hirt (1968), see also Zalesak (1981). A fourth order ZIP transportive flux, written in one-dimensional form (dropping the index j) is

$$F^{H}_{i+\frac{1}{2}} = \frac{2}{3} \left[U_{i+1} c_{i} + U_{i} c_{i+1} \right] - \frac{1}{12} \left[U_{i+1} c_{i-1} + U_{i+2} c_{i} + U_{i-1} c_{i+1} + U_{i} c_{i+2} \right] . \qquad (2.8.6a)$$

At the boundaries a second order ZIP flux is implemented, which has the form

$$F^{H}_{i+\frac{1}{2}} = \tfrac{1}{2} \left[U_{i+1} c_{i} + U_{i} c_{i+1} \right] \qquad (2.8.6b)$$

Next the special form of the limiter in step (5) which Zalesak uses for his Multidimensional-FCT algorithm, will be reproduced here without the subtle reasoning that is given in Zalesak (1979). Some intermediate quantities are needed for the limiter. These are the fluxes P and Q and their ratio R. Moreover, the later to be defined c^{max} and c^{min} are used to

set bounds to c^{n+1}. The mass that flows into ΔV as a consequence of the antidiffusive fluxes is given by P^+_{ij}, see figure 2.8.1. The expression is

$$P^+_{ij} = [\ \max(0, A_{i-\frac{1}{2},j}) - \min(0, A_{i+\frac{1}{2},j})\ ]\ \Delta y + \\ + [\ \max(0, A_{i,j-\frac{1}{2}}) - \min(0, A_{i,j+\frac{1}{2}})\ ]\ \Delta x\ . \qquad (2.8.7)$$

The allowed increase in mass in ΔV per unit time is

$$Q^+_{ij} = \frac{\Delta V}{\Delta t}\ [\ c^{max}_{ij} - c^{td}_{ij}\ ]\ . \qquad (2.8.8)$$

Their ratio is

$$R^+_{ij} = \begin{cases} \min(1,\ Q^+_{ij} / P^+_{ij}) & \text{if} \quad P^+_{ij} > 0\ , \\ 0 & \text{if} \quad P^+_{ij} = 0\ , \end{cases} \qquad (2.8.9)$$

Similar quantities are introduced for the sum of the masses that flow away from ΔV, caused by the antidiffusive fluxes:

$$P^-_{ij} = [\ \max(0, A_{i+\frac{1}{2},j}) - \min(0, A_{i-\frac{1}{2},j})\ ]\ \Delta y + \\ + [\ \max(0, A_{i,j+\frac{1}{2}}) - \min(0, A_{i,j-\frac{1}{2}})\ ]\ \Delta x\ , \qquad (2.8.10)$$

$$Q^-_{ij} = \frac{\Delta V}{\Delta t}\ [\ c^{td}_{ij} - c^{min}_{ij}\ ]\ , \qquad (2.8.11)$$

$$R^-_{ij} = \begin{cases} \min(1,\ Q^-_{ij} / P^-_{ij}) & \text{if} \quad P^-_{ij} > 0\ , \\ 0 & \text{if} \quad P^-_{ij} = 0\ . \end{cases} \qquad (2.8.12)$$

The bounds on c are defined by,

$$c^a_{ij} = \max(c^n_{ij},\ c^{td}_{ij})\ ,$$

$$c^{max}_{ij} = \max(c^a_{i-1,j},\ c^a_{ij},\ c^a_{i+1,j},\ c^a_{i,j-1},\ c^a_{i,j+1})\ , \qquad (2.8.13)$$

$$c^b_{ij} = \min(c^n_{ij},\ c^{td}_{ij})\ ,$$

$$c^{min}_{ij} = \min(c^b_{i-1,j},\ c^b_{ij},\ c^b_{i+1,j},\ c^b_{i,j-1},\ c^b_{i,j+1})\ . \qquad (2.8.14)$$

Finally, the limiting factors become

$$\mu_{i+\frac{1}{2},j} = \begin{cases} \min\left(R^{+}_{i+1,j},\ R^{-}_{ij}\right) & \text{if} \quad A_{i+\frac{1}{2},j} \geq 0\ , \\ \min\left(R^{+}_{ij},\ R^{-}_{i+1,j}\right) & \text{if} \quad A_{i+\frac{1}{2},j} < 0\ . \end{cases} \tag{2.8.15}$$

$$\mu_{i,j+\frac{1}{2}} = \begin{cases} \min\left(R^{+}_{i,j+1},\ R^{-}_{ij}\right) & \text{if} \quad A_{i,j+\frac{1}{2}} \geq 0\ , \\ \min\left(R^{+}_{ij},\ R^{-}_{i,j+1}\right) & \text{if} \quad A_{i,j+\frac{1}{2}} < 0\ . \end{cases} \tag{2.8.16}$$

The complexity of the above described limiter of Zalesak shows that it is an art to design a suitable limiter. At the moment the theory is still developing and phase and amplification behaviour of the scheme or the stability condition can be found only by trial and error for a problem at hand.

In the actual implementation the quantities are cell-normalized, which means that fluxes are multiplied by $\Delta t/\Delta x$ or $\Delta t/\Delta y$ and masses by $\Delta t/\Delta V$.

From the foregoing theory it can be concluded that

- the hybridization technique eliminates high-wavenumber oscillations, while still attaining a fair degree of spatial accuracy;
- the method is multi-dimensional and according to Schere (1983) has a better performance than the fractional step version SHASTA of Boris and Book (1973);
- the storage requirements are minimal, i.e. one array per concentration element and five local help arrays.

2.9 A particle method

In the particle methods the advection equation (2.1) is solved in a full Lagrangian manner. Although the method followed here is slightly different many proposals, being more or less similar, can be found in the literature (see for references Roache, 1976).

It is assumed that the velocity-vector (U,V) has been given in the nodal points on the domain of interest Ω and also that the structure of this domain being either a finite element of a finite difference grid, is

known. Using these discrete velocity nodal points, the velocity vector in each internal point is obtained by interpolation.

An initial concentration field is created by covering the whole domain of interest (see figure 2.9.1) by small squares and by assigning to each the representative amount of the species considered. Each square keeps its identity as long as it remains within Ω.

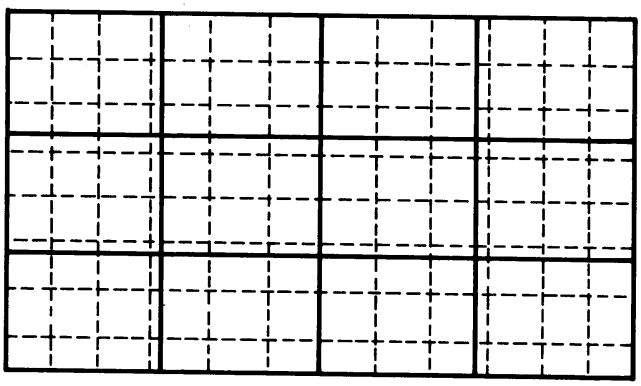

Figure 2.9.1 Ω: Eulerian grid ————————
Particle squares — — — — — —

Once the field of squares has been created the transport of each of these "particle" squares is computed by solving the ordinary differential equations:

$$\begin{cases} \dfrac{dx}{dt} = U(x,y,t), & x(t^o) = x^o \\ \dfrac{dy}{dt} = V(x,y,t), & y(t^o) = y^o \end{cases} \tag{2.9.1}$$

numerically, where (x^o, y^o) is the position of the barycenter of the square at time $t = t^o$.

The numerical solution of (2.9.1) is obtained utilizing the classical fourth order Runge-Kutta method (see Lambert (1973)). During the computational process the right hand side functions U and V are being adjusted each substep, using the interpolated values of the velocity field.

Unlike the Second Moment Method (see section 2.5) no special administration is kept in order to maintain the form of the concentration profile.

Boundaries do not cause problems for the method: at all boundary points new "particles" are being released with a specific user prescribed

concentration if there is a net discharge into Ω.

Since the classical Runge-Kutta 4 method has very good amplification and phase error properties (see also the CF method) the advection of the squares will almost be optimal and positiveness and mass conservation are guaranteed.

The specific properties of the method with respect to stability and storage requirements are:

- stability: $|\gamma| \leq \sqrt{8}$ (see Praagman (1979));

- storage: for each particle extra files are needed, which contain:
  - x resp. y coordinate of the barycenter of the square;
  - indication in which part (element) of the domain the particle is situated;
  - concentration of each of the species to be considered.

  So in total if N particles are used and s species are considered N * (s+3) positions are needed for storage.

A disadvantage of the method is encountered if the results are needed on the Eulerian grid. Several smoothing effects are present due to the fact that the concentrations are given on the squares and not in the nodal points.

2.10 Results

In this section the results of the numerical experiments are presented. The tests are performed on a VAX 11/750 computer under UNIX 4.1 operating system. In order to avoid a "lucky choice" of the Courant number, a Courant number of 0.83 times maximum possible is used with an upperbound of 0.83. The time step was chosen automatically. In the presentation the schemes have been numbered as follows.

1A Pseudo spectral (polynomial)[a,b]
1B Pseudo spectral (decay)[a,b]
2 Second moment[b]
3A Chapeau function[b]
3B Lumped chapeau function[b]
4 Smolarkiewicz (with 2 corrections)[b]
5 Multidimensional flux corrected transport[b]
6 Particles method.

The superscripts "a" and "b" stand for the spatial discretization that has been used: a = 17 x 17 nodal points, and b = 33 x 33 nodal points.

The methods are compared with respect to accuracy and non-negativity (theoretical demands) and with respect to cpu-time and storage requirements (practical demands).

For the theoretical demands each run was post-processed in order to obtain 2D- and 3D-plots of the evolution in time of the calculated concentration field. Also plots were obtained of the evolution in time of the objective criteria of section 2.3. In the latter the length of the positive vertical axis has unit 1.

For the practical demands in each run the cpu-time was monitored, while the storage requirements follow from the description of the methods in the sections 2.4 - 2.9.

In the following four sections the results of the four tests as described in section 2.3 are given. First a short examination of the results in comparison with the theoretical demands is followed by a collection of the criteria in tabulated form. Next the results are shown graphically. In section 2.10.5 the comparison with respect to the practical demands is included.

2.10.1 Molenkamp test (see figures 2.10.1 - 2.10.10)

$1A^a$ In spite of the low grid resolution there is a good accuracy. A slight negativity is introduced ($\approx 2\%$).

$1A^b$ Almost perfect. A very slight negativity is introduced ($\approx 3\,^o/_{oo}$).

$1B^a$ Less accurate than $1A^a$. $2\Delta x$ ripples are introduced. Negativity about 4%.

$1B_b$ As $1A^b$ almost perfect. Negativity $\approx 5\,^o/_{oo}$.

2 The maximum is decreasing linearly in time. The radius of the center of mass is increasing linearly in time.

3A Very good accuracy. Negativity about $1\,^o/_{oo}$.

3B A great wave train following the cosine hill with negative concentrations of about 10% is introduced.

4 In spite of 2 corrections there is serious diffusion: the maximum decreases almost linearly in time and the hill symmetry is disturbed. Adding more corrections did not result in essentially more accurate results.

5 The cosine hill form and symmetry is seriously disturbed. The profile becomes of a shock-wave type. Also, the concentration is smeared out

in directions perpendicular to the wind velocity. The radius of the centre of mass is slightly increasing.

6 The projection of the concentration to the Eulerian grid causes a projection error, which is constant, indicating that the Lagrangian method itself works perfectly well.

The results for the objective criteria are tabulated in table 1.

Table 1. Objective criteria,
Molenkamp test

	1A[a]	1A[b]	1B[a]	1B[b]	2	3A	3B	4	5	6
max	1.	1.	1.1	1.	0.7	1.	0.82	0.7	1.	0.8
min	-0.03	-0.004	-0.05	-0.007	0.	-0.001	-0.13	0.	-0.	0.
mass	1.	1.	0.75	1.	1.	1.	1.	1.	1.	1.
$\|\|_{\ell_1}$	0.15	0.	0.4	0.	0.55	0.05	0.8	0.5	0.55	0.2
$\|\|_{\ell_2}$	0.05	0.	0.3	0.002	0.45	0.05	0.5	0.4	0.55	0.15
$\|\|_{\ell_\infty}$	0.05	0.	0.4	0.02	0.45	0.05	0.5	0.4	0.8	0.15
radius	0.95	1.	0.9	1.	1.2	1.	1.	1.	1.05	1.
$\Delta\phi$	0.	0.	0.	0.	0.	0.	0.	0.	0.	0.

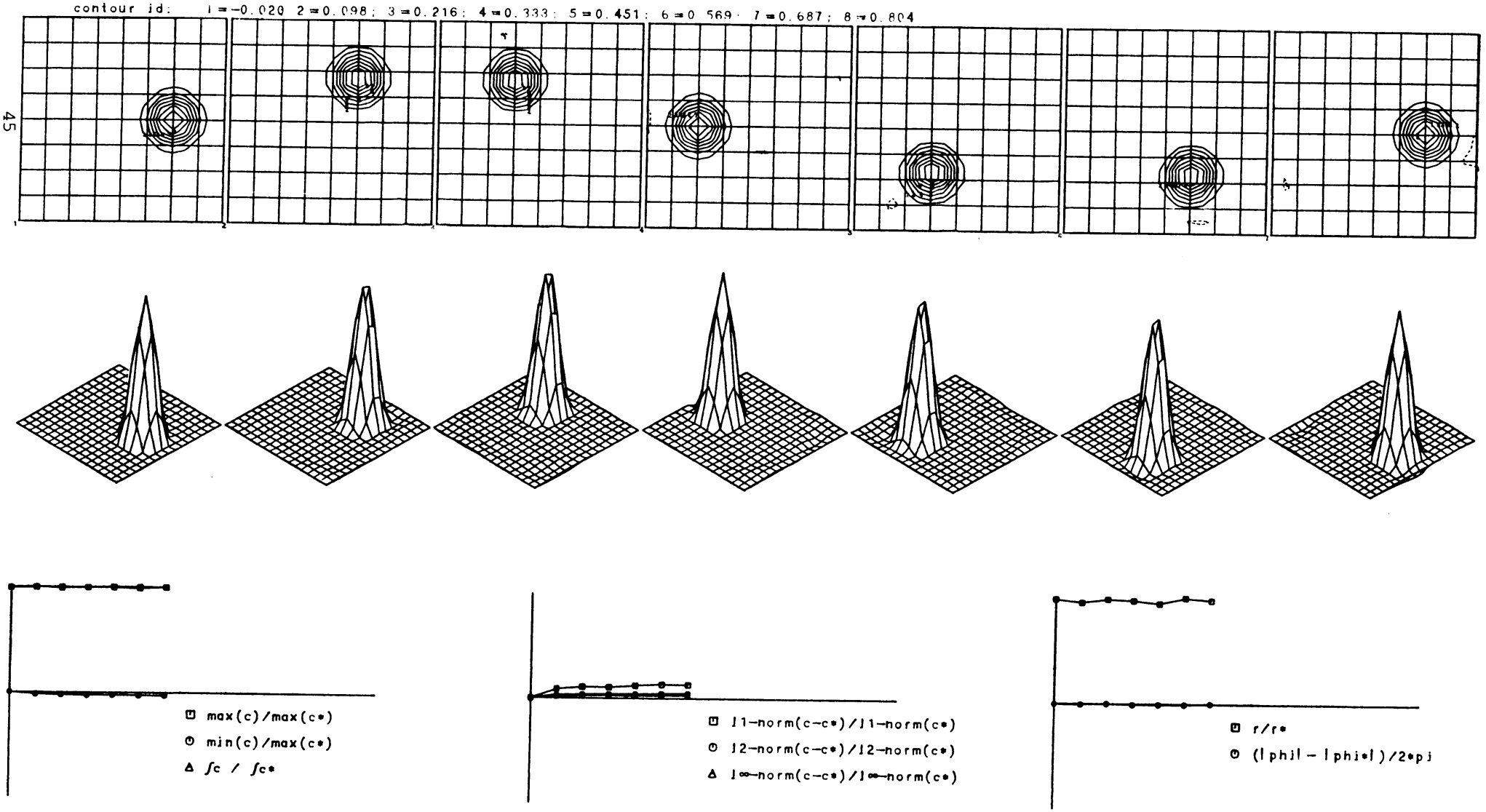

Pseudo spectral (polynomial); #points=17; Courant=.747; Molenkamp test

Figure 2.10.1

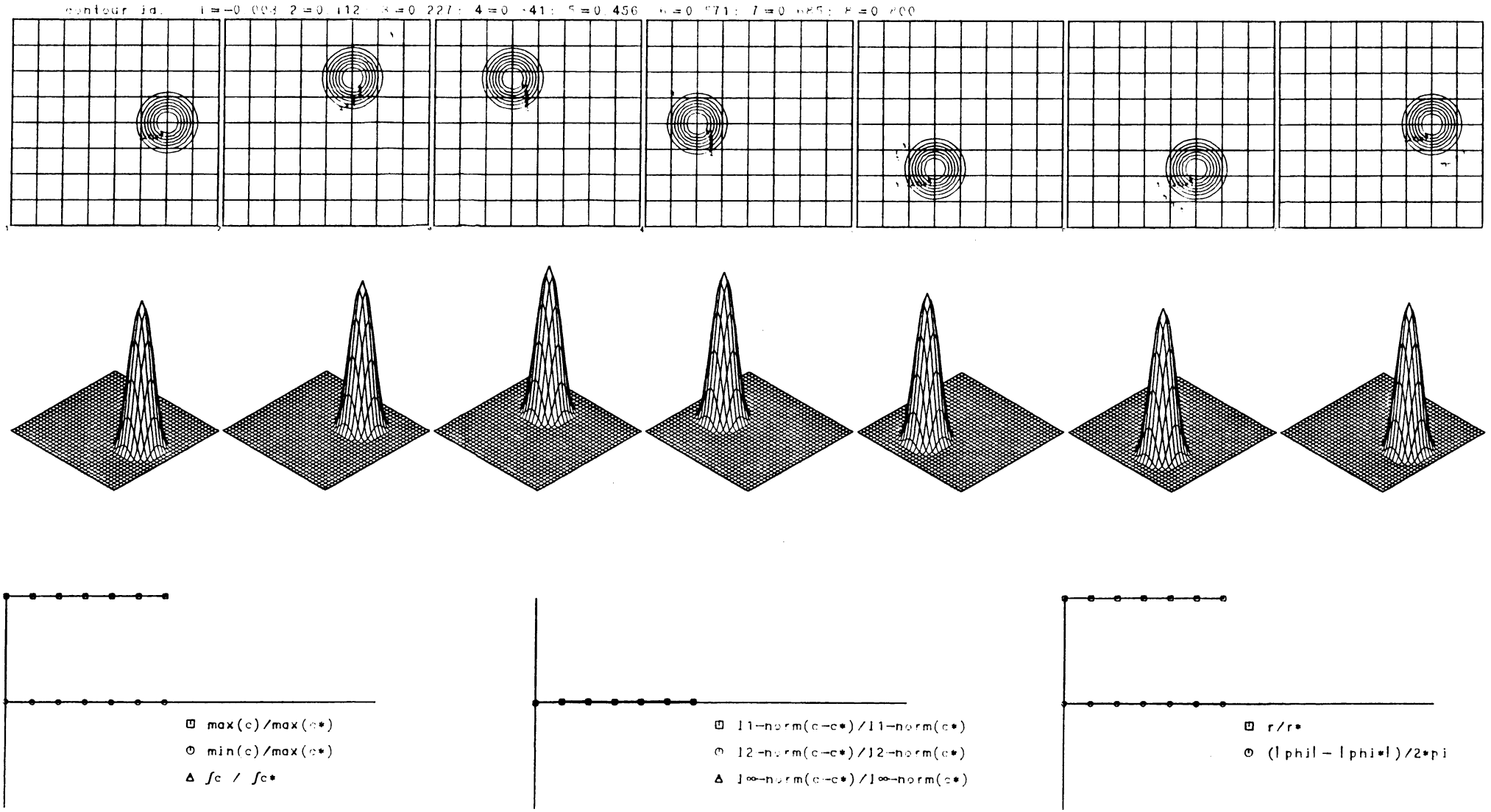

Pseudo spectral (polynomial); #points=33; Courant=.747; Molenkamp test

Figure 2.10.2

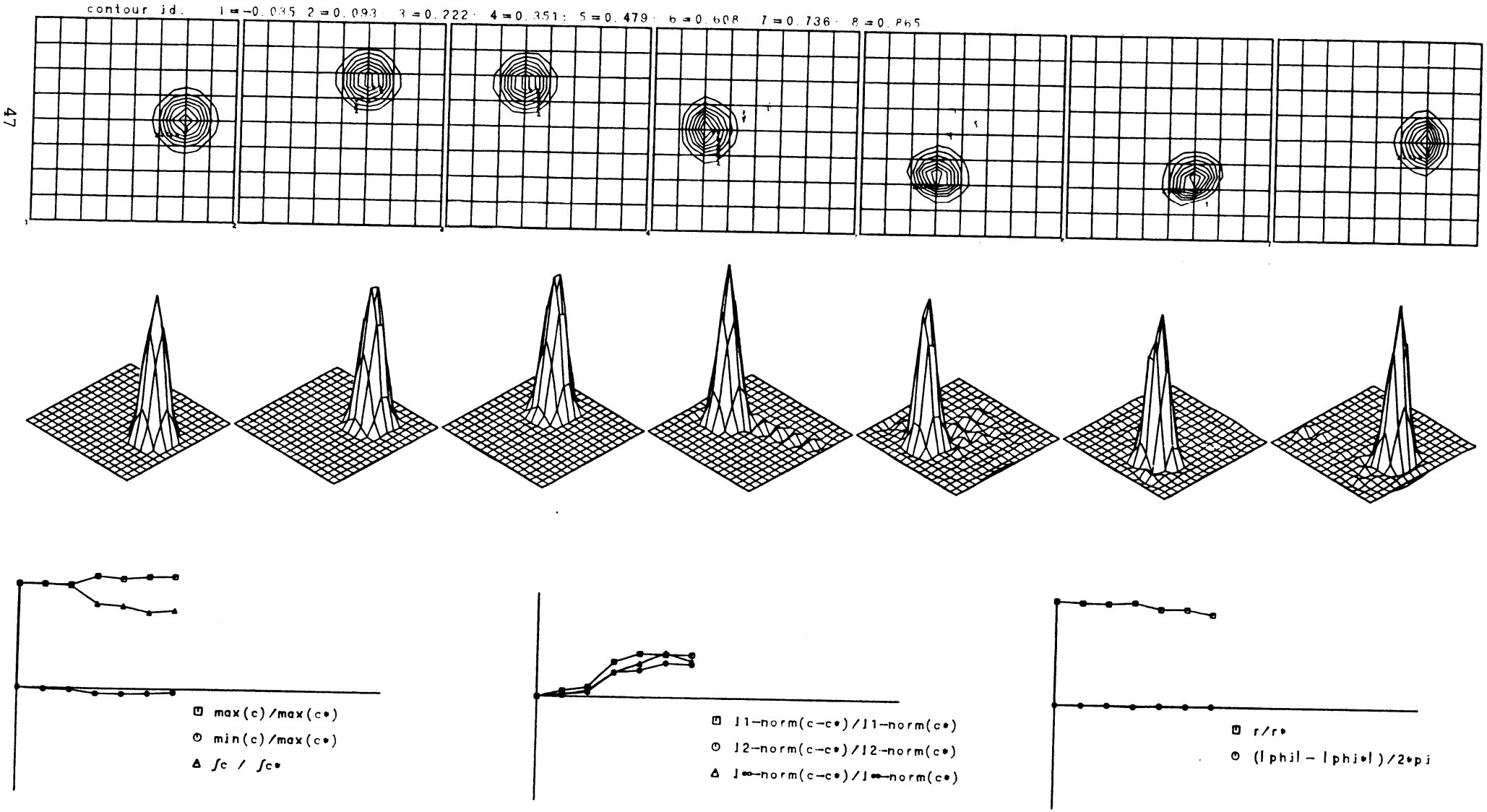

Pseudo spectral (decay); #points=17; Courant=.74; Molenkamp test

Figure 2.10.3

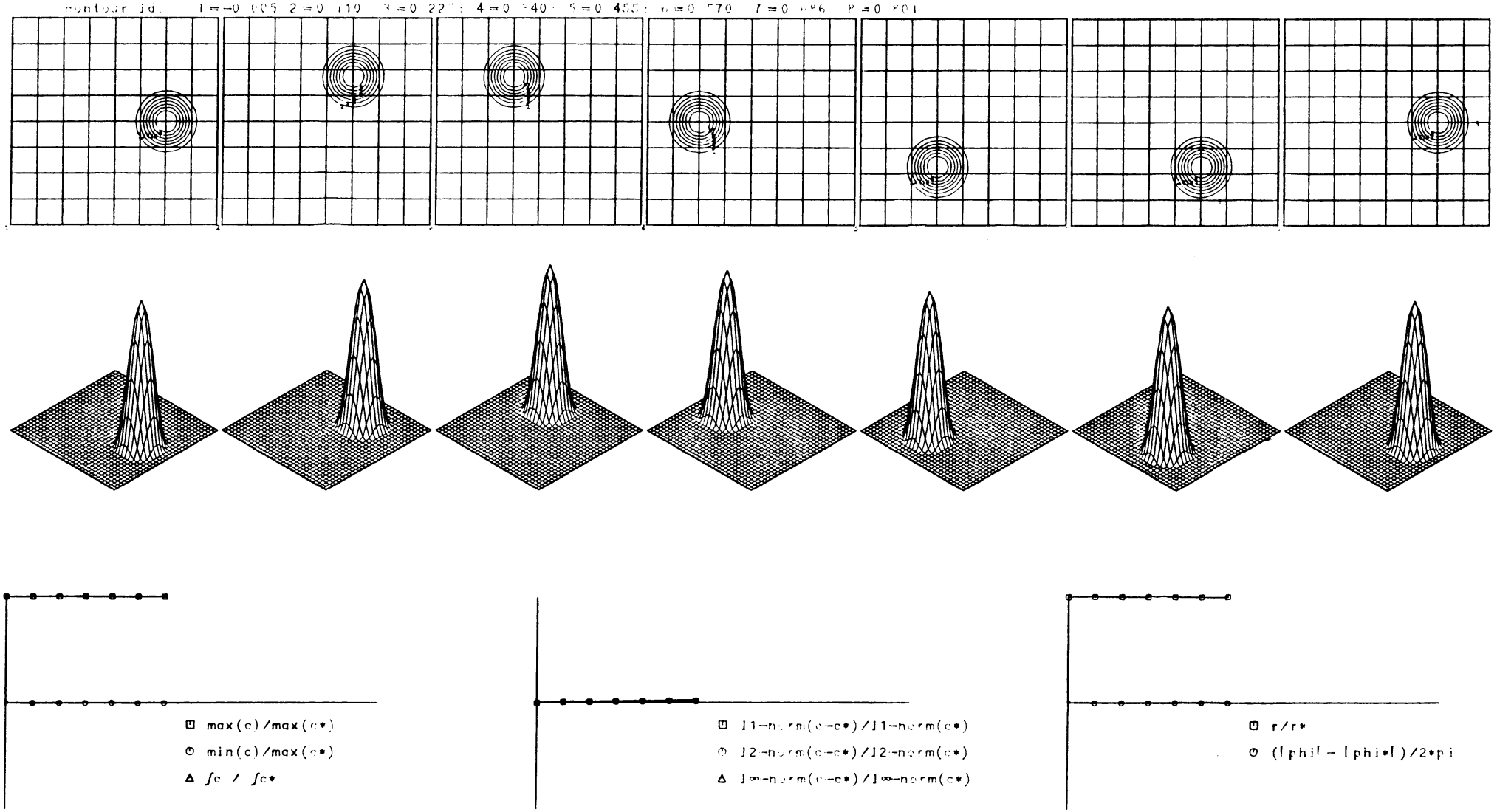

Pseudo spectral (decay): #points=33: Courant=.74: Molenkamp test

Figure 2.10.4

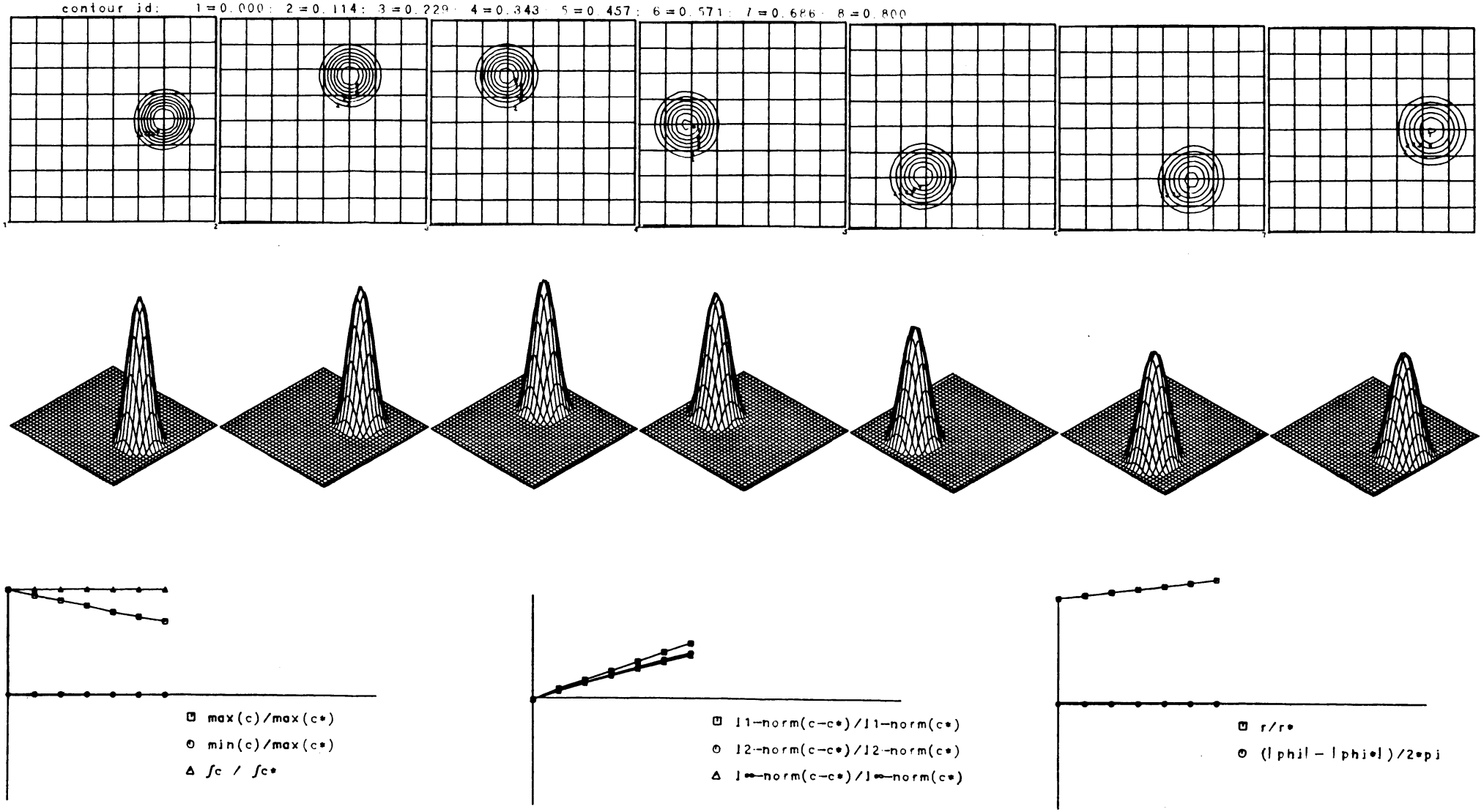

Second moment; #points=33; Courant number=0.83; Molenkamp test

Figure 2.10.5

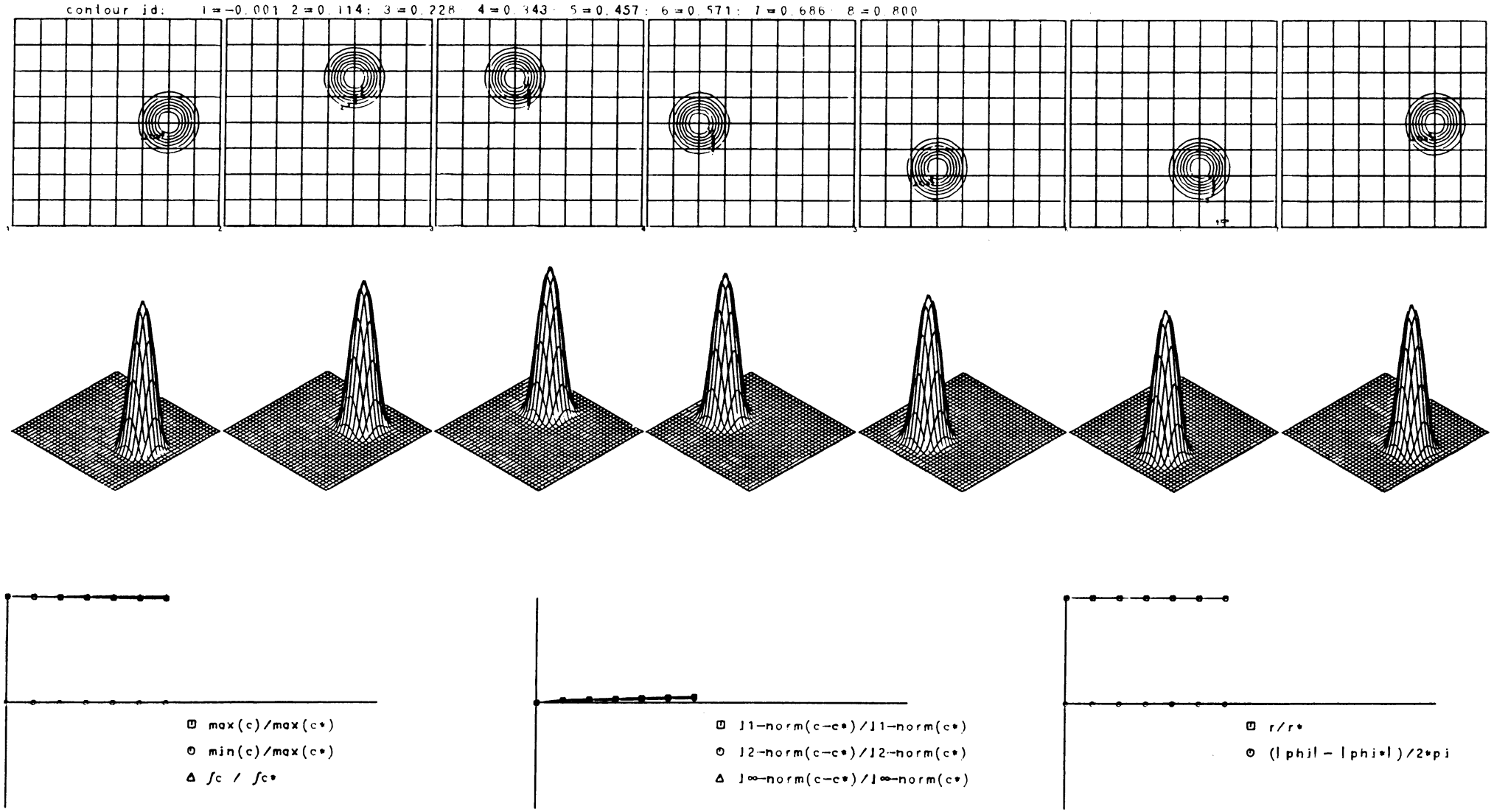

Chapeau, Forester filter: #points=33; Courant =.479; Molenkamp test

Figure 2.10.6

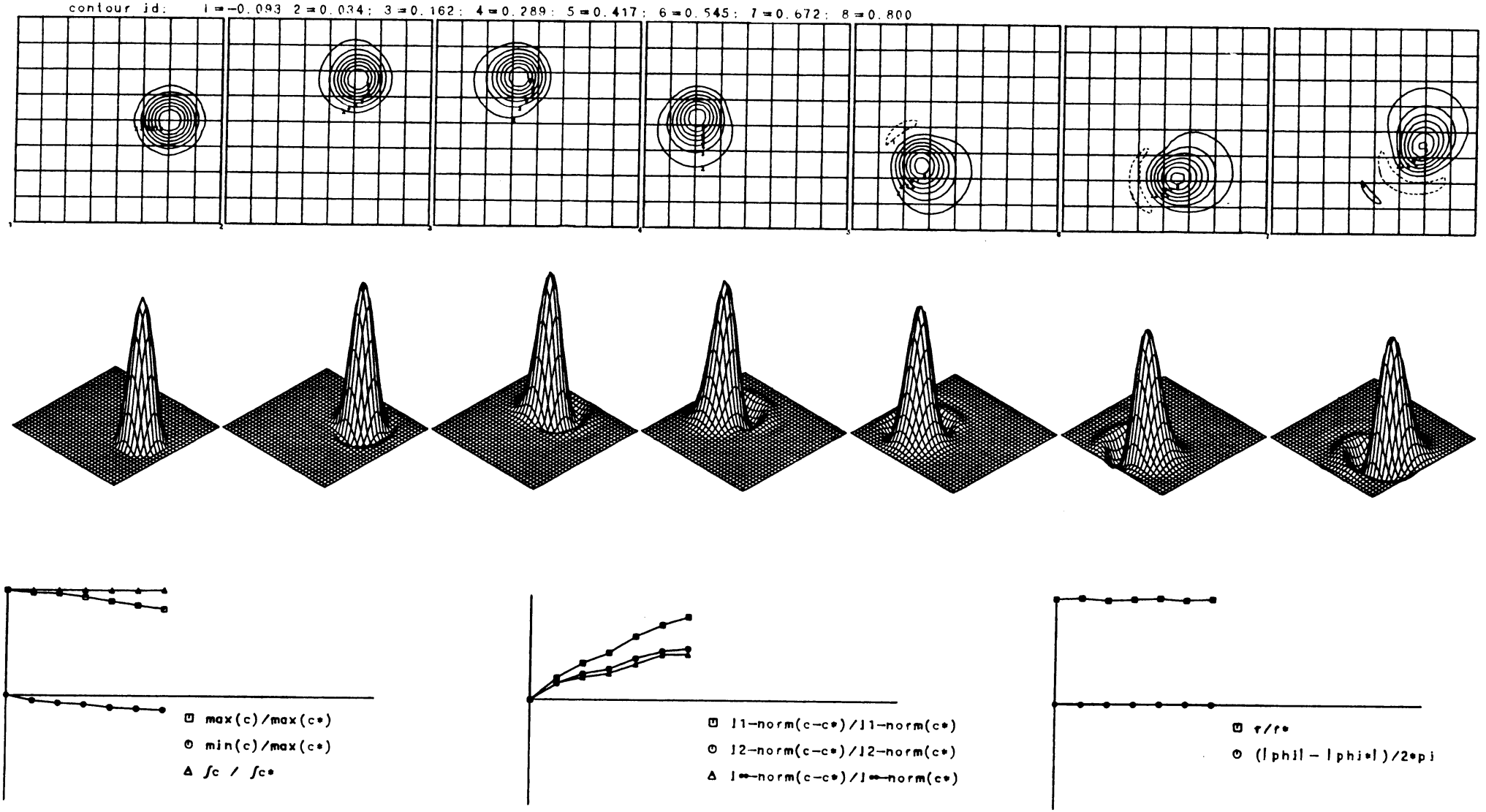

Chapeau-lumped method; #points=33; Courant number=0.83; Molenkamp test

Figure 2.10.7

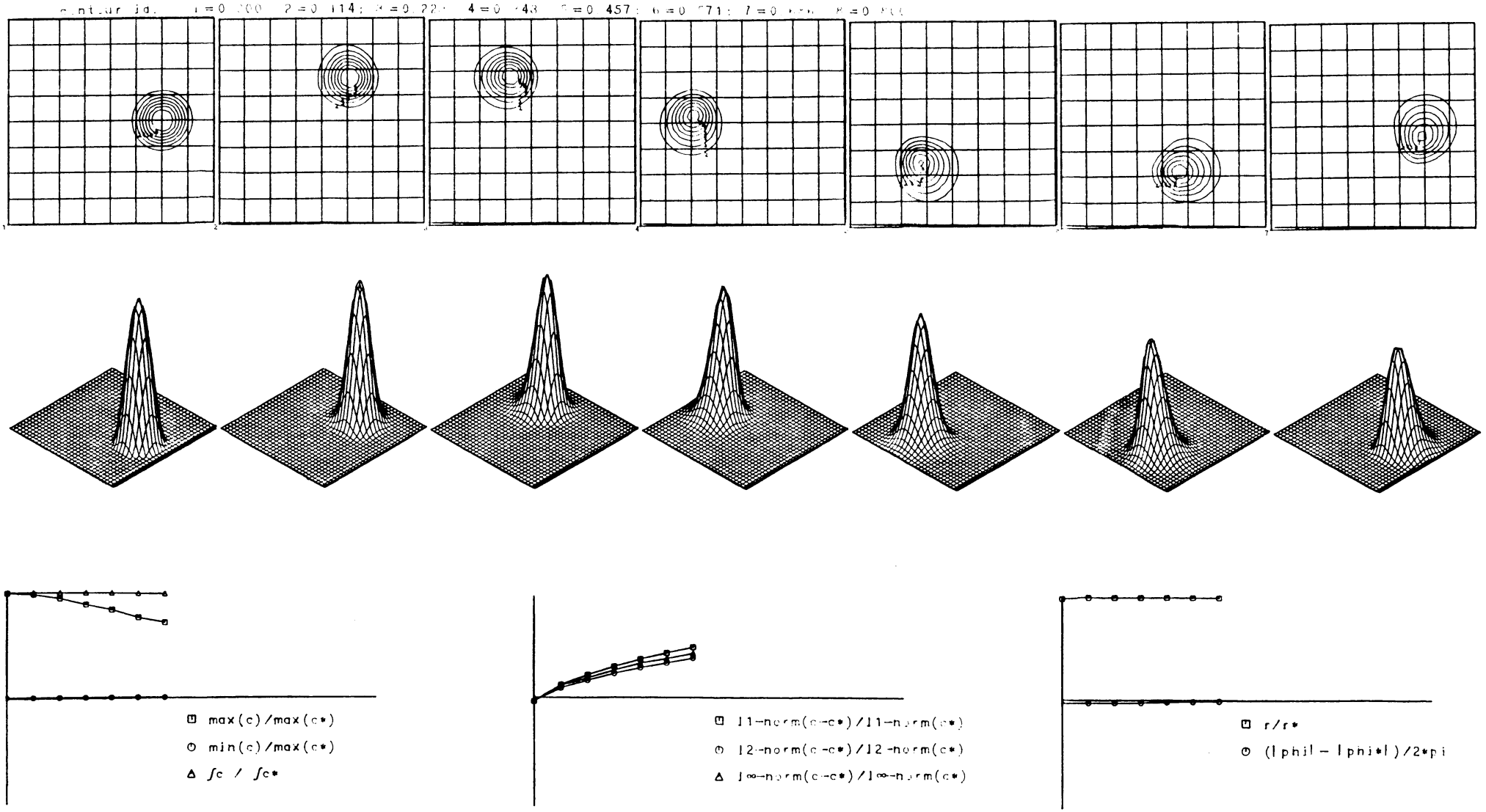

Smolarkiewicz(2); #points=64; Courant number=.486; Molenkamp test

Figure 2.10.8

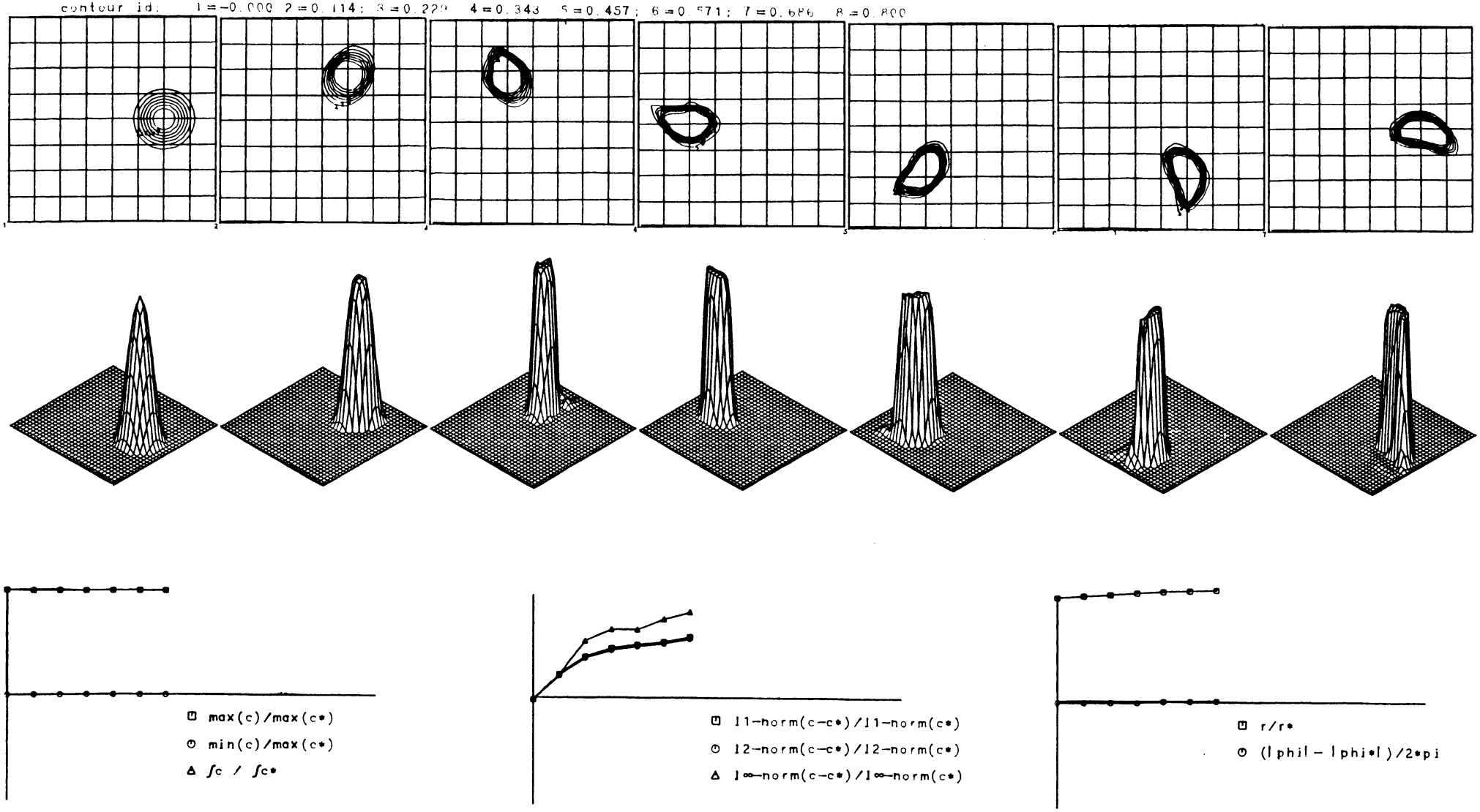

MFCT; #points=33; Courant number=.43; Molenkamp test

Figure 2.10.9

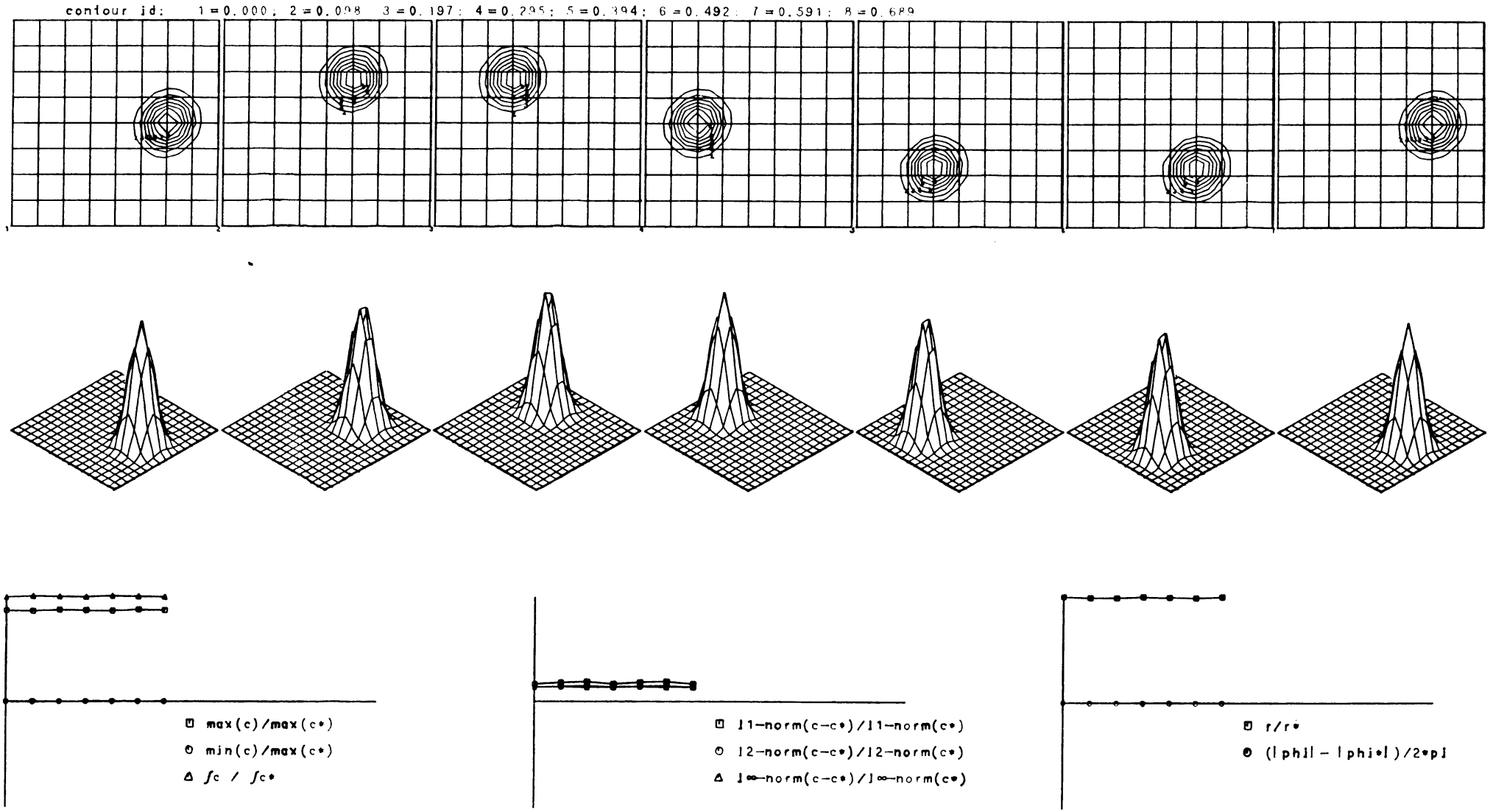

Particles method (1000); #points=17; Courant=.83; Molenkamp test

Figure 2.10.10

2.10.2 Source test (see figures 2.10.11 - 2.10.20)

1A[a] Obviously the grid resolution of 17 x 17 grid points is too low. Large oscillations with large negative values occur.

1A[b] This grid resolution yields good results, negative values of about 2% and reasonable errors. Note the reflexion of the outflowing concentration at the opposite side.

1B[a] As for 1A[a], the grid resolution is too low.

1B[b] Oscillations of higher frequency and amplitude occur. The reflexion is clearly too large.

2 Good accuracy. Because the exact solution tends to zero when leaving the domain small absolute errors introduce great relative errors. This remark holds for all the methods.

3A The origin of the great peak at the right and the smaller peak at the left is unknown. There seems to be no bug in the program. Perhaps the interpretation of what the numerical formulation at the boundary should be is wrong. Apart from the boundaries the method performs good. Slight negative values (≈2%) are introduced.

3B For this steep gradient problem the method performs better than for the smooth Molenkamp test. Negative values of about 5% are introduced.

4 The method performs well. The steep gradients are smoothed.

5 The steep gradients are made still steeper. This shows again that the method deforms the concentration profile into a shock-wave type profile.

6 Obviously too much mass has been introduced. Apart from this problem the method performs good.

The results for the objective criteria are tabulated in table 2. Here only the first 5 output results have been used.

Table 2. Objective criteria,
Source test

	$1A^a$	$1A^b$	$1B^a$	$1B^b$	2	3A	3B	4	5	6
max	1.1	1.	1.1	1.1	1.	3.6	1.05	1.05	1.	1.35
min	-0.36	-0.02	-0.15	-0.05	0.	-0.02	-0.05	0.	-0.	0.
mass	0.58	1.	0.65	0.95	1.	1.	1.05	1.05	1.1	1.5
$\|\ \|_{\ell_1}$	0.8	0.2	0.6	0.5	0.05	0.15	0.35	0.25	0.25	0.5
$\|\ \|_{\ell_2}$	0.5	0.15	0.4	0.45	0.05	0.45	0.3	0.25	0.35	0.5
$\|\ \|_{\ell_\infty}$	0.35	0.15	0.3	0.6	0.05	3.6	0.3	0.25	0.5	0.6

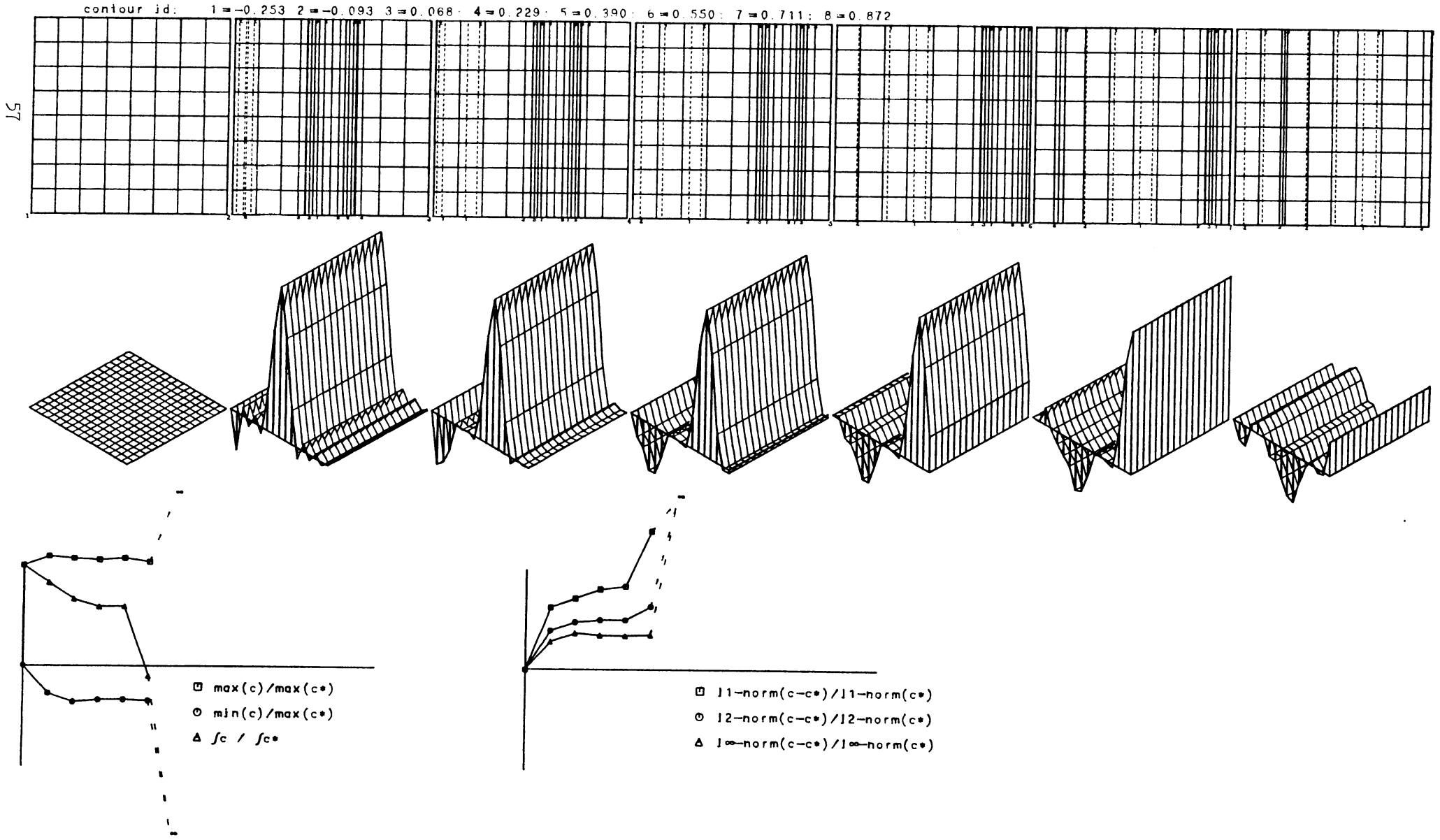

Pseudo spectral (polynomial); #points=17; Courant=0.747; Source test

Figure 2.10.11

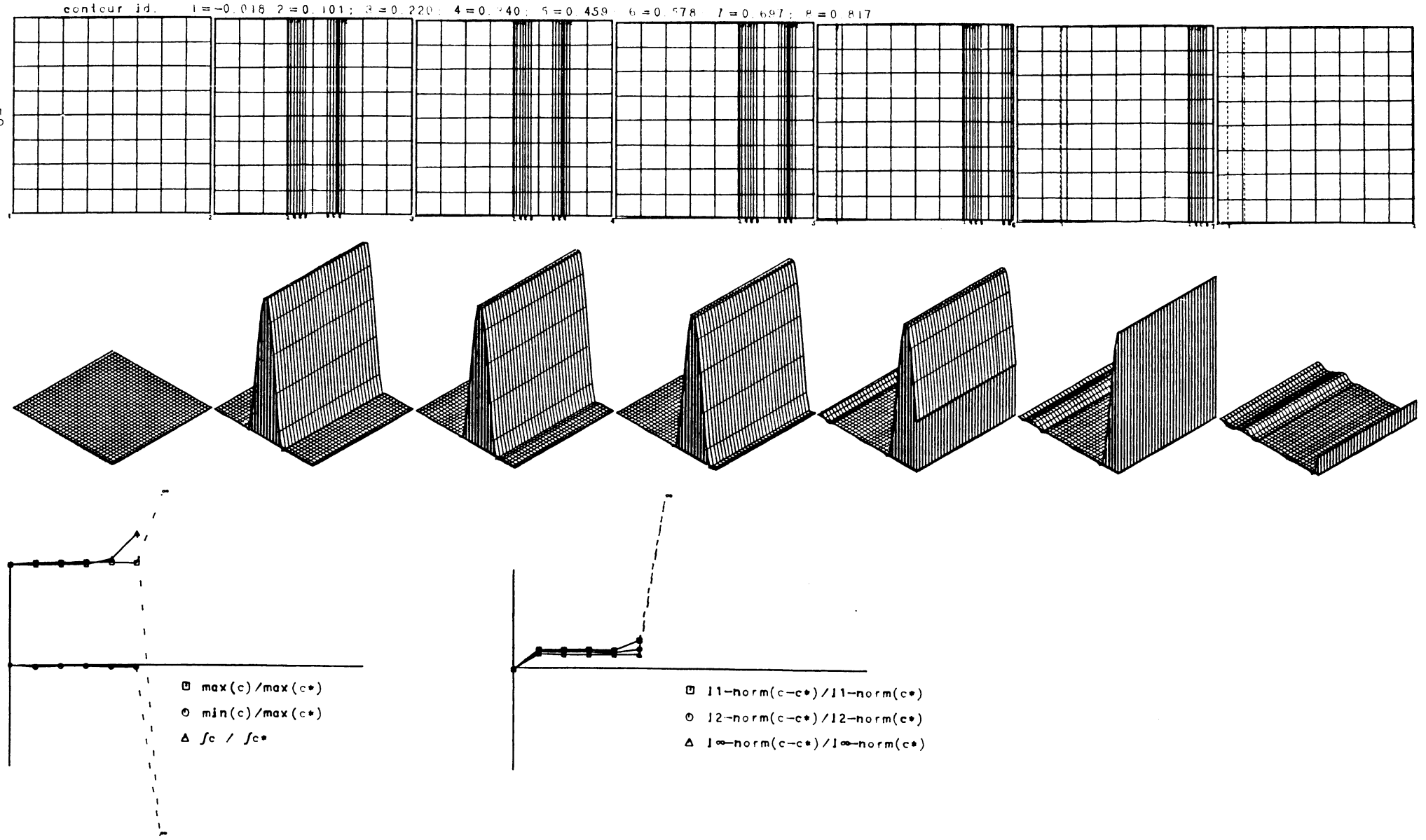

Pseudo spectral (polynomial): #points=33; Courant=.747; Source test

Figure 2.10.12

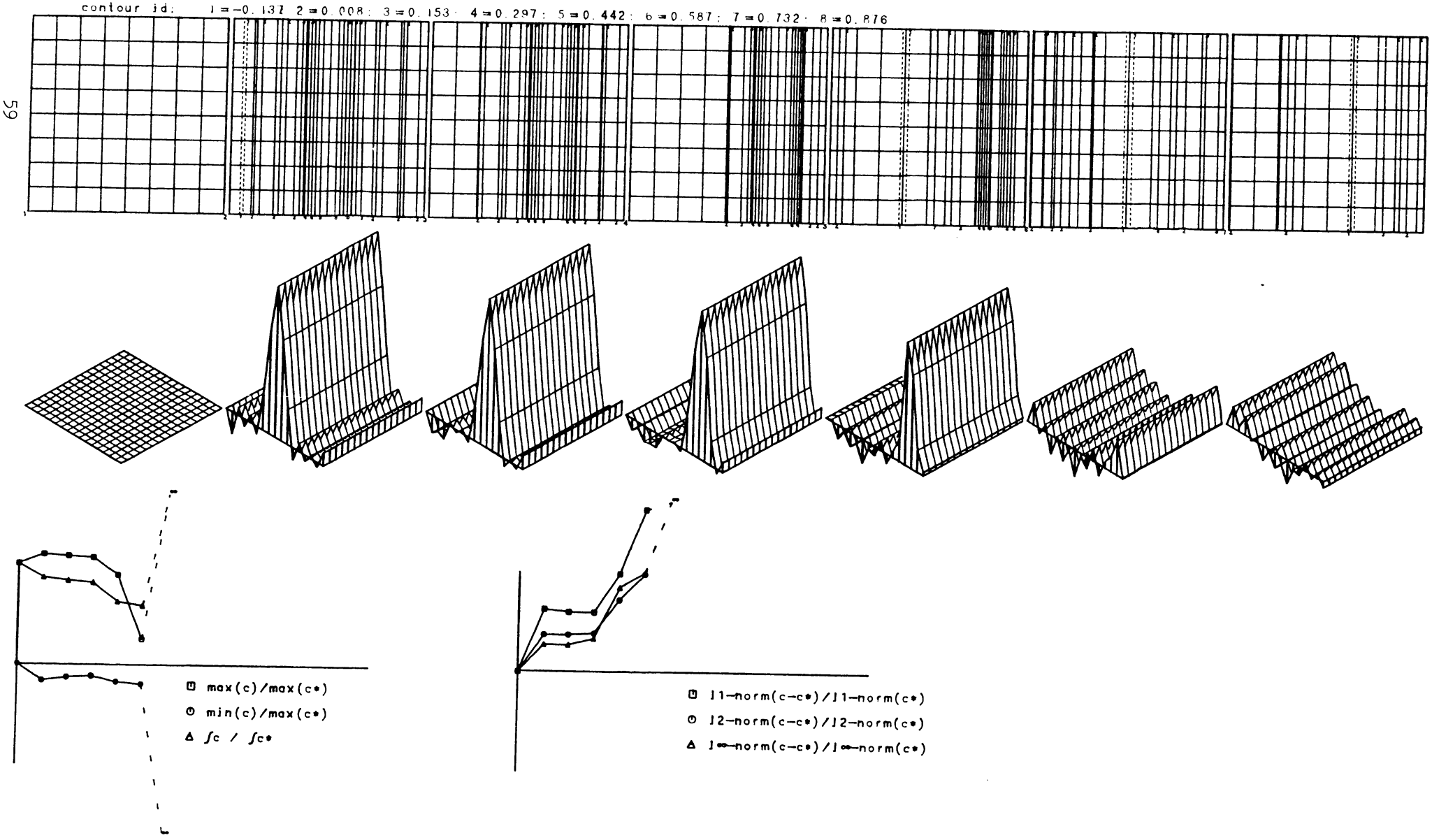

Pseudo spectral (decay); #points=17; Courant=0.74; Source test

Figure 2.10.13

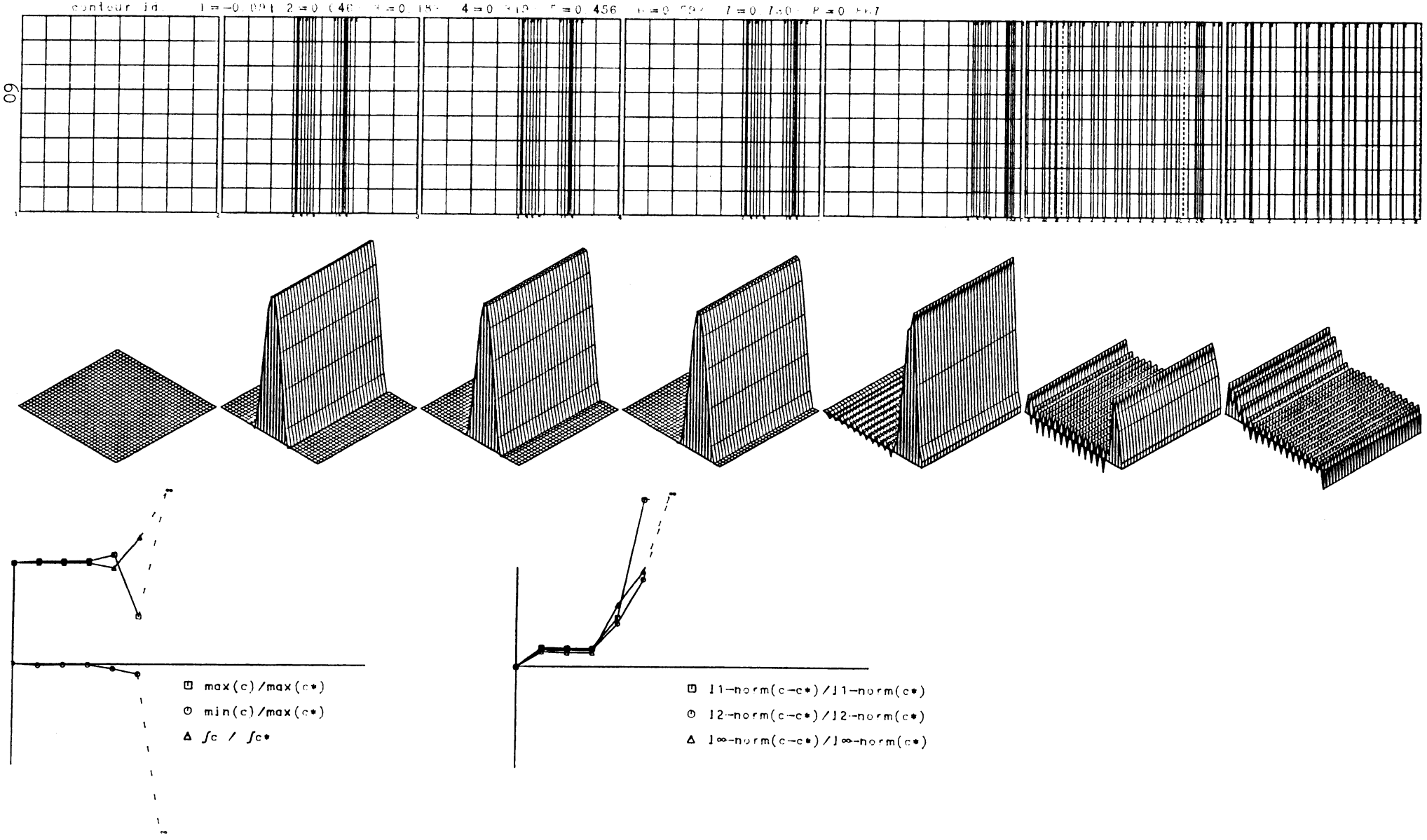

Figure 2.10.14

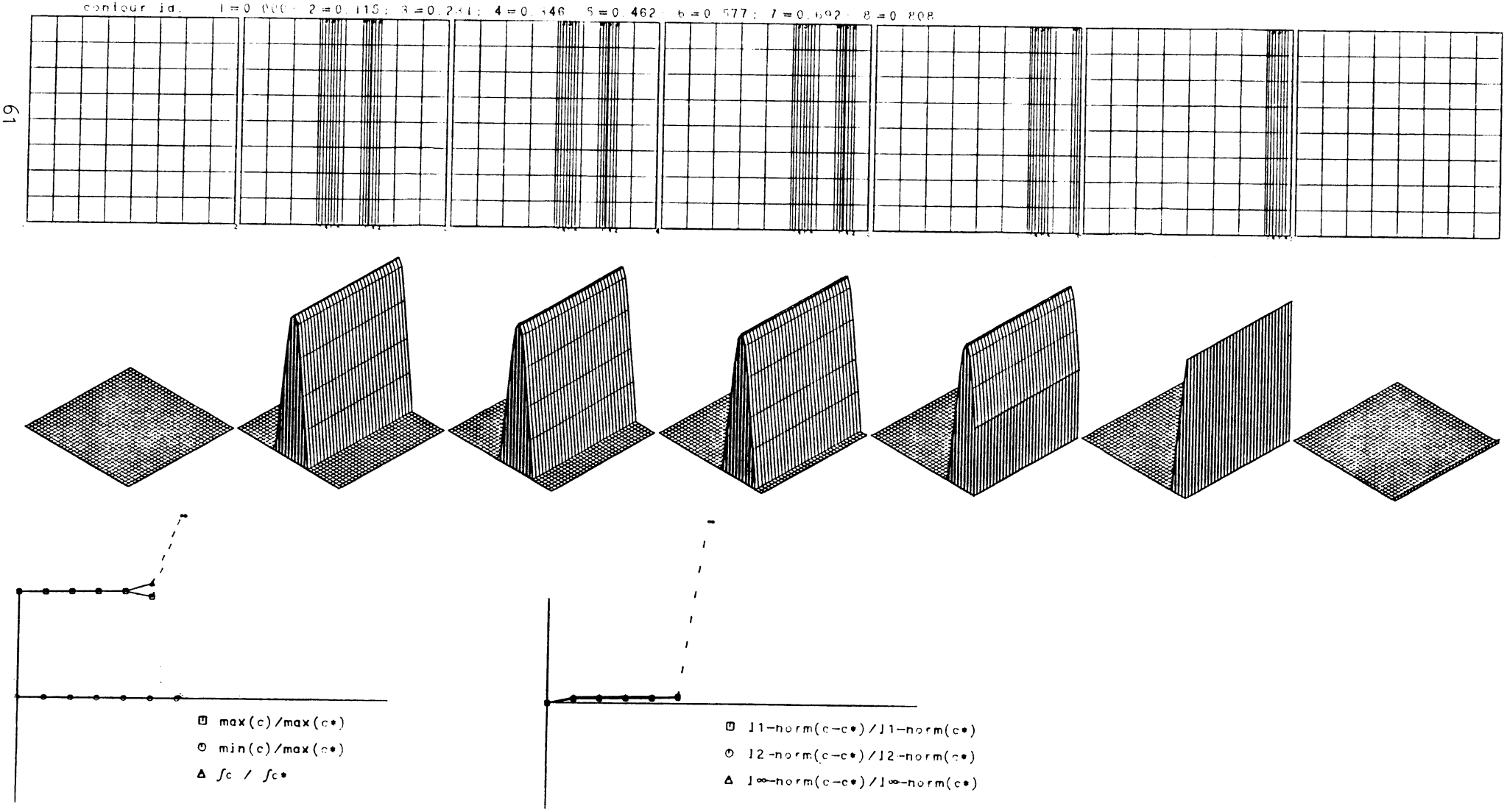

Second moment; #points=33; Courant number=.83; Source test

Figure 2.10.15

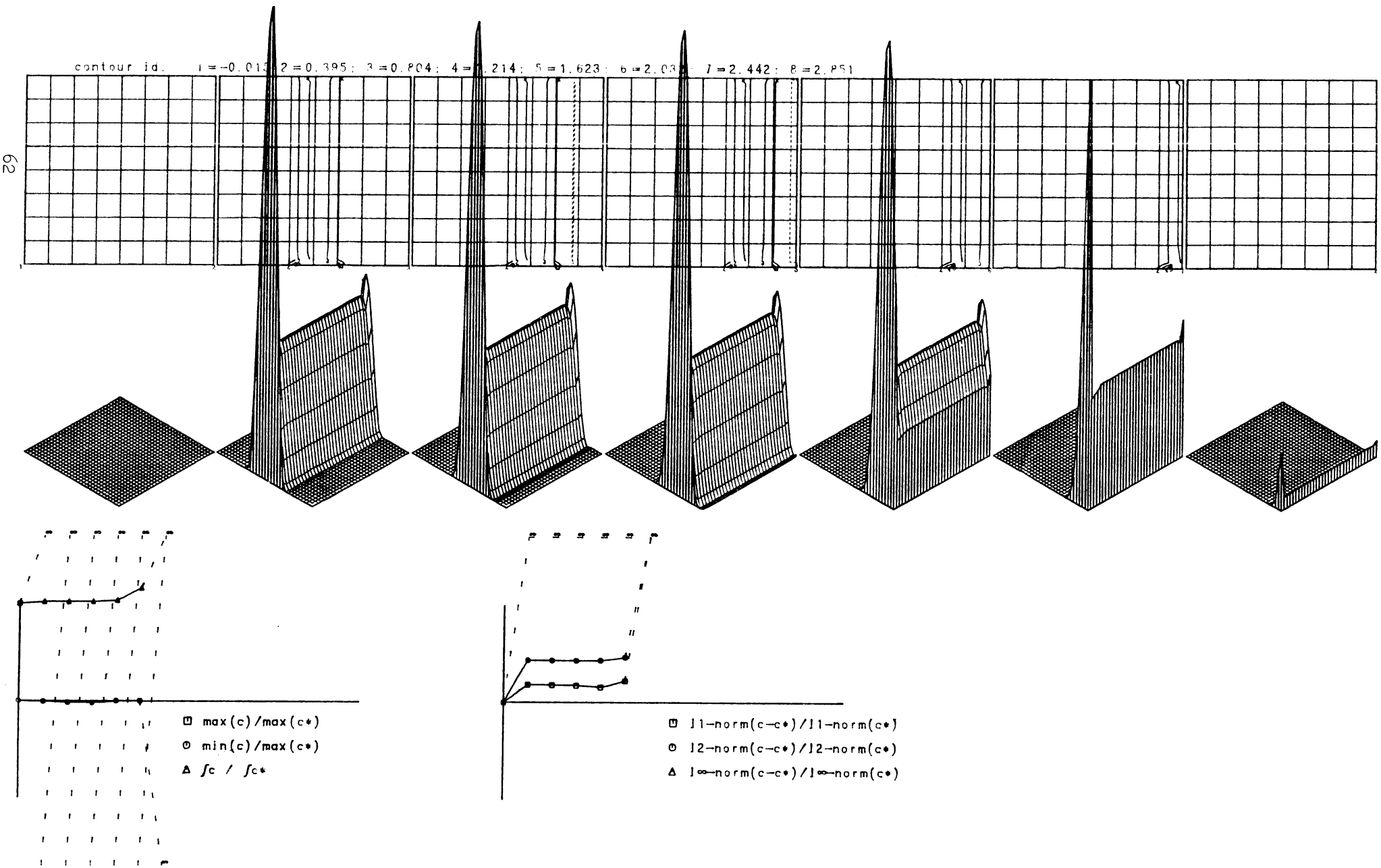

Chapeau, Forester filter: #points=33; Courant number=.479: Source test

Figure 2.10.16

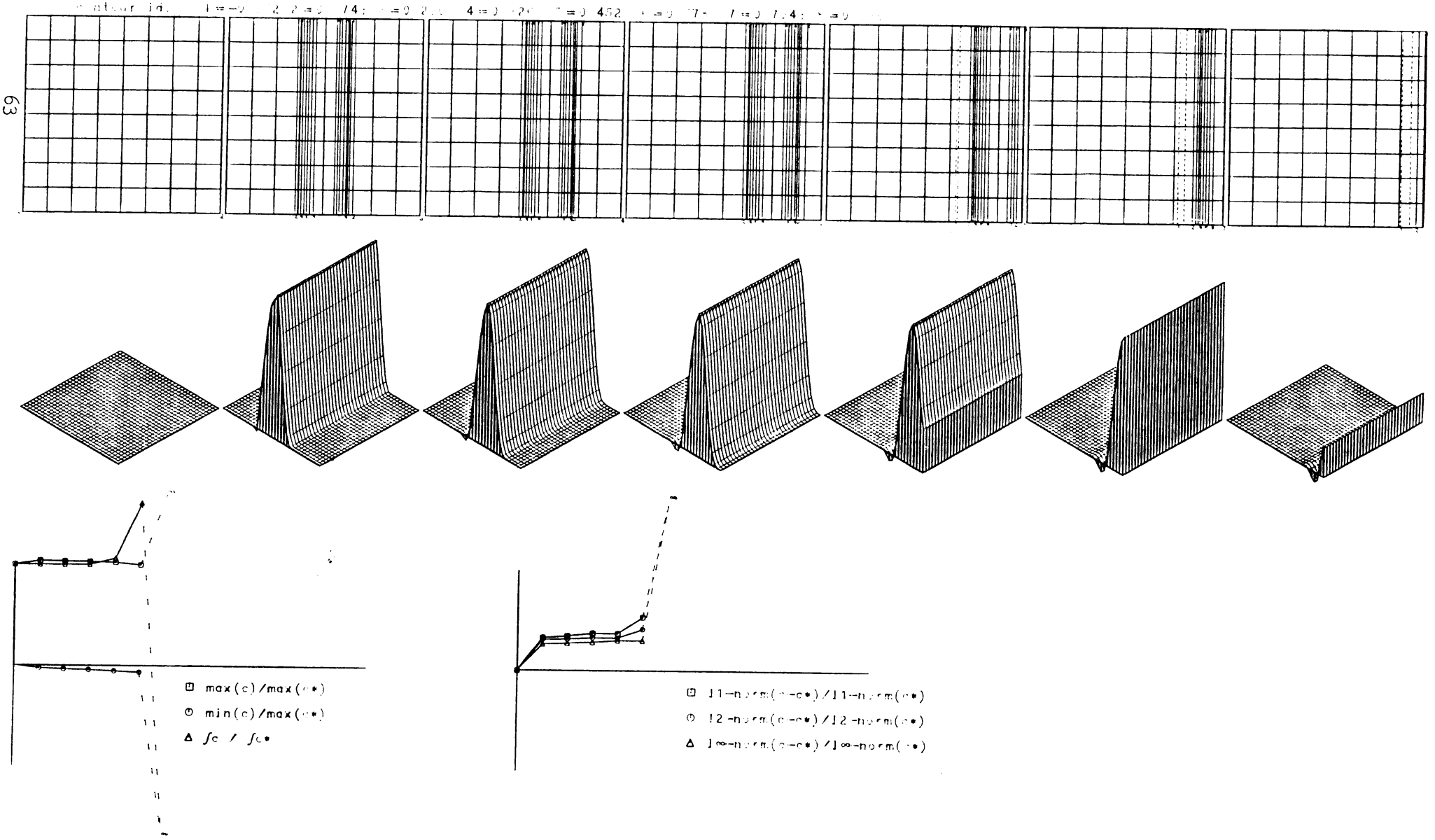

Figure 2.10.17

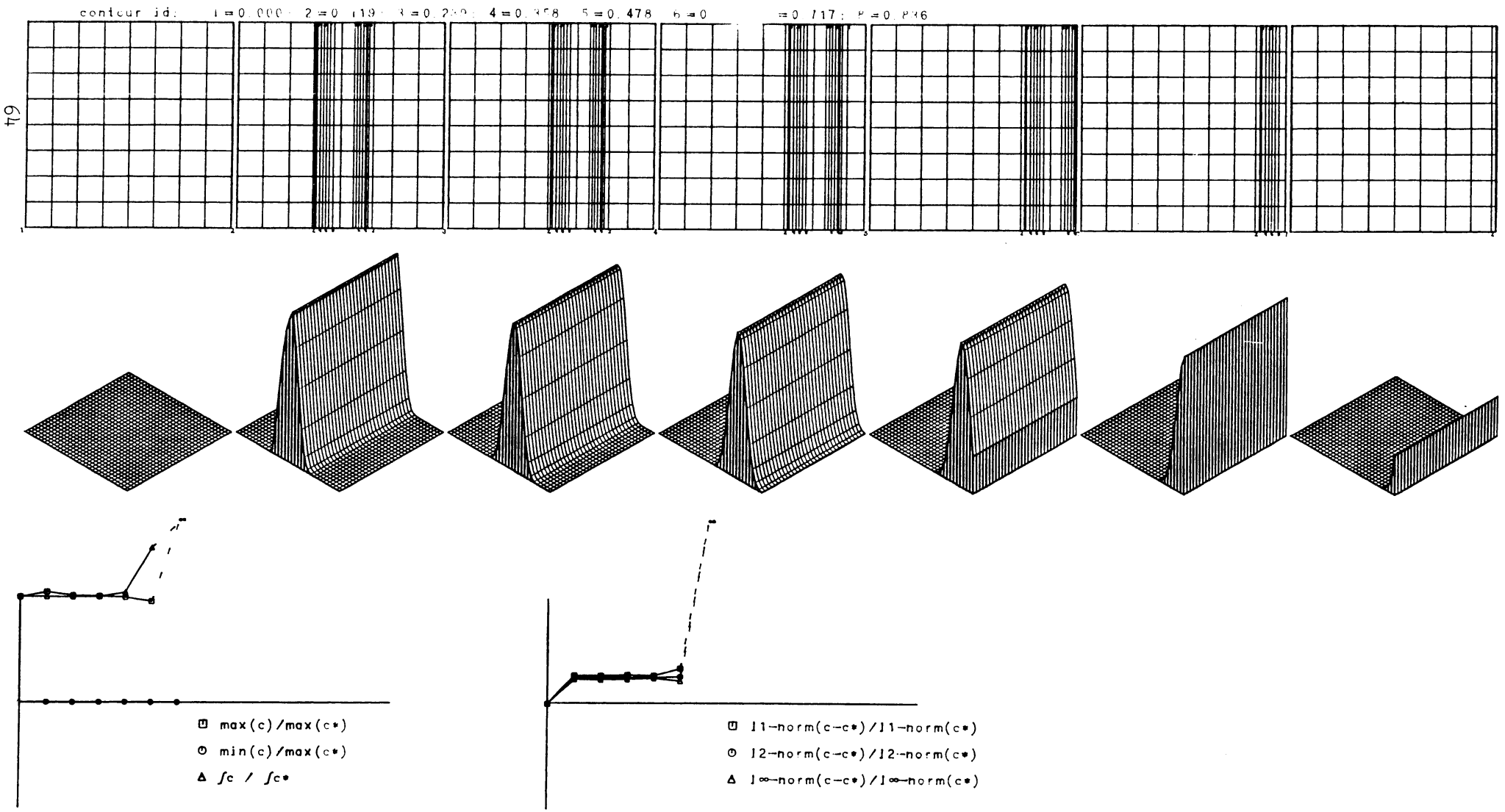

Smolarkiewicz(2); #points=33; Courant number=.486; Source test

Figure 2.10.18

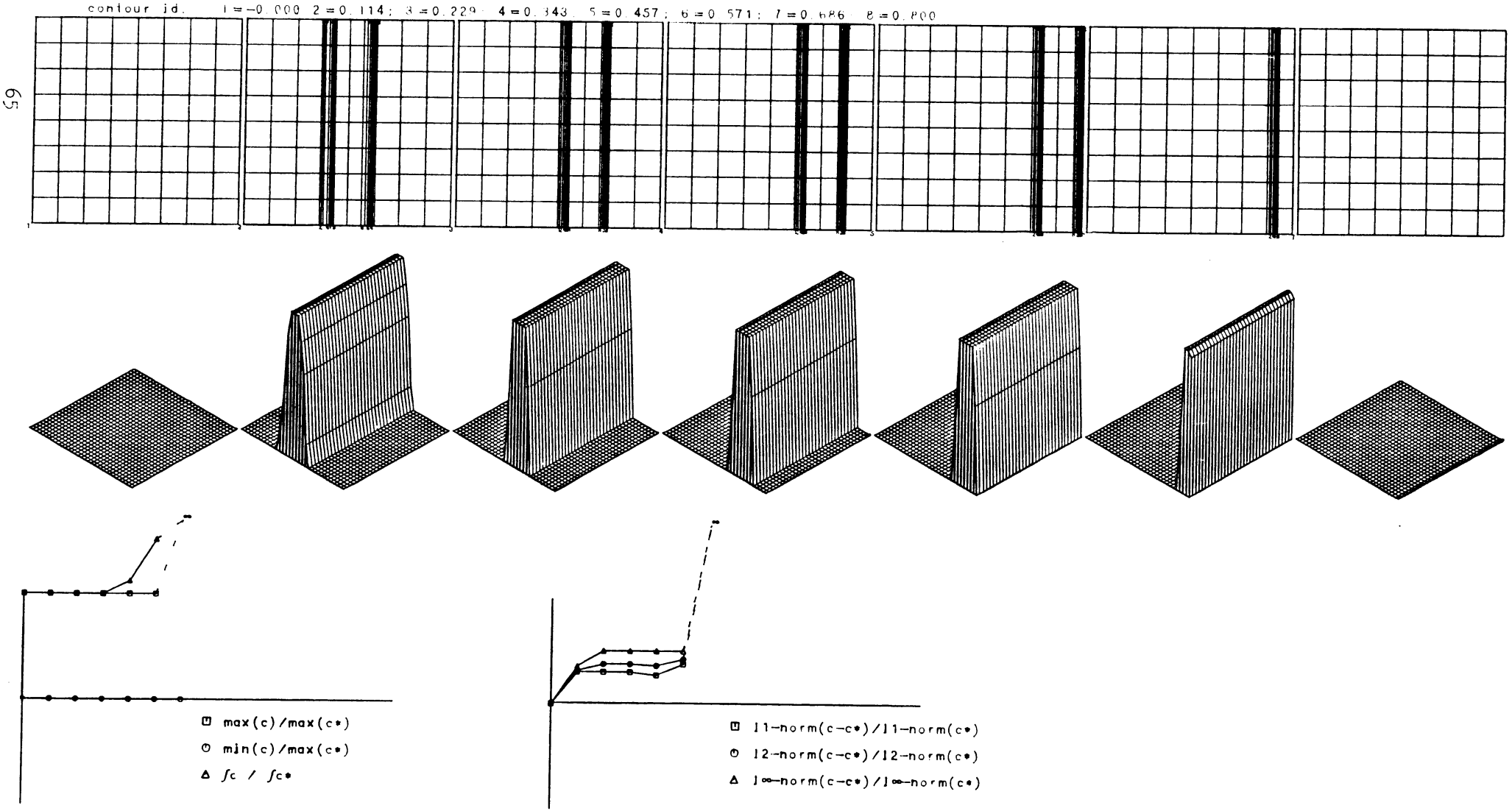

MFCT: #points=33; Courant=.83; Source test

Figure 2.10.19

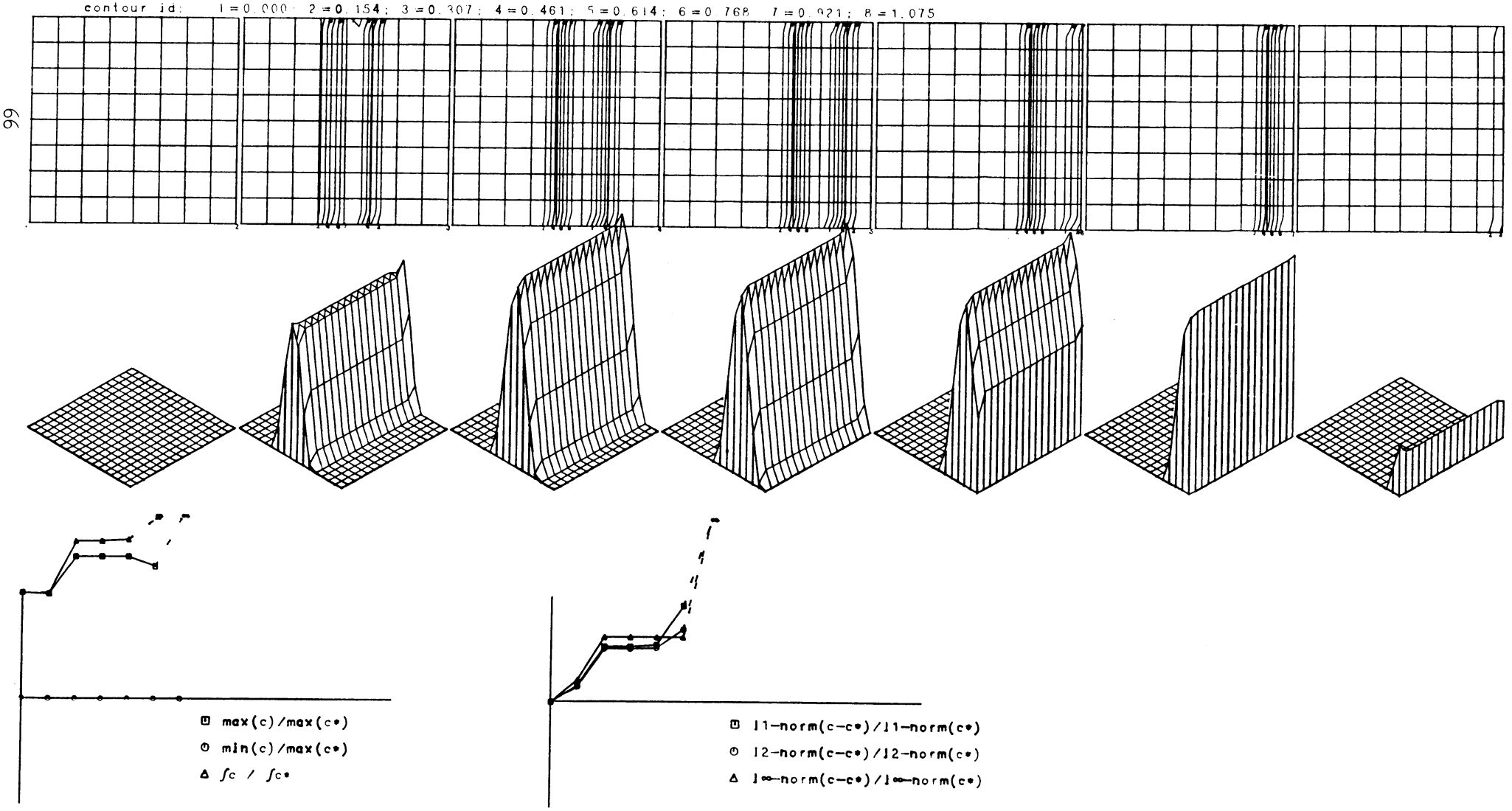

Particles method (1000); #points=17; Courant=.83; Source test

Figure 2.10.20

2.10.3 Block test, inflow boundary (see figures 2.10.21 - 2.10.30)

Generally, the inflow boundary seems problematic. Surprisingly, for almost each method only about 70% of the mass enters the region. A run of the second moment method with Courant number 1 (figure 2.10.25b) showed, however, that the implementation of the inflow boundary condition was correct: an almost exact result was obtained.

1A[a] The block shape is deformed into a hill shape. Peak values introduced at the beginning are decreased to the correct maximum value of 1. Negative values of about 6% occur.

1A[b] The concentration is less smeared out than for 1A[a]. Also, from the 2-D plot it is seen that the square shape is better conserved. About 90% mass enters the region. The peak value, however, increases slightly, and negative values of about 10% occur.

1B[a] From this picture one can conclude that this method is totally unfit for this kind of problem.

1B[b] See 1B[a].

2 Even this method which seems to be well fit for steep and discontinuous data produces large errors caused by the mass deficiency. Compared, however, with the other methods the results are good. It is the only method that more or less maintains the block shaped concentation profile.

3A When the block enters the region large negative values are introduced. It is not clear whether this phenomenon is caused for the same reason as in the source test. The difference is that this is an inflow boundary problem, while in the source test problems arise at outflow boundaries (V=0). Compare also figure 2.10.36, where the block leaves the region (outflow boundary!) and no large negative values are introduced.

3B Apart from the large negative peak value in 3A this method performs almost as 3A: a maximum value overshoot of 20% and a maximum negative value of ≈9%.

4 Note the diffusive effects of this method: the maximum decreases and the block shape is deformed into a hill shape that is flat at the downwind side.

5 The block shaped concentration profile is seriously deformed into a shock-wave type profile, and the concentration has been smeared out in directions normal to the wind velocity. Negative values of about

10^{-16} (machine precision) occur.

6 There seems to be a small lag with respect to the distance that should have been travelled.

The results for the objective criteria are tabulated in table 3.

Table 3. Objective criteria,
block test - inflow boundary

	1A[a]	1A[b]	1B[a]	1B[b]	2	3A	3B	4	5	6
max	1.35	1.3	2.6	2.7	1.	1.15	1.2	1.25	1.	0.9
min	-0.06	-0.1	-1.15	-1.8	0.	-1.4	-0.11	0.	-0.	0.
mass	0.65	0.94	0.55	0.8	0.7	0.7	0.7	0.6	0.65	0.55
$\|\|_{\ell_1}$	0.85	0.55	-	-	0.6	0.65	0.7	0.85	0.85	0.6
$\|\|_{\ell_2}$	0.65	0.45	1.6	1.9	0.65	0.55	0.55	0.7	0.9	0.6
$\|\|_{\ell_\infty}$	0.85	0.85	1.55	-	1.	1.8	0.95	0.9	1.	0.9

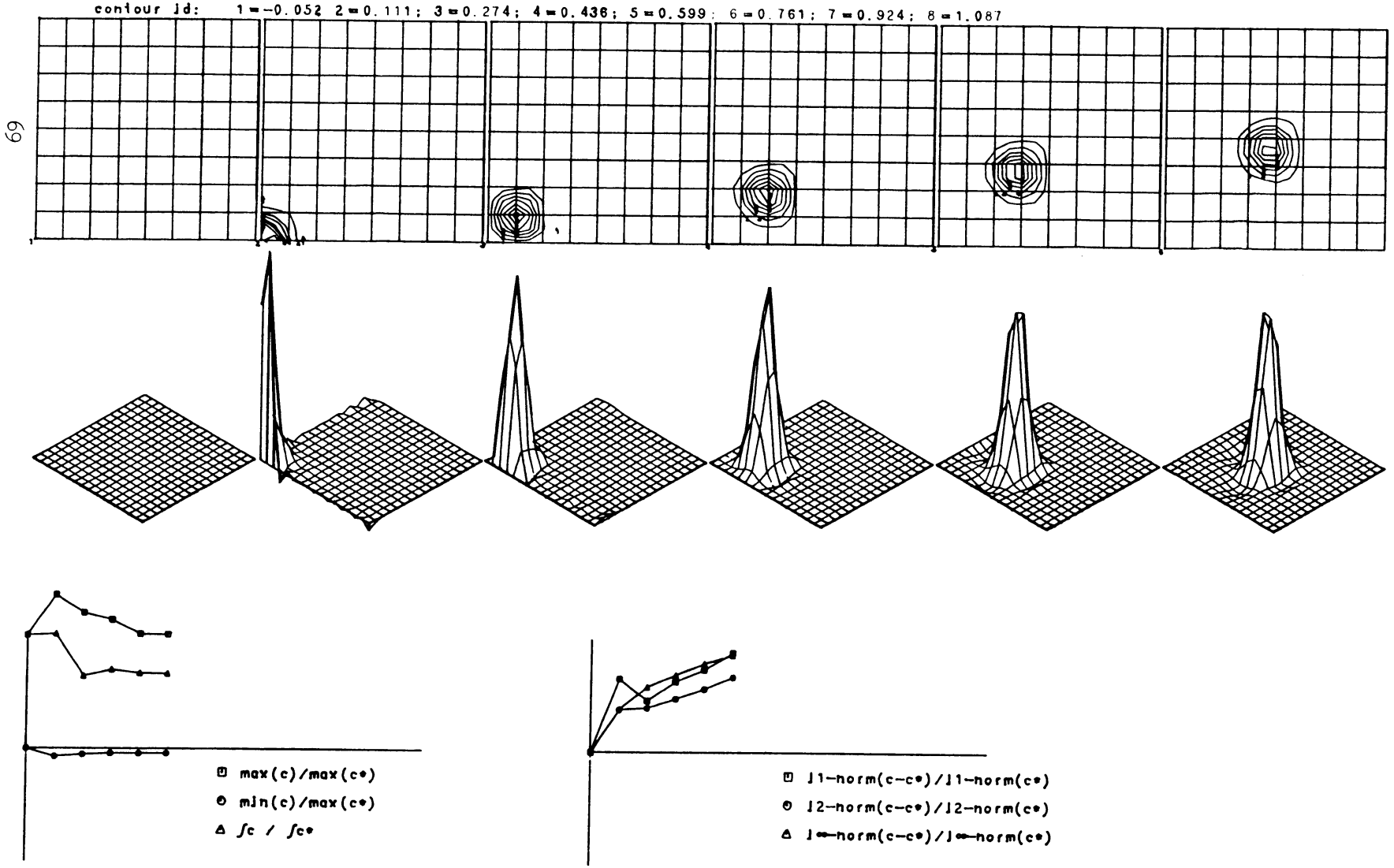

Pseudo spectral (polynomial); #points=17; Courant=0.747; Block test

Figure 2.10.21

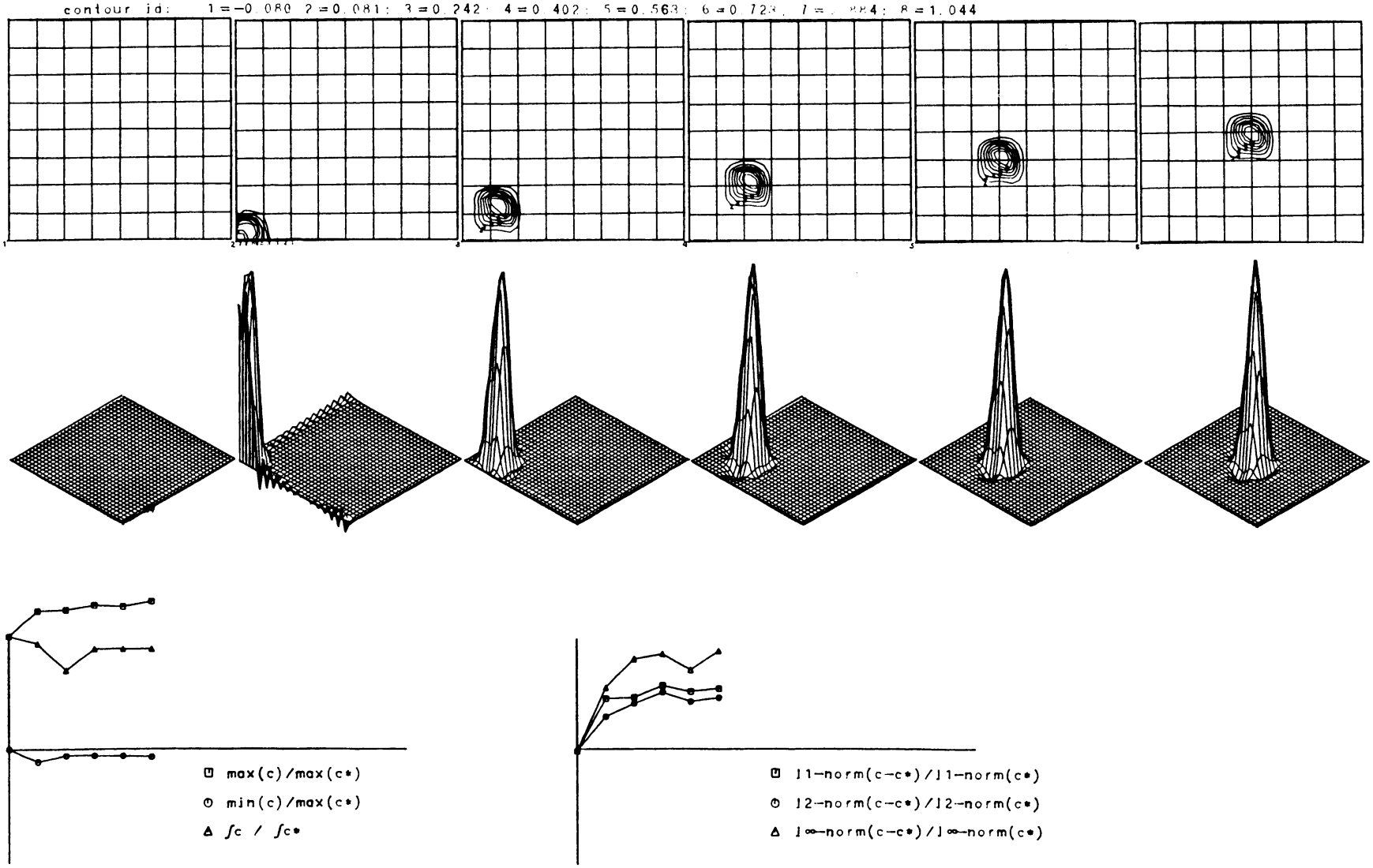

Pseudo spectral (polynomial); #points=33; Courant=0.747; Block test

Figure 2.10.22

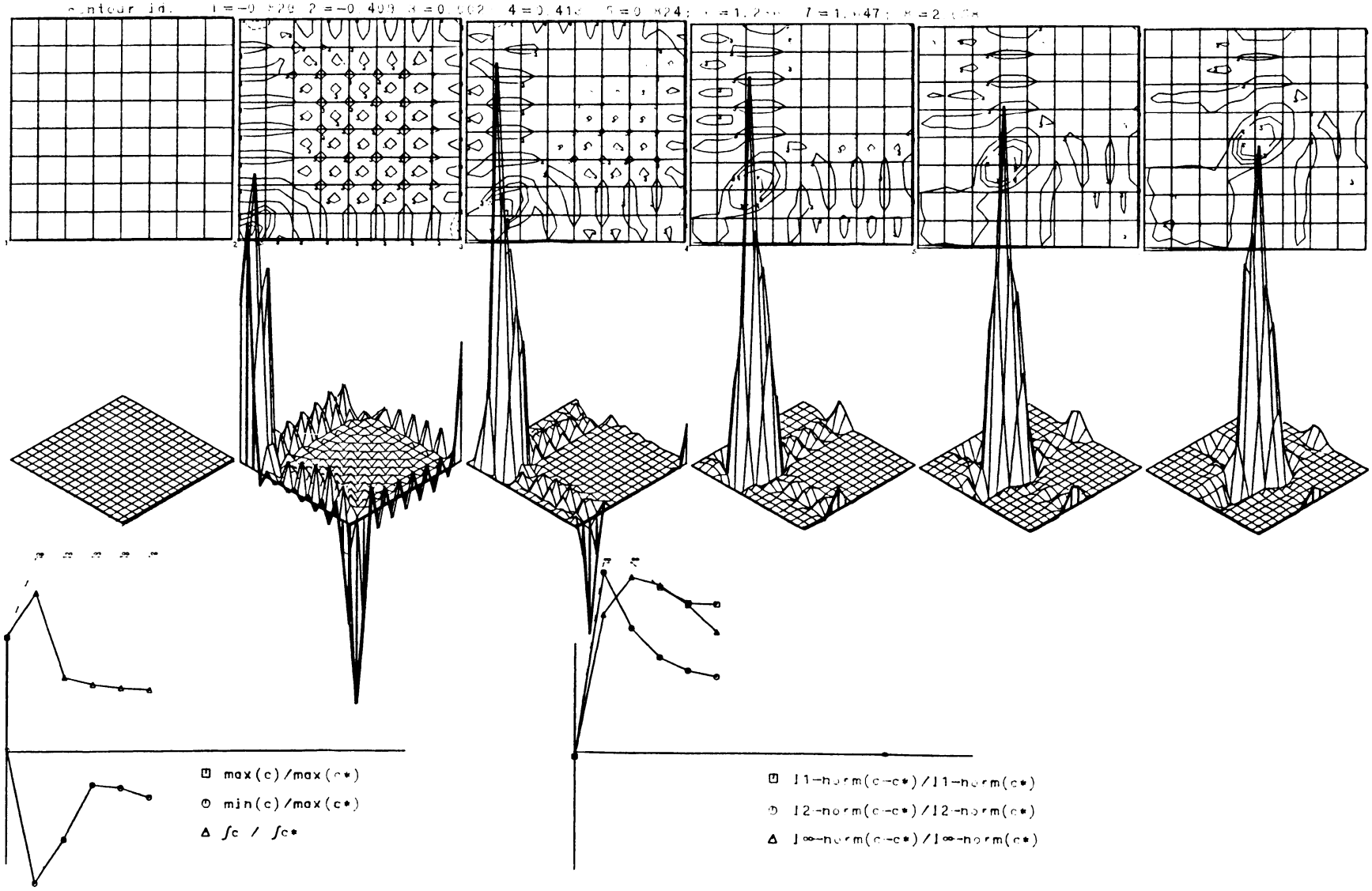

Pseudo spectral (decay): #points=17; Courant=0.74; Block test

Figure 2.10.23

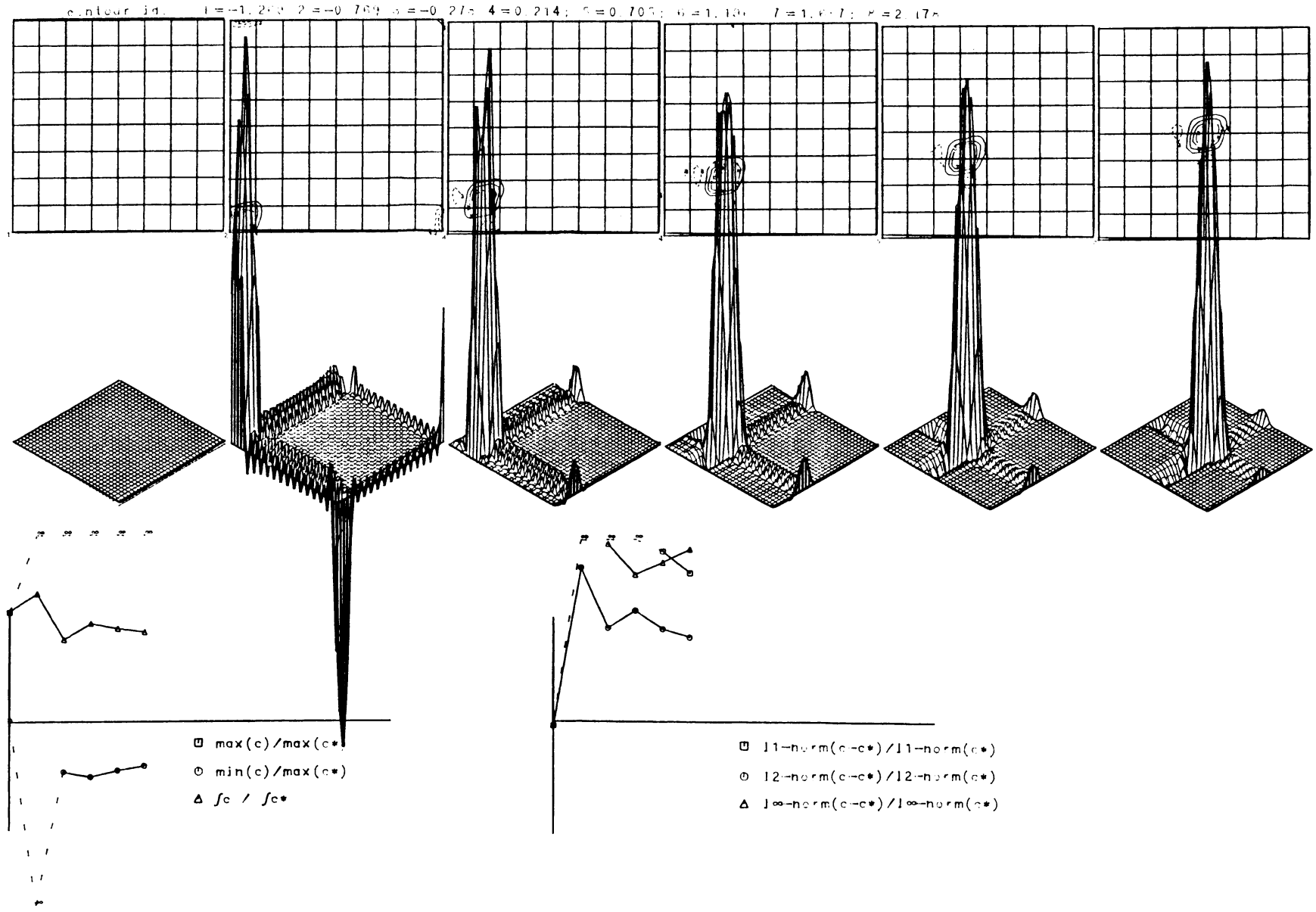

Figure 2.10.24

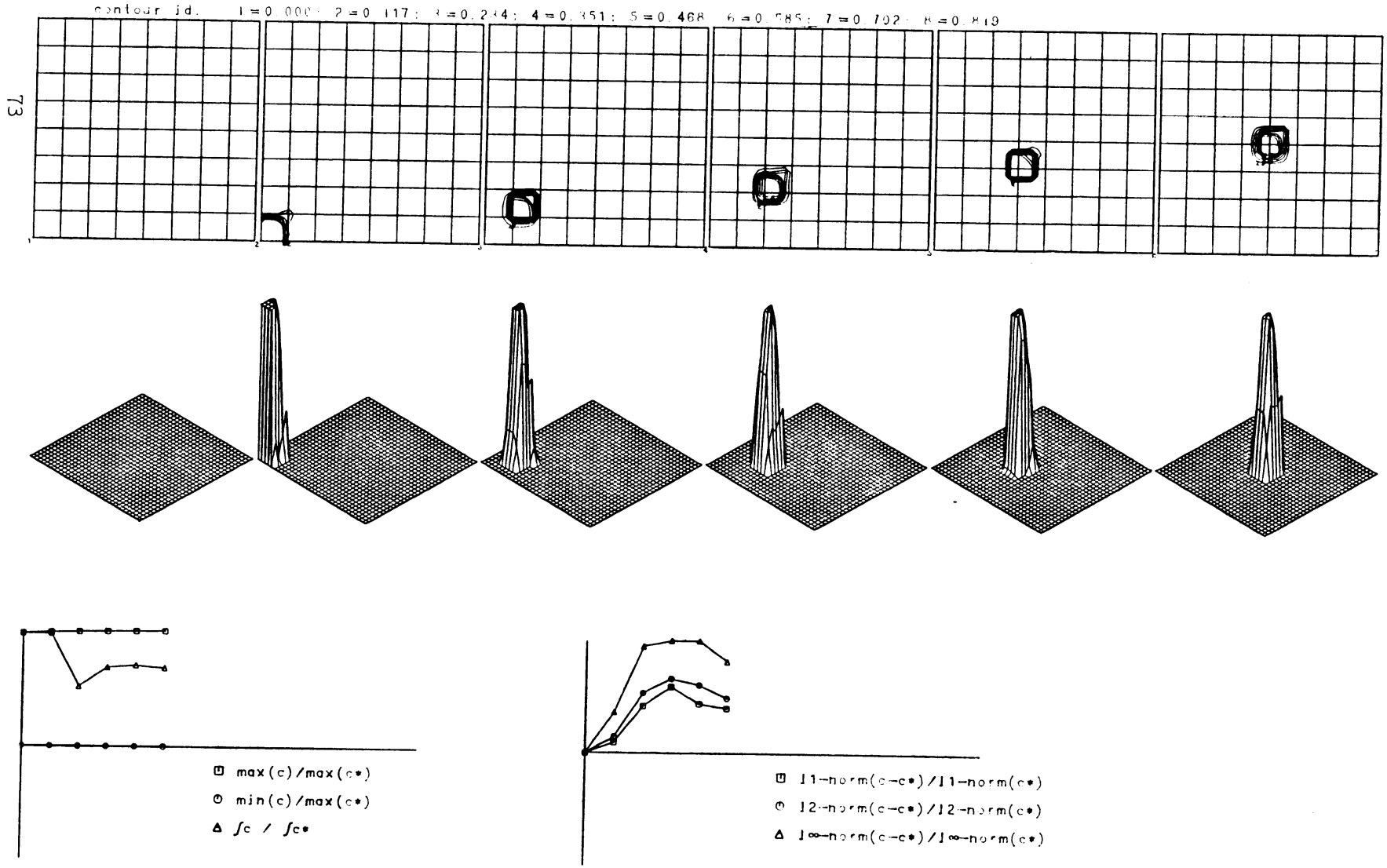

Second moment; #points=33; Courant number=0.83; Block test

Figure 2.10.25a

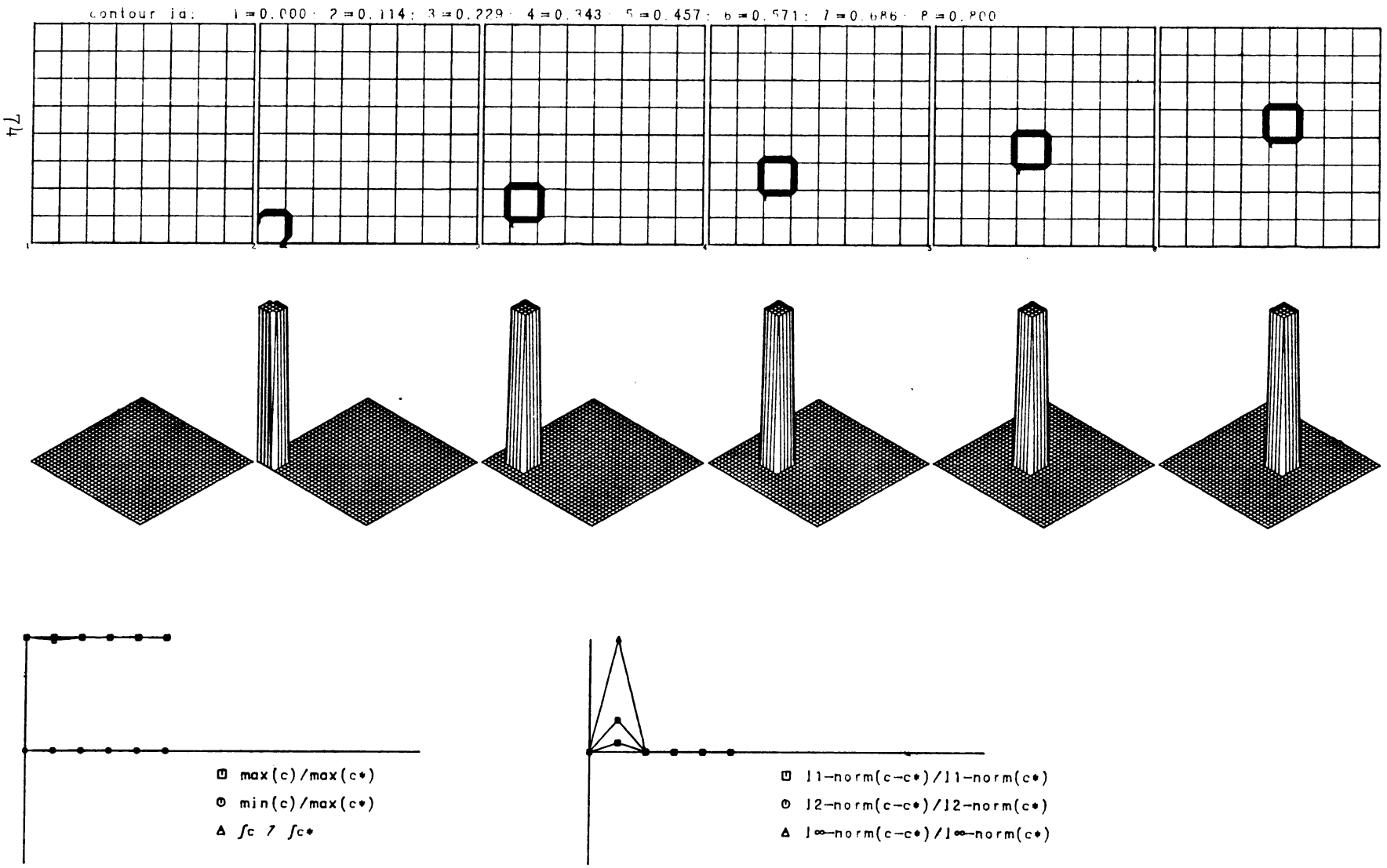

Second moment; #points=33; Courant number=1.0; Block test

Figure 2.10.25b

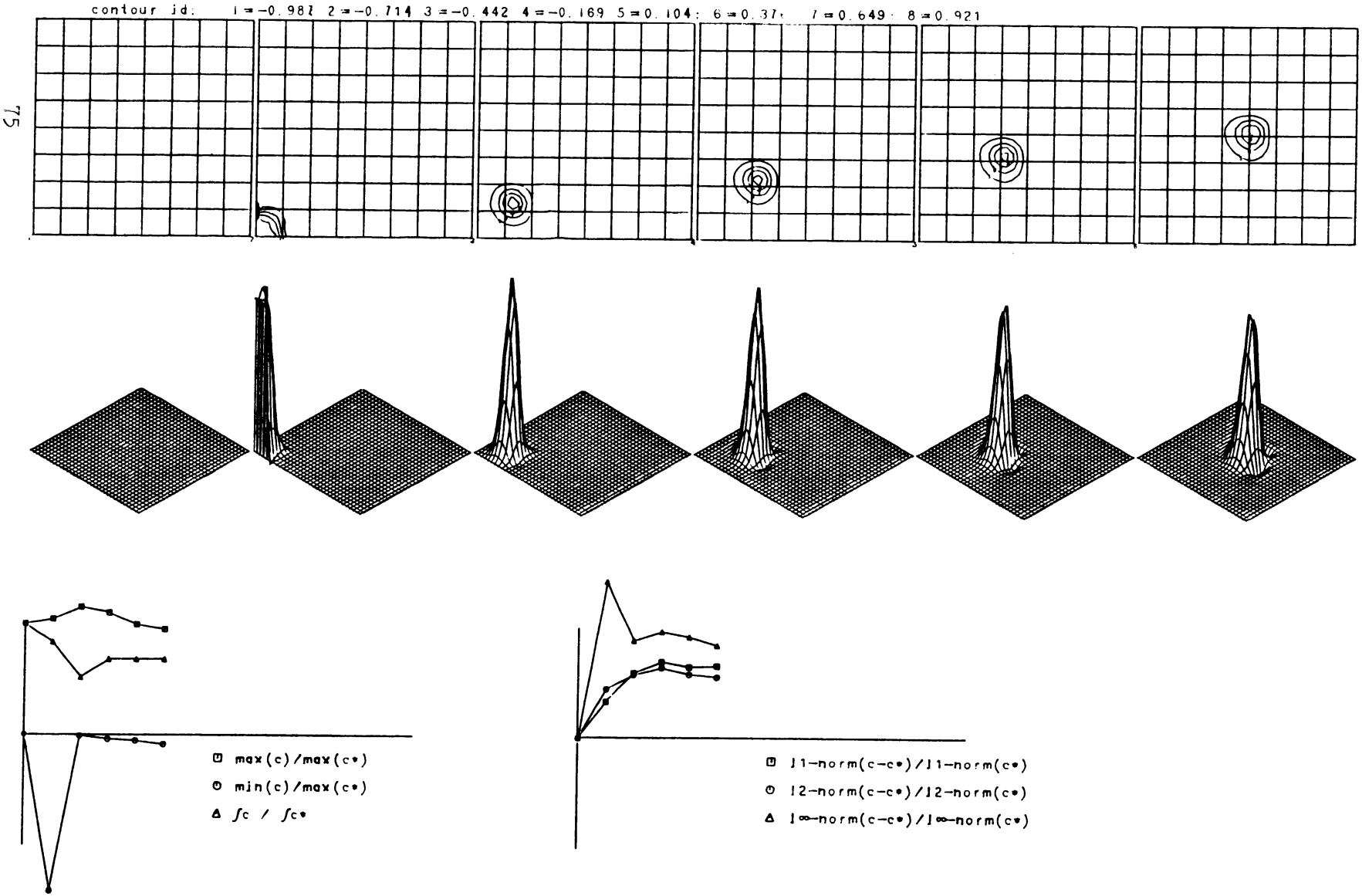

Chapeau, Forester filter: #points=33; Courant number=.479; Block test

Figure 2.10.26

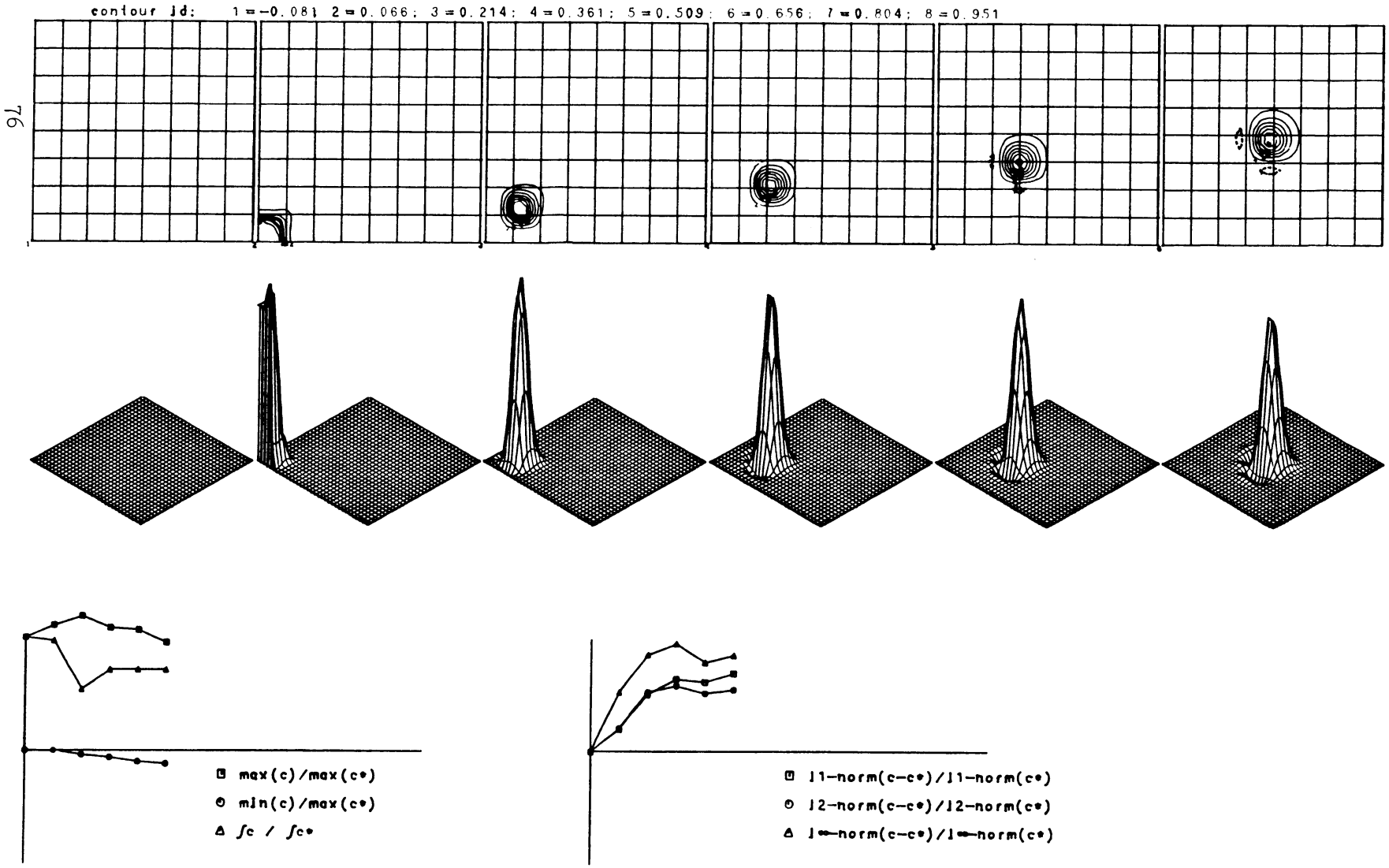

Chapeau-lumped method; #points=33; Courant number=.83; Block test

Figure 2.10.27

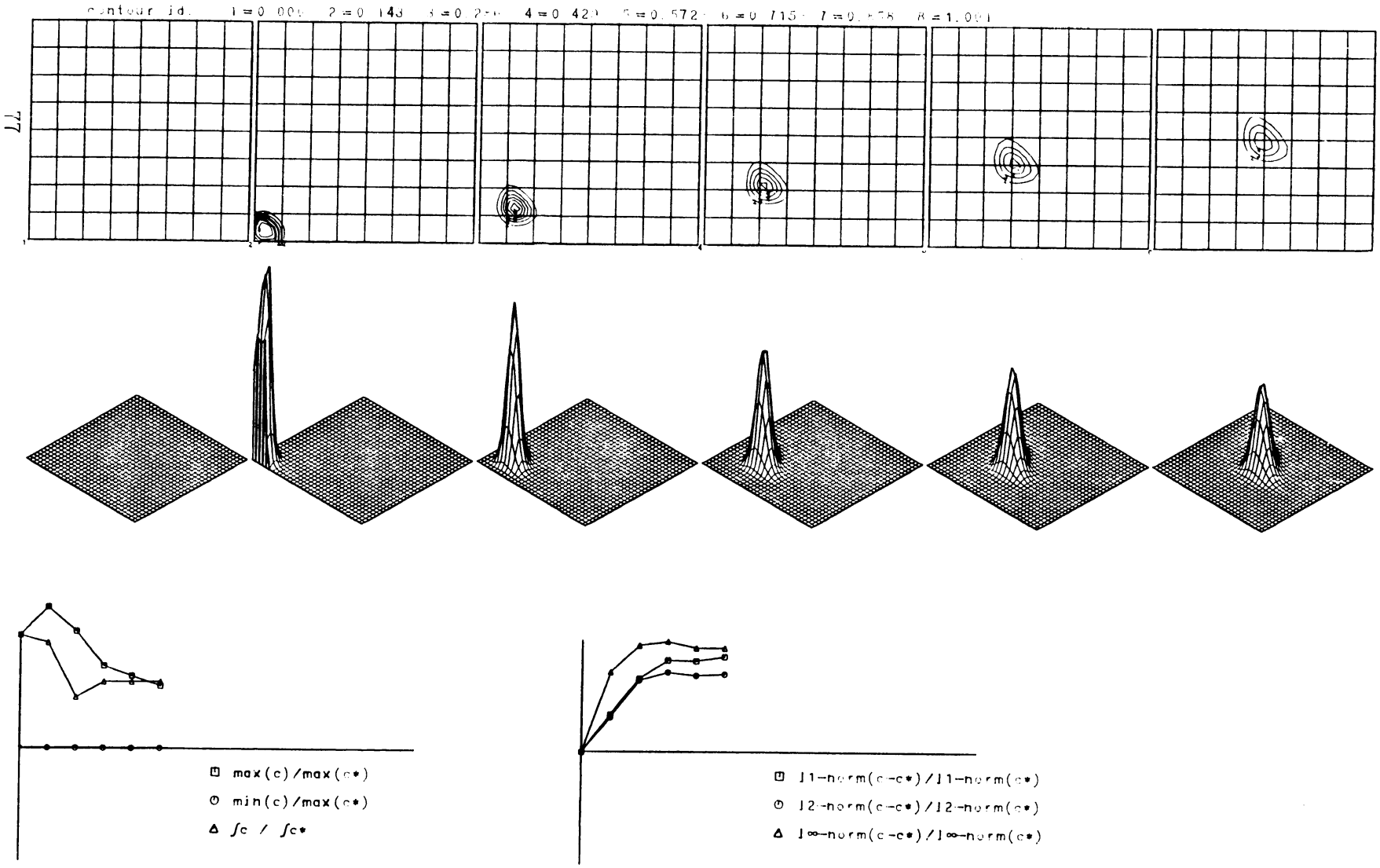

Figure 2.10.28

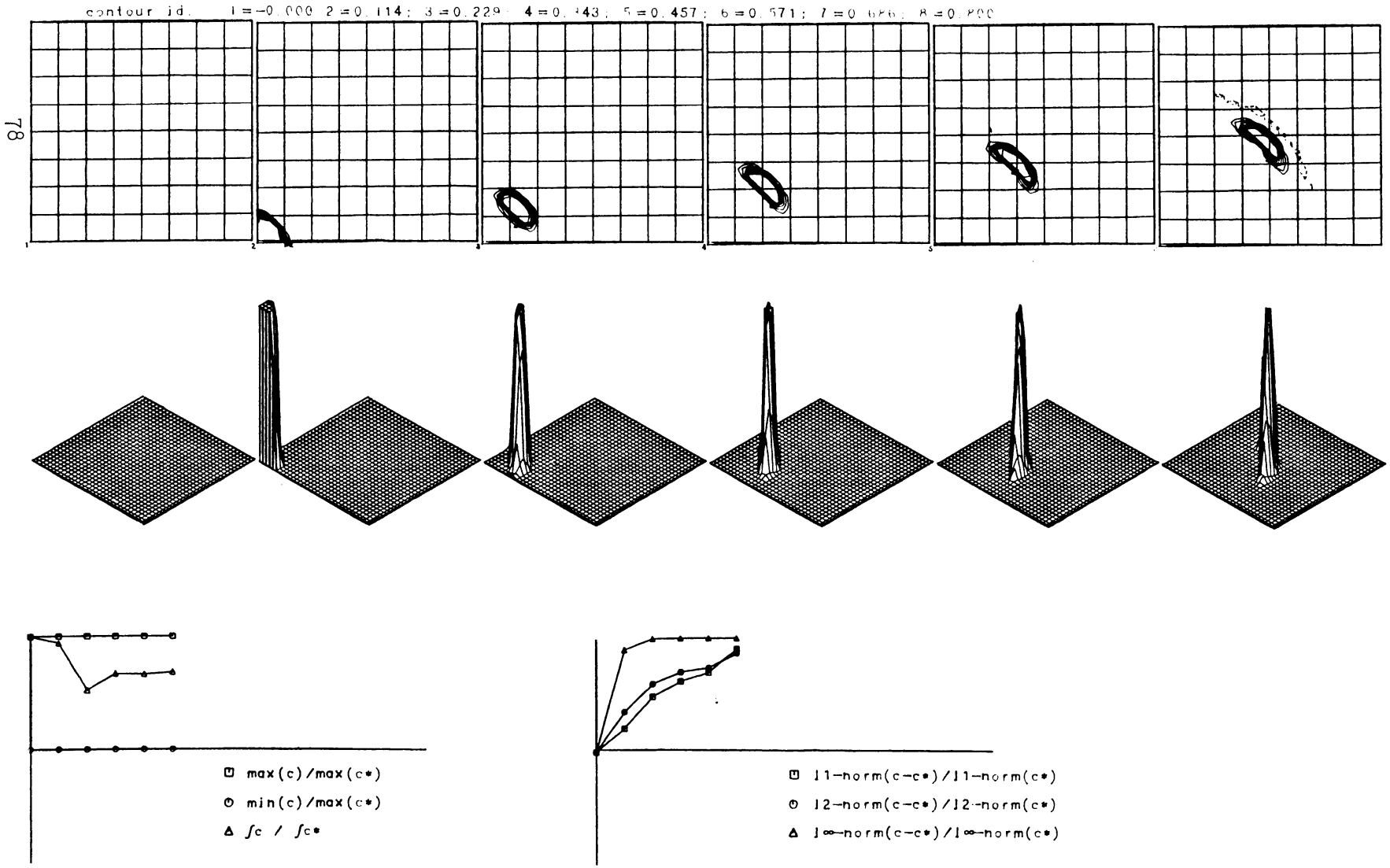

MFCT: #points=33; Courant=.43; Block test

Figure 2.10.29

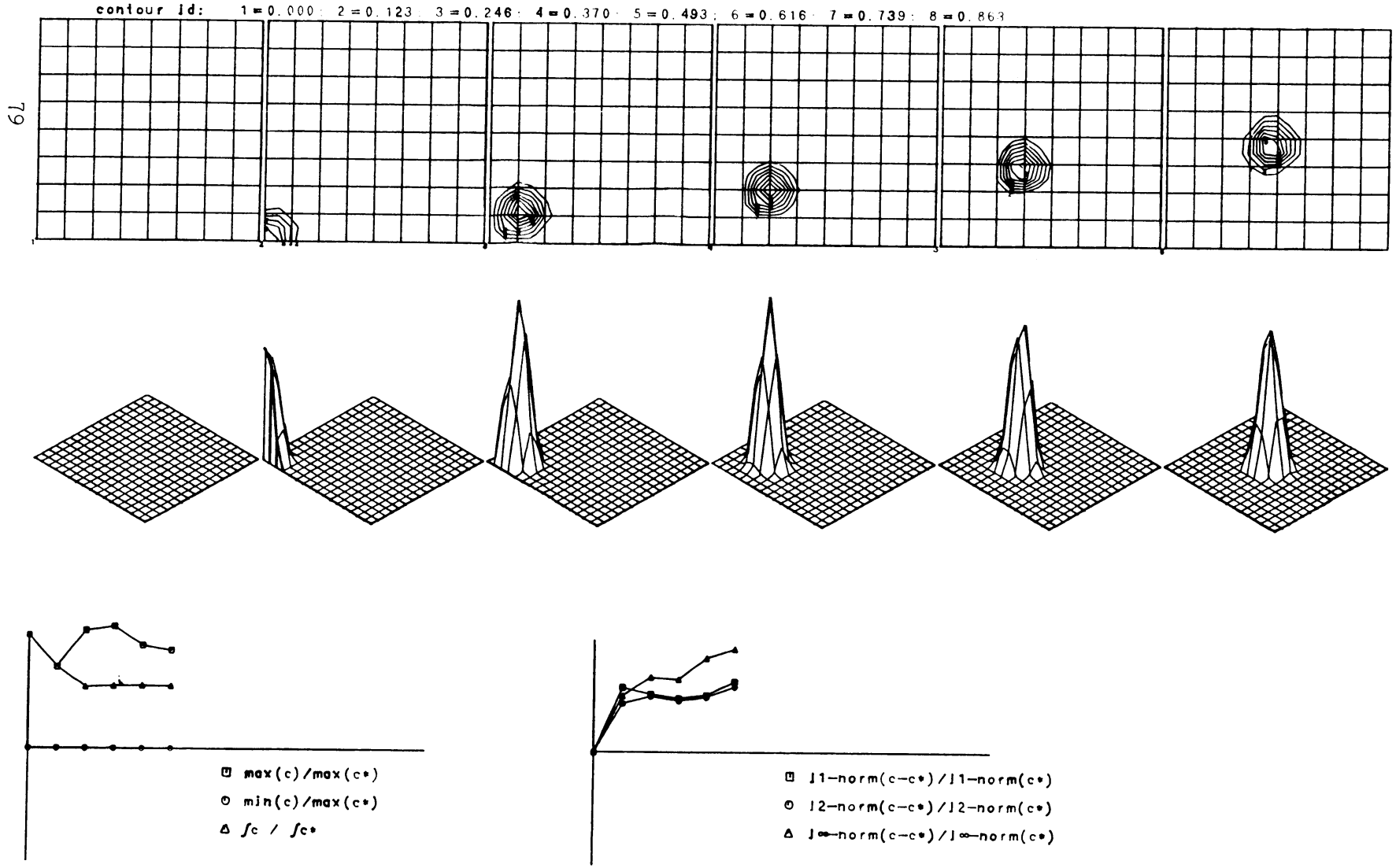

Particles method (1000); #points=17; Courant=.83; Block test

Figure 2.10.30

2.10.4 Block test, outflow boundary (see figures 2.10.31 - 2.10.40)

1A[a] Obviously the grid resolution is too low: large positive peaks are formed upstream in x-, and y-direction (remember that the method is fractional) and as a combined effect, but attenuated, in the cross-wind direction. Note that the errors are only introduced upwind.

1A[b] The higher grid resolution yields better results, but large negative errors (≈25%) are introduced. Again, as for 1A[a], errors occur mainly upwind.

1B[a] In contrast to the inflow boundary test the method performs better than 1A[a], but it is still too inaccurate.

1B[b] As for 1B[a], the method performs slightly better than 1A[b].

2 The method performs best of all. Note the oscillating behaviour of the error norms and the mass. This is due to a representation error by considering only the concentration (0^{th} moment) and not the higher moments for output. If the time periods for output were chosen such that an integer number of grids would have been passed, then the representation would have been exact. Performing this test with a Courant number of 1 will yield the same result, and performing a test with a choice for output that fits exact representation will yield an exact result independently of the Courant number. However, for the inflow boundary the lucky choise of both Courant number and output time period is necessary to obtain exact results.

3A The block shape is deformed into a hill shape with a peak value that is about 25% too large. Negative values of about 6% are introduced.

3B Almost the same performance as 3A. Negative values ≈10%.

4 The diffusion effect seems to be less than for the inflow boundary block test.

5 Again, a severe disturbance of the block shape into a shock-wave type shape, and smearing of the concentration.

6 Obviously, there is too few mass (≈50%). The peak value can be 25% too low.

The results for the objective criteria are tabulated in table 4.

Table 4. Objective criteria,
block test ⊟ outflow boundary

	$1A^a$	$1A^b$	$1B^a$	$1B^b$	2	3A	3B	4	5	6
max	1.3	1.2	1.5	1.2	1.	1.25	1.25	1.2	1.	0.75
min	-0.11	-0.25	-0.12	-0.17	0.	-0.07	-0.12	0.	-0.	0.
mass	⊢	0.45	⊢	0.4	1.25	0.9	0.9	0.9	1.15	0.55
$\|\ \|_{\ell_1}$	-	1.25	1.5	1.15	0.6	0.8	0.7	0.8	0.65	0.8
$\|\ \|_{\ell_2}$	0.95	0.8	0.95	1.	0.7	0.65	0.5	0.55	0.7	0.75
$\|\ \|_{\ell_\infty}$	0.9	0.9	1.	1.	0.95	0.9	0.75	0.85	1.	0.95

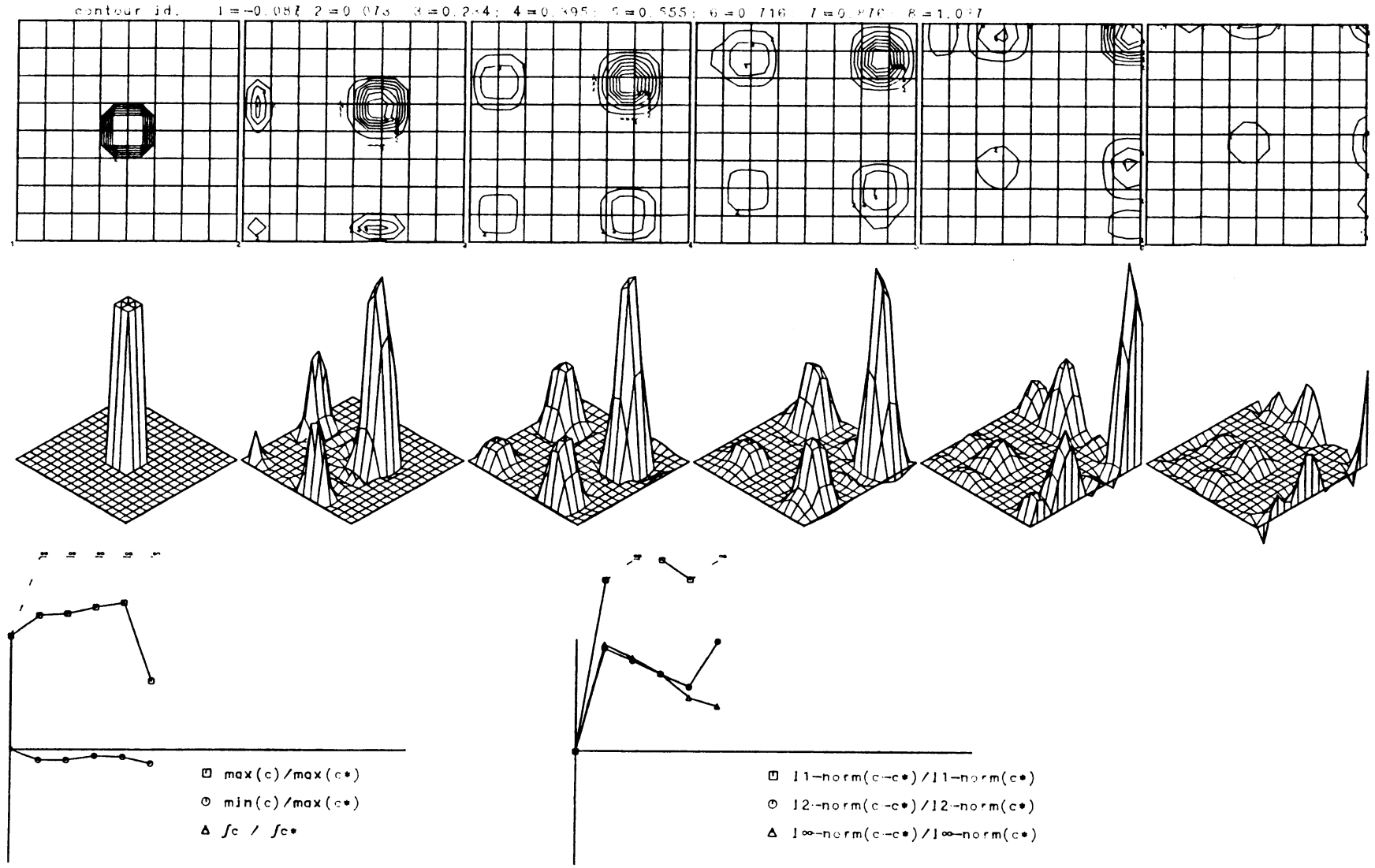

Pseudo spectral (polynomial): #points=17; Courant=0.747; Block test

Figure 2.10.31

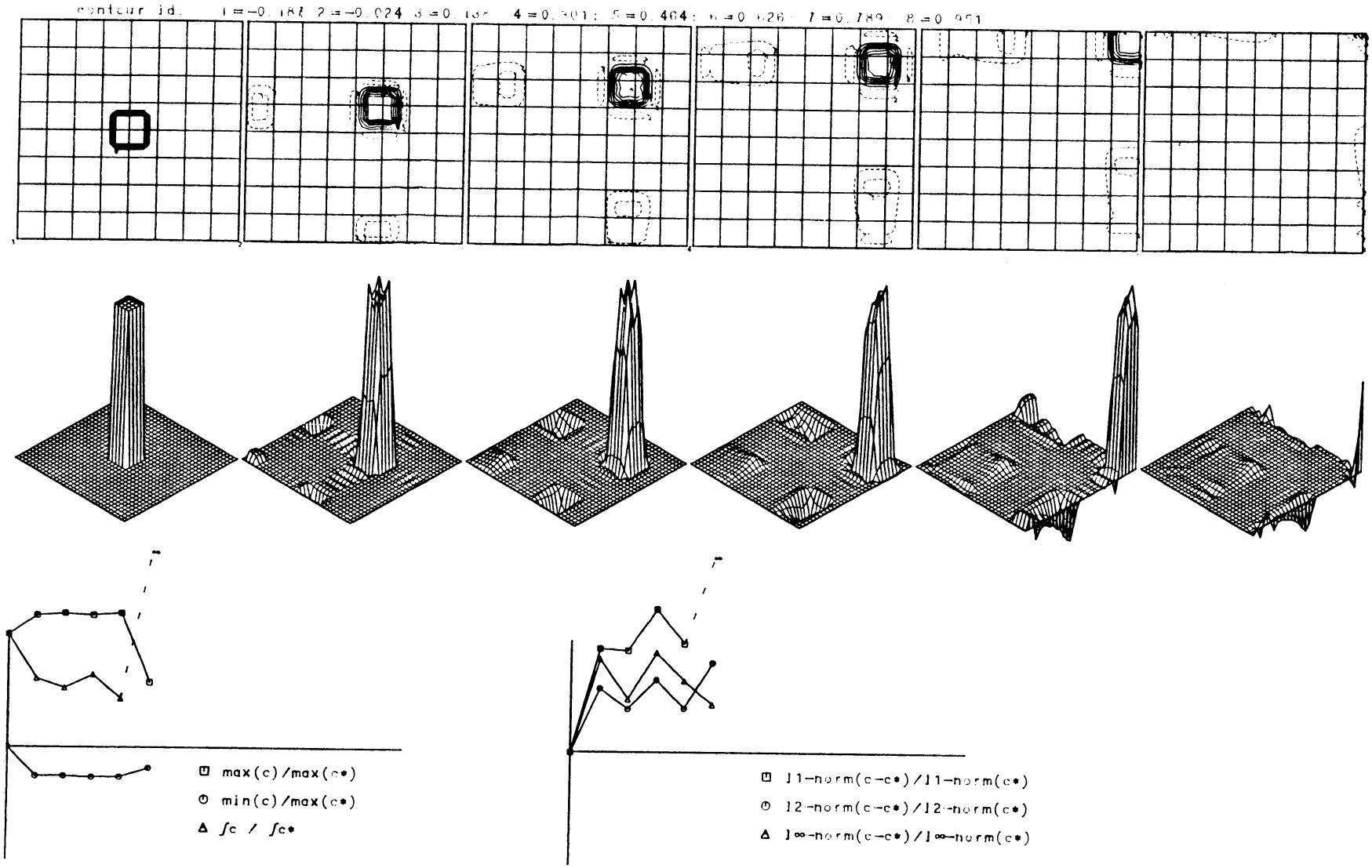

Pseudo spectral (polynomial); #points=33; Courant=0.747; Block test

Figure 2.10.32

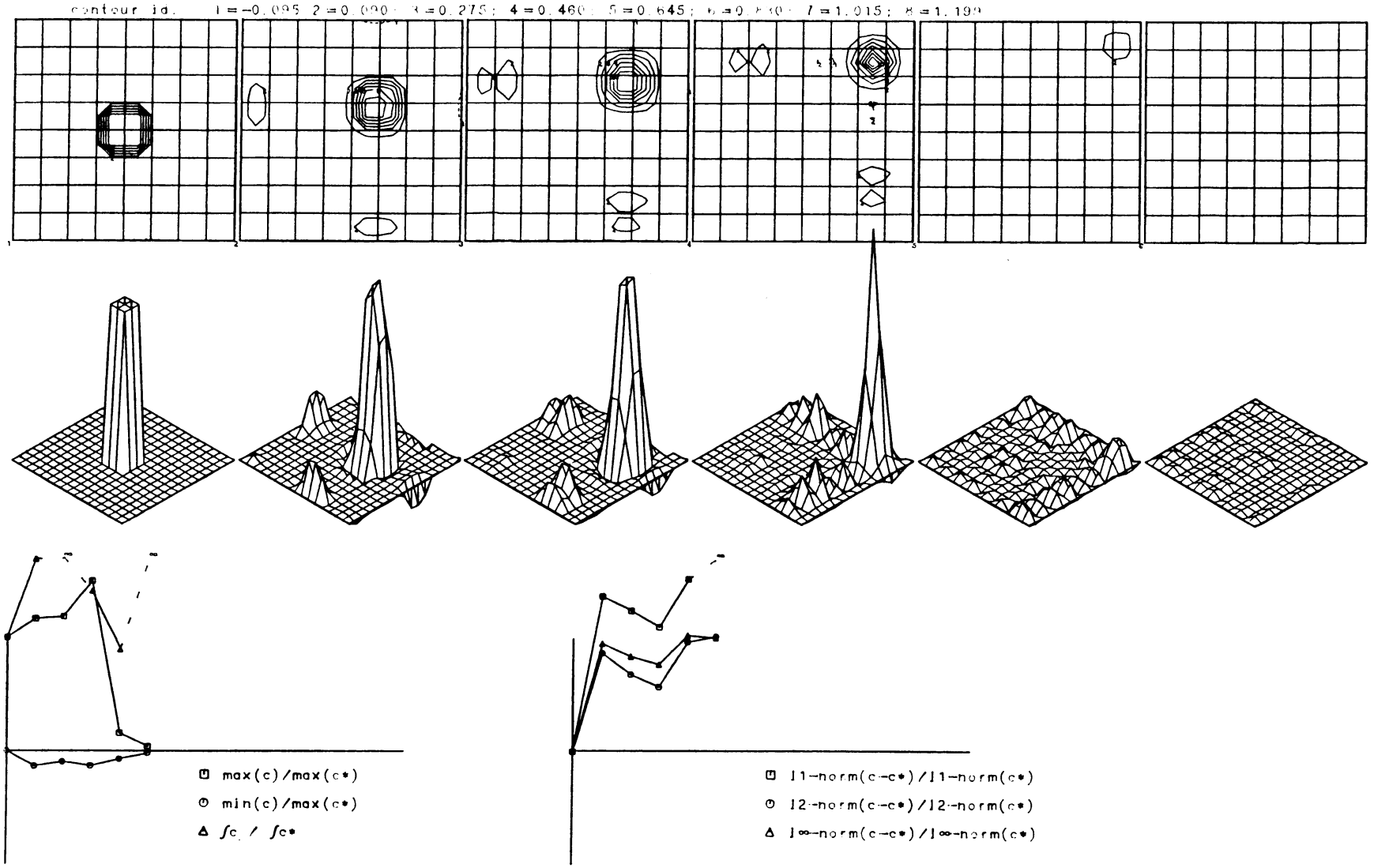

Pseudo spectral (decay); #points=17; Courant=0.74; Block test

Figure 2.10.33

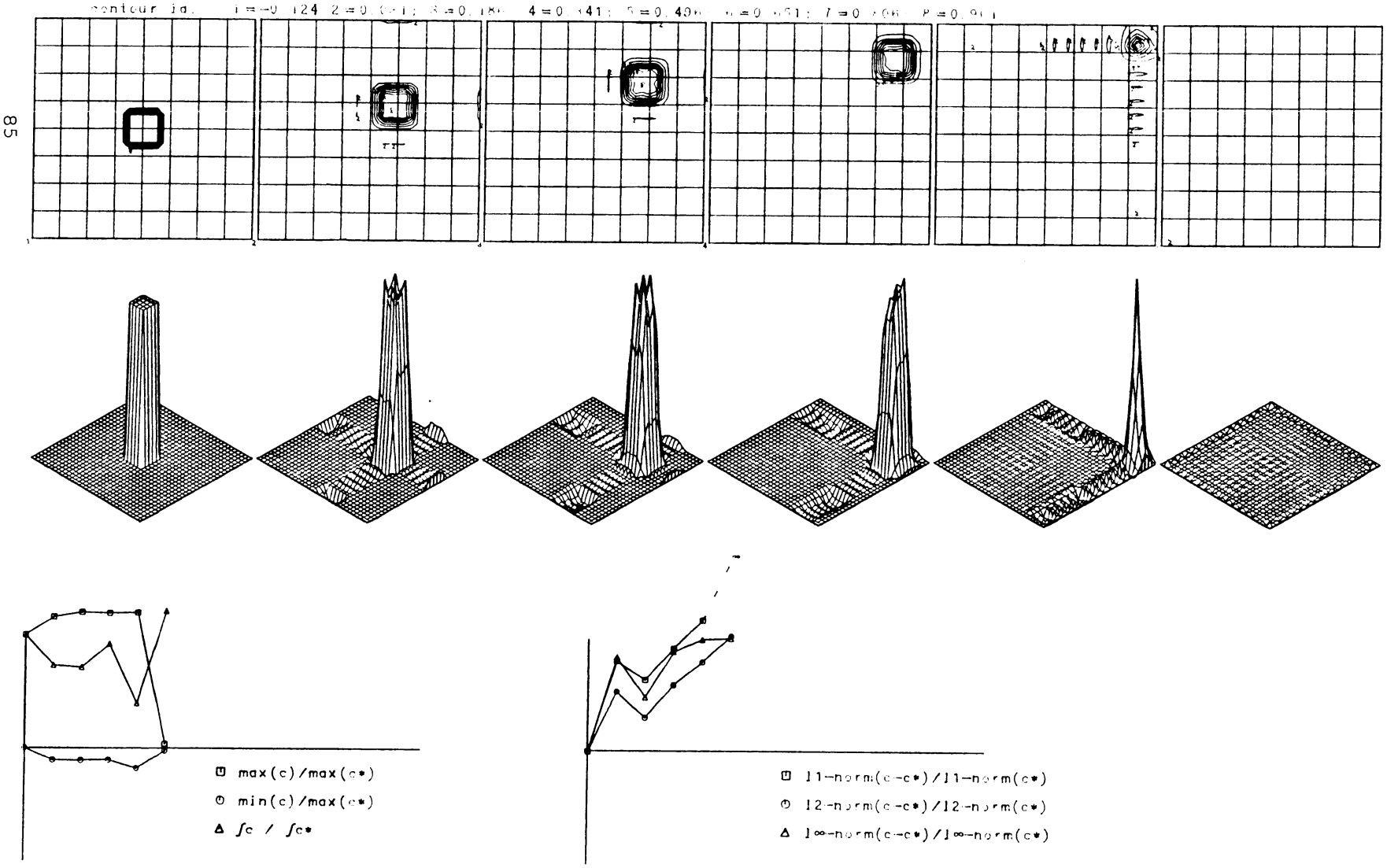

Pseudo spectral (decay): #points=33 Courant=0.74: Block test

Figure 2.10.34

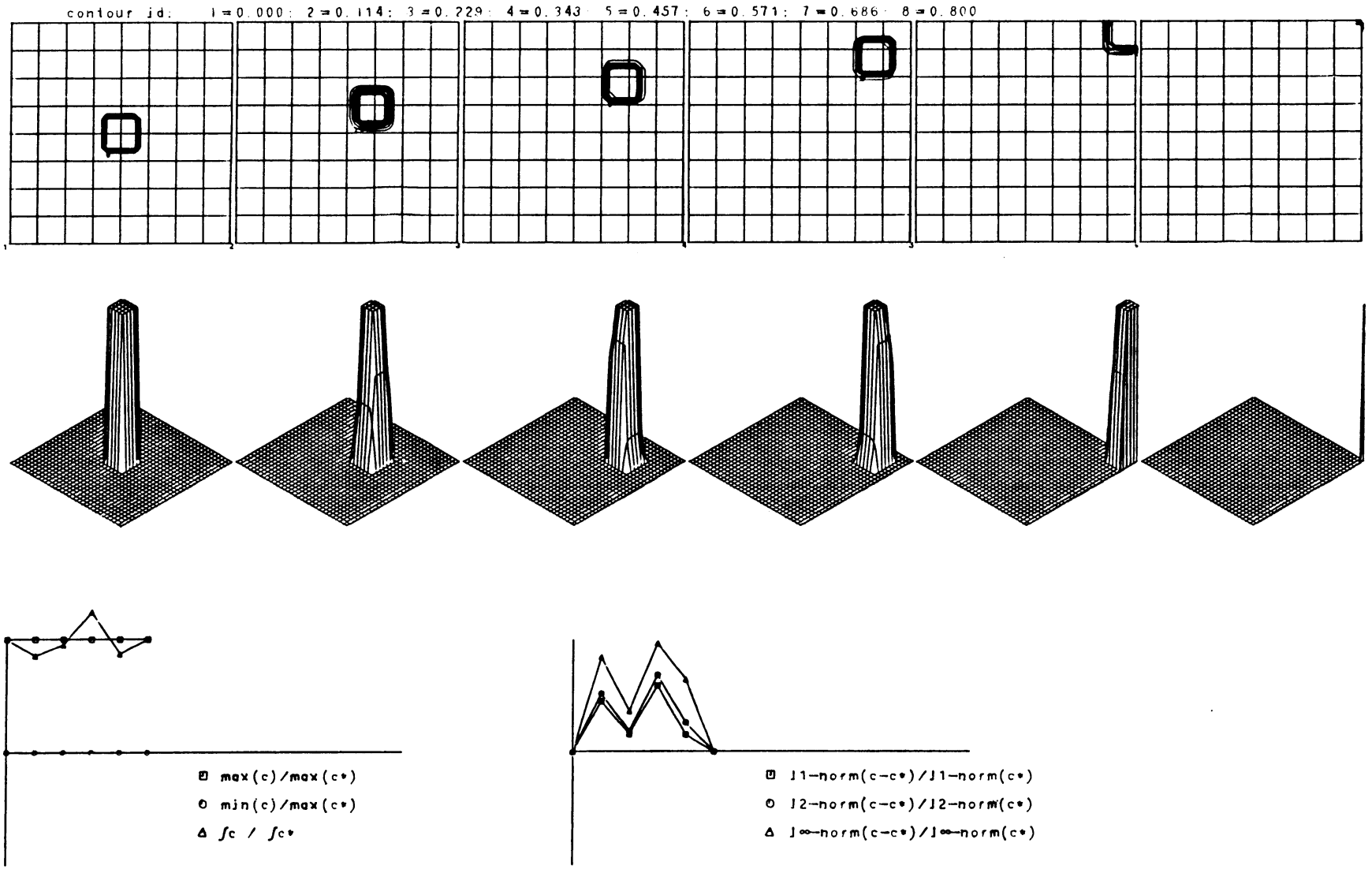

Second moment: #points=33; Courant number=0.83; Block test

Figure 2.10.35

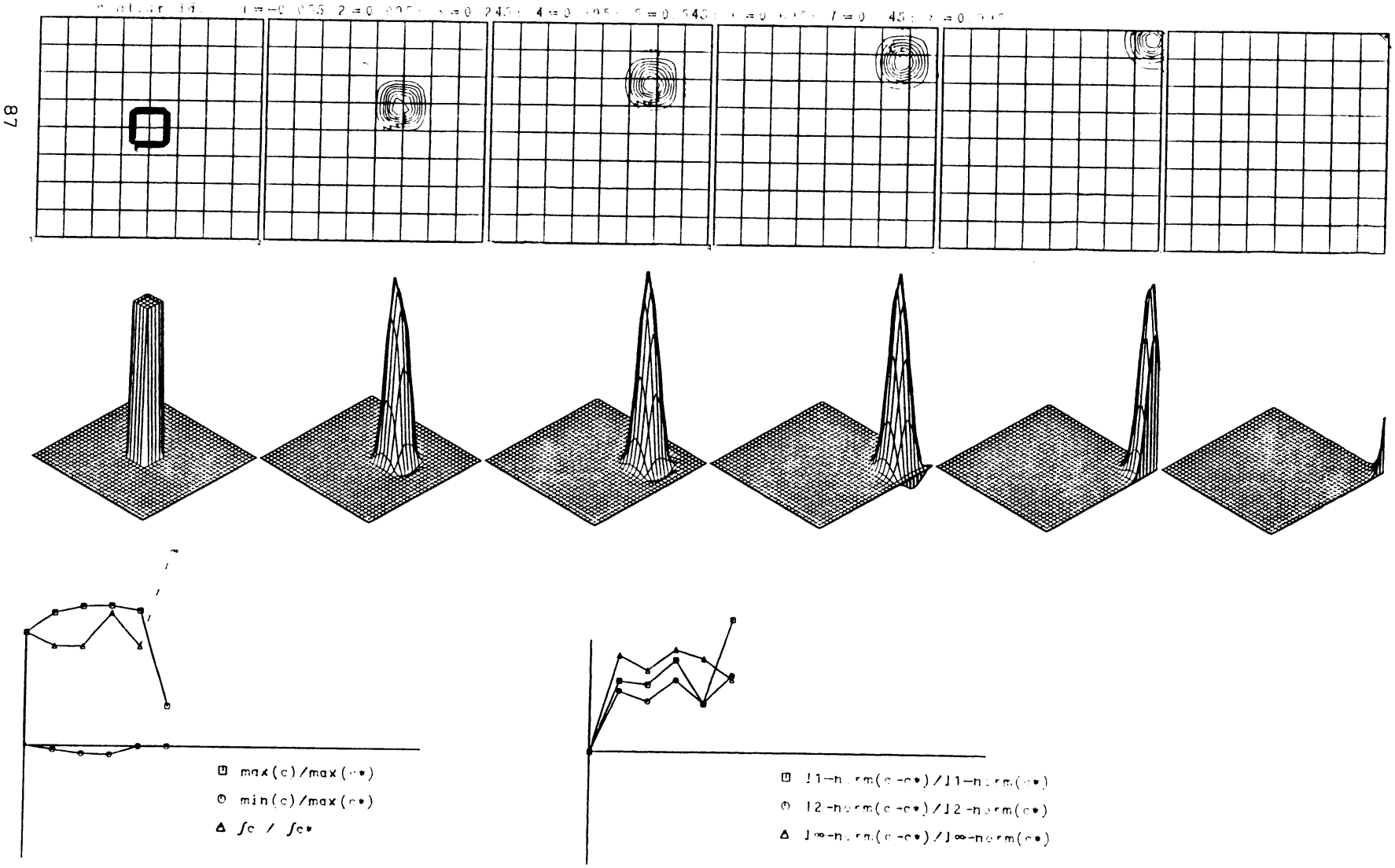

Figure 2.10.36

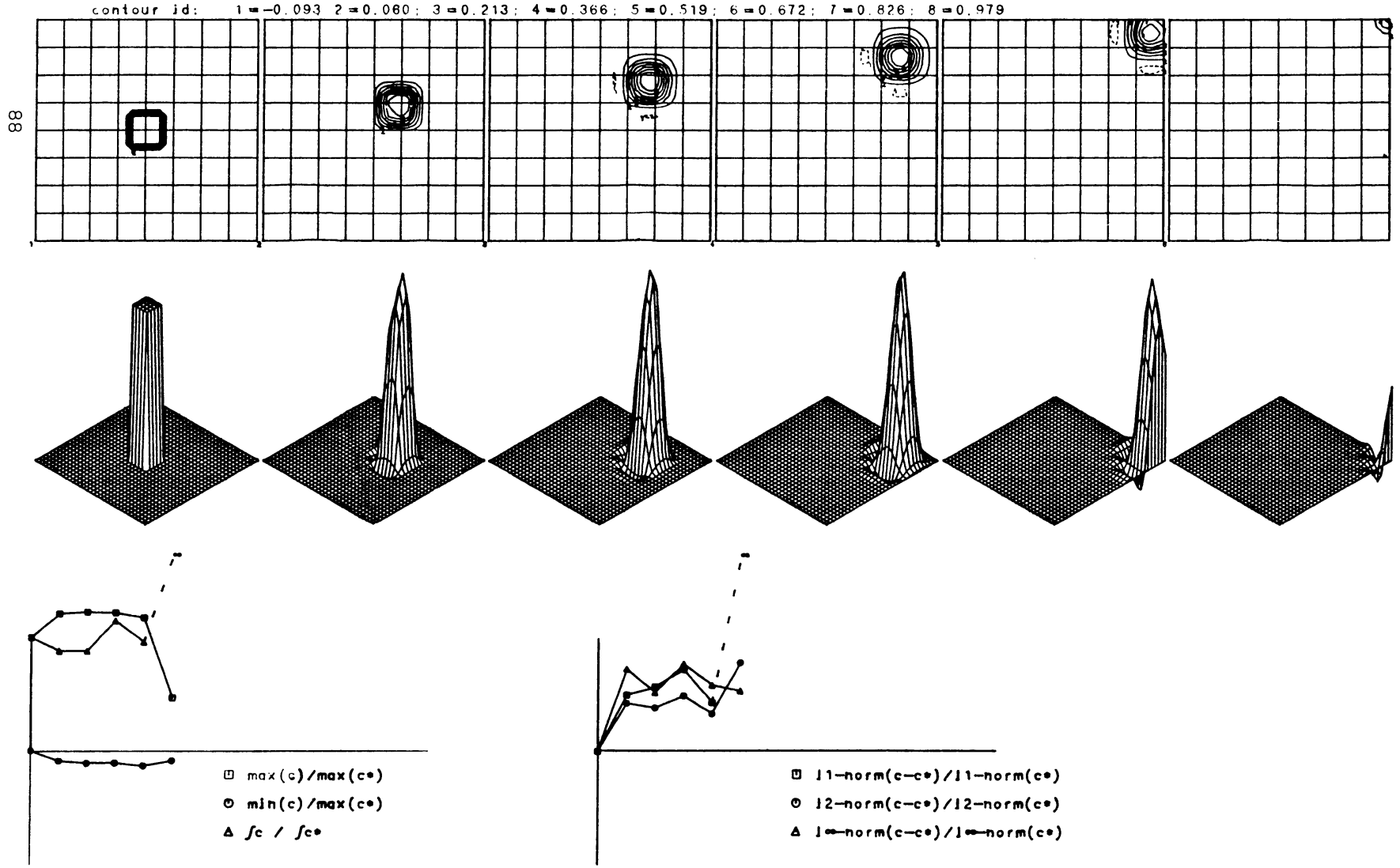

shape-lumped method: #points= Courant number=.8 Block test

Figure 2.10.37

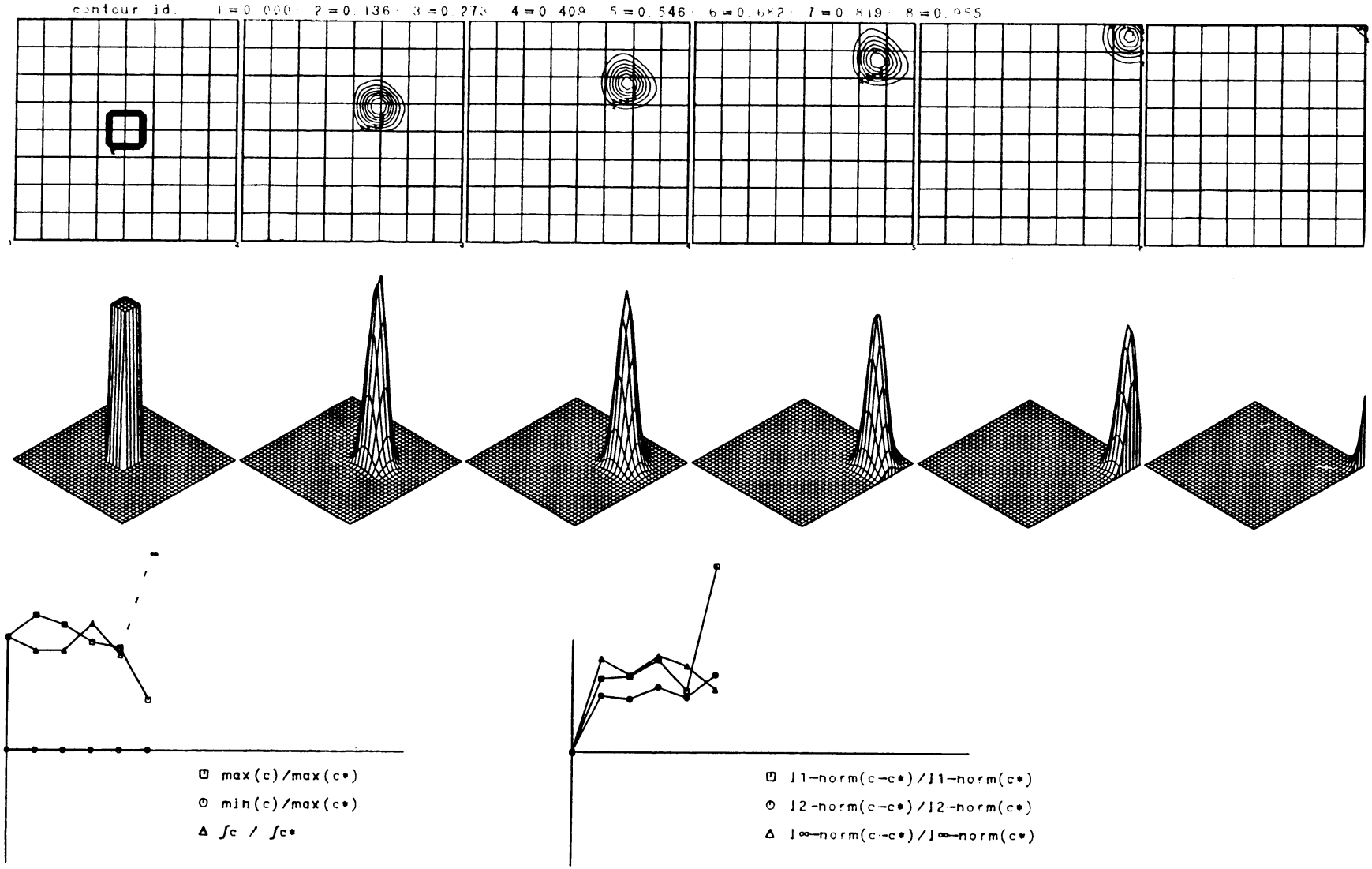

Smolarkiewicz(2): #points=33; Courant number=.486; Block test

Figure 2.10.38

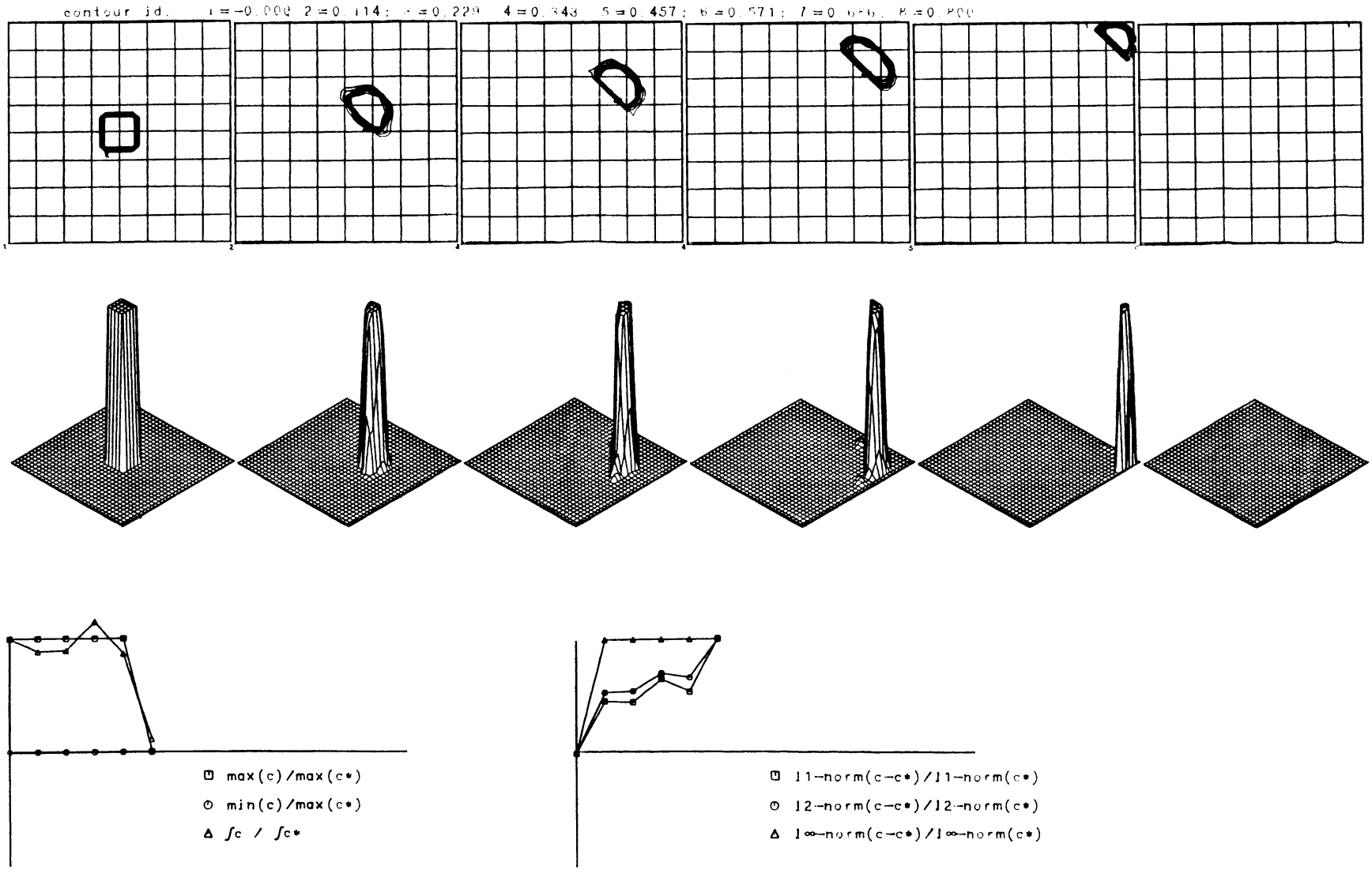

MFCT: #points=33; Courant=.43; Block test

Figure 2.10.39

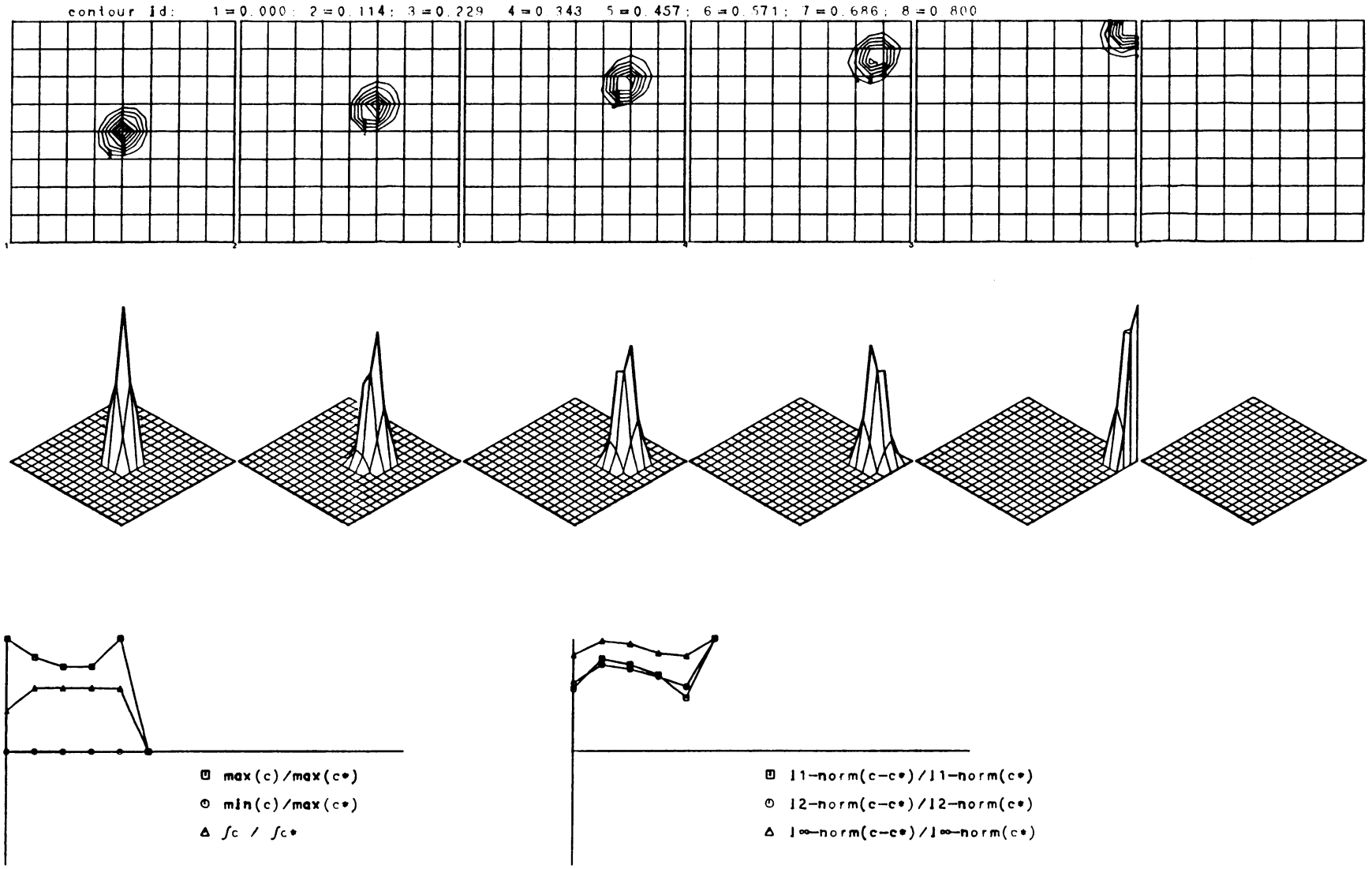

Particles method (1000); #points=17; Courant=.83; Block test

Figure 2.10.40

2.10.5 Comparison of practical demands

Time consumption and storage requirements are tabulated in table 5. The time consumption is in units of cpu-seconds. The storage requirements are given for s chemical species to be advected in units of the total number of grid points $n_x.n_y$. In the particles method the number

p = number of particles / total number of grid points

had to be introduced.

Note that for the pseudo-spectral methods with 17 x 17 grid points the storage requirements are about one quarter of other methods. Also, the factor p in the particles method is less severe as it might seem when a low Eulerian grid resolution is applied. In fact, a 17 x 17 grid was used together with 1000 particles ($p \approx 4$), so the storage requirements are about the same as for other methods. Note also the factor 5 of the second moment method: for this method the storage requirements are quite severe.

However, concerning the cpu-time consumption, the second moment came out as one of best together with the pseudo-spectral methods with low grid resolution and the chapeau function, lumped version, method.

Table 5. Consumption time and storage requirements

	1A[a]	1A[b]	1B[a]	1B[b]	2	3A	3B	4	5	6
cpu:										
Molenkamp	155	1139	144	1038	185	327	174	2475	454	626
Source	65	387	42	313	65	103	55	479	80	185
Block-in	37	208	36	219	31	75	43	1690	100	324
Block-out	44	239	33	202	34	72	45	1690	98	213
Storage:	s+6	s+6	s+6	s+6	5s+5	s+1	s+1	s+3	s+5	p(s+3)

2.11 Discussion

Six different methods are compared on the basis of four test problems. Three of these methods are strictly non-negative: the second moment method, the method due to Smolarkiewicz and the particles method. All other methods introduce negative concentration values during the calculations, be it that the MFCT algorithm never introduces negative values less than -10^{-16}. A relation seems to exist between steepness of data and the negative values: the steeper the data, the greater (in absolute value) the negative values. All methods except for the second moment method essentially deform a block shaped concentration field. The MFCT algorithm deforms all profiles into a shock-wave type and smears out the concentration in directions perpendicular to the local wind velocity.

Apart form the Molenkamp test the second moment method performed best with respect to the theoretical demands and the practical demand of computation-time consumption. In order to gain accuracy in problems with space-dependent wind fields as e.g. in the Molenkamp test it is proposed to calculate the transportation of the center of masses in the SMM by a 4^{th} order Runge-Kutta method instead of the forward Euler method that is used now.

The above considerations lead to the problem of choosing an algorithm for use in air quality models which include photochemical interactions.

A. Strict non-negativity is demanded.
This rules out three methods. From the three that remain, Smolarkiewicz' method is very expensive, while it is still quite diffusive. The particles method lacks an accurate projection procedure onto the Eulerian grid. Also, the right way for the source definition and for the initial concentration implementation are not well understood yet (source: too much mass; block-out: too few mass). The only method that rests is the second moment method which in fact performed best for all tests involving steep data. Nevertheless, one may have to resort to the two other methods because of the severe storage requirements. However, considering the enormous developments in computer architecture this may be not a problem any more within a decade.

B. Slight negative values are acceptable.

In case of steep gradients, only the MFCT algorithm competes with the second moment method, because the other methods introduce too large negative values. However, MFCT rules itself out because of its implied deforming property, which makes the method inaccurate. In case of fairly smooth gradients, the pseudo-spectral methods with low grid resolution (small negative values, relative small storage requirements) and the chapeau function method (very small negative values) are competing. However, the use of these methods together with smooth inflow boundary conditions has to be considered yet in more detail.

ACKNOWLEDGEMENT

The authors would like to thank Marleen Kaltofen for her accurate and quick typing of the manuscript.

REFERENCES

Boris J.P. and Book D.L. (1973) Flux-Corrected Transport I. J. Comp. Phys. 11, 38-69.

Boris J.P. and Book D.L. (1976) Flux-Corrected Transport III. J. Comp. Phys. 20, 397-431.

Businger J.A. (1984) Equations and Concepts in: Atmospheric Turbulence and Air Pollution Modelling, F.T.M. Nieuwstadt and H. van Dop (eds.) D. Reidel, Dordrecht.

Chock D.P. and Dunker A.M. (1983) A comparison of numerical schemes for solving the advection equation. Atmospheric Environment 17, 11-24.

Chock D.P. (1985) A comparison of numerical schemes for solving the advection equation II. Atmospheric Environment 19, 571-586.

Christensen O. and Prahm L.P. (1976) A pseudospectral method for dispersion of atmospheric pollutants. J. Appl. Meteor. 15, 1284-1294.

Cooley J.W. and Tukey J.W. (1965) An algorithm for the machine calculation of complex Fourier series. Math. Comput. 19, 297-301.

De Haan B. (1981) A comparison of finite difference schemes, describing the two-dimensional advection equation, in: Air pollution modelling and its application I, C. de Wispelaere (ed.), Plenum Press, New York.

Egan B.A. and Mahoney J.R. (1971) Numerical modelling of advection and diffusion of urban area source pollutants. J. Appl. Meteor. 11, 312-322.

Forester C.K. (1977) Higher order monotonic convective difference schemes. J. Comp. Phys. 23, 1-22.

Gottlieb D. and Orszag S.A. (1977) Numerical Analysis of Spectral Methods: Theory and Applications. NSF-CBMS Monograph no. 26 SIAM.

Gresho P.M., Lee R.L. and Sani R.L. (1978) Advection dominated flows, with emphasis on the consequences of mass lumping. In: Finite Elements in Fluids (E. Gallagher, ed.) Vol. 3, Ch. 19, 335-350.

Hirt C.W. (1968) Heuristic stability theory for finite-difference equations. J. Comp. Phys. 2, 339-355.

Karamchandani P. and Peters L.K. (1983) Analysis of the error associated with grid representation of point sources. Atmospheric Environment 17, 927-933.

Lambert J.D. (1973) Computational Methods in Ordinary Differential Equations. J. Wiley and Sons, New York.

Long P.E. and Pepper D.W. (1981) An examination of some simple numerical schemes for calculating scalar advection. J. Appl. Meteor. 20, 146-156.

Marchuk G.I. (1975) Methods of Numerical Mathematics, Springer Verlag, New York.

McRae G.J., Goodin W.R. and Seinfeld J.H. (1982) Numerical solution of the atmospheric diffusion equation for chemically reacting flows. J. Comp. Phys. 45, 1-42.

Molenkamp C.R. (1968) Accuracy of finite-difference methods applied to the advection equation, J. Appl. Meteor. 7, 160-167.

Pasquill F. and Smith F.B. (1983) Atmospheric Diffusion, John Wiley, New York.

Pedersen L.B. and Prahm L.P. (1974) A method for numerical solution of the advection equation. Tellus XXVI, 594-602.

Peyret R. and Taylor T.D. (1983) Computational Methods for Fluid Flow, Springer Verlag, New York.

Praagman N. (1979) Numerical solution of the shallow water equations by a finite element method, Thesis, University of Technology Delft.

Praagman N. (1986) TRASIL: A numerical simulation model for the transport of silt. Internal Report, Svasek B.V., Rotterdam.

Richtmyer R.D. and Morton K.W. (1967) Difference Methods for Initial-Value Problems, Interscience Publishers, New York.

Roache P.J. (1976) Computational Fluid Dynamics. Hermosa, Albequerque.

Roe P.L. (1986) Characteristic-based schemes for the Euler equations. Ann. Rev. Fluid Mech. 18, 337-365.

Schere K. (1983) An evaluation of several numerical advection schemes. Atmospheric Environment 17, 1897-1907.

Sheih C.M. and Ludwig F.L. (1985) A comparison of numerical pseudo-diffusion and atmospheric diffusion. Atmospheric Environment 19, 1065-1068.

Smolarkiewicz P.K. (1983) A simple positive definite advection scheme with small implicit diffusion, Mon. Wea. Rev. 111, 479-486.

Smolarkiewicz P.K. (1984) A fully multidimensional positive definite advection transport algorithm with small implicit diffusion, J. Comp. Phys. 54, 325-362.

Spekreyse S.P. (1986) Multigrid solution of monotone second-order discretizations of hyperbolic conservation laws. Centre for Mathematics and Computer Science, Report NM-R8611, Amsterdam.

Strang G. and Fix G.J. (1973) An Analysis of the Finite Element Method, Prentice-Hall, Englewood Cliffs, N.J.

Trefethen L.N. (1985) Stability of hyperbolic finite-difference models with one and two boundaries, Lectures in Applied Mathematics 22, 311-326.

Van Dop H., De Haan B.J., Engeldal C. (1982) The KNMI mesoscale air pollution model, Royal Netherlands Meteorological Institute, Scientific Report W.R. 82-6.

Van Leer B. (1979) Toward the ultimate conservative difference scheme V. J. Comp. Phys. 32, 101-136.

Whitham G.B. (1974) Linear and Nonlinear Waves, Wiley-Interscience, New York.

Yanenko N.N. (1971) The Method of Fractional Steps, Springer, New York.

Zalesak S.T. (1979) A fully multidimensional flux-corrected transport algorithm for fluids, J. Comp. Phys. 31, 335-362.

Zalesak S.T. (1981) High order "ZIP" differencing of convective terms, J. Comp. Phys. 40, 497-508.

[1] Numerical Advection Schemes: The pseudospectral method. RIVM report 958702001 (to be published 1987).

[2] Numerical Advection Schemes: The second moment method. RIVM report 958702002 (to be published 1987).

[3] Numerical Advection Schemes: The chapeau function method. RIVM report 958702003 (to be published 1987).

[4] Numerical Advection Schemes: The method of Smolarkiewicz. RIVM report 958702004 (to be published 1987).

[5] Numerical Advection Schemes: The MFCT method. RIVM report 958702005 (to be published 1987).

[6] Numerical Advection Schemes: The particles method. RIVM report 958702006 (to be published 1987).